Enhancing the performance of transparent electrodes through the design of new silver nanostructures

Alexandra Madeira

THÈSE EN COTUTELLE PRÉSENTÉE
POUR OBTENIR LE GRADE DE

DOCTEUR DE L'UNIVERSITÉ DE BORDEAUX ET DE L'UNIVERSITÉ DE WATERLOO

ÉCOLE DOCTORALE DES SCIENCES CHIMIQUES
ELECTRICAL AND COMPUTER ENGINEERING

Spécialité : Physico-Chimie de la Matière Condensée
Par Alexandra Madeira

Enhancing the performance of transparent electrodes through the design of new silver nanostructures

Sous la direction d'Irene Goldthorpe
et Mona Tréguer-Delapierre

Membres du jury de l'université de Bordeaux:

M. Viau Guillaume	Professeur, INSA Toulouse	Rapporteur
M. Piquemal Jean-Yves	Professeur, U.Paris Diderot	Rapporteur
M. Bellet Daniel	Professeur, INP Grenoble	Examinateur
M. Maglione Mario	Directeur de recherche, CNRS	Examinateur
M. Wasilewski Zbigniew	Professeur, University of Waterloo	Invité
M. Servant Laurent	Professeur, U.Bordeaux	Invité

Abstract

Transparent electrodes are a necessary component in a number of devices such as solar cells, flat panel displays, touch screens and light emitting diodes. The most commonly used transparent conductor, indium tin oxide (ITO), is expensive and brittle, the latter property making it inappropriate for up-and-coming flexible devices. Films consisting of random networks of solution-synthesized silver nanowires have emerged as a promising alternative to ITO. They have transparency and conductivity values better than competing new technologies (e.g. carbon nanotubes films, graphene, conductive polymers, etc.) and comparable to ITO. Furthermore, these silver nanowire films are cheap, flexible, and compatible with roll-to-roll deposition techniques. The main objectives of this PhD work are to improve the properties of silver nanowire electrodes and to study and solve issues that are currently hindering their use in commercial devices. Specifically, I studied the important areas of electrode conductivity and stability. To increase the conductivity of nanowire electrodes, two silver nanostructures different from what is commercially available were synthesized i) ultra-long nanowires and (ii) branched nanowires. Regarding (i), by using 1.2-propanediol as the medium rather than the typical ethylene glycol in the polyol synthesis process, as well as the molecular weight of PVP, the temperature of the process, or the concentration of silver nitrate, we obtained silver nanowires with an aspect ratio between their lengths and diameters of 1050. Among all the ultra-long silver nanowires elaborated in polyol process reported in the literature, they have the maximum length. The synthesis developed is also cheap and the reaction time takes less than 2h. Moreover, they have a high yield of 2 mg/ml. Electrodes with a sheet resistance of 5 Ω/Sq for a transparency of 94% were obtained (with post thermal treatment applied). However, this post-deposition anneal is shown to have a small influence on the decrease of the sheet resistance. It is thus not required to elaborate electrodes with good performance, which is very advantageous for the elaboration of electrodes on plastic substrates. Regarding (ii), "V-like

shape" or "Y-like branched" nanowires were elaborated thanks to the input of ultrasonic irradiation during the polyol process. Unfortunately, their length being short (6 µm), their interest is limited to enhance the performance of transparent electrodes. In addition, structural analyses of both branched and unbranched nanowires revealed the nanostructures not monocrystalline. Concerning the stabilities issues, the thermal stability of silver nanowire electrodes coated with graphene was investigated. This coating allows a better homogeneity of the heat through the network, decreasing the number of hot spots and thus increasing the lifetime of the electrodes. The corrosion of silver nanowire and the resulting electrode resistance increase over time is a severe problem hindering their use in commercial devices. 11-mercaptoundecanoic acid (MuA) was identified as a promising passivation agent of silver nanowires. Lifetime testing showed that the electrode resistance increased more slowly (12%) than any other passivated electrodes reported in the literature. Furthermore, unlike many other passivation methods, the MuA molecule itself does not negatively affect the conductivity or transparency of the electrode and is very inexpensive, all contributing to the commercial viability of the passivation method.

Résumé

Les électrodes transparentes sont les composants indispensables de nombreux dispositifs optoélectroniques commerciaux (cellules solaires, écrans plats, écrans tactiles ou encore diodes électroluminescentes). Elles sont constituées le plus souvent d'oxyde d'indium et d'étain (ITO). Les électrodes à base d'ITO sont produites par un procédé relativement coûteux et sont très fragiles à la contrainte mécanique, ce qui limite leur utilisation au sein de dispositifs optoélectroniques flexibles. Des matériaux alternatifs, sans indium, à base de réseaux de nano-fils d'argent, font actuellement l'objet d'un grand nombre de recherches. Ces réseaux à base de nanostructures métalliques ont des propriétés opto-électroniques comparables voire supérieures à celles de l'ITO. Ils sont adaptables à des substrats flexibles et sont compatibles avec les procédés de dépôt « roll to roll ». L'objectif de cette thèse est d'explorer de nouvelles voies de synthèse et de modification de surface de nanofils d'argent pour développer des électrodes transparentes plus performantes. De nouvelles nanostructures métalliques, différentes de celles commercialisées, ont été élaborées : (i) des fils d'argent ultra-longs (ii) des fils d'argent présentant une architecture inhabituelle i.e avec des ramifications. Des paramètres clés du procédé polyol ont été modifiés pour élaborer les fils à facteur de forme très élevé. Ils ont permis d'accroître les performances résistance/transparence des dispositifs conventionnels. Des nano-fils d'argent de forme « Y » ou « V » ont également été synthétisés en soumettant le milieu de croissance à des ultra-sons. Ces nanostructures devraient permettre de limiter les problèmes de conduction qui apparaissent, à l'heure actuelle, au niveau des contacts entre les fils dans les dispositifs nanostructurés. Par ailleurs, des réseaux de fils d'argent modifiés en surface avec de l'acide 11-mercaptoundecanoïque (MuA) ont été élaborés. Ils constituent une solution très intéressante pour améliorer la stabilité chimique des réseaux métalliques. Le MuA limite

l'oxydation de surface du métal et permet aux électrodes de conserver leurs transparence et conductivité initiales.

Remerciements

J'ai effectué une grande partie de cette thèse à l'Institut de Chimie de la Matière Condensée de Bordeaux au sein du groupe V « Chimie des nanomatériaux ». Je tiens donc tout d'abord à remercier Monsieur Mario Maglione pour m'avoir accueillie au sein de son laboratoire.

Je remercie grandement Guillaume Viau et Jean-Yves Piquemal d'avoir consacré du temps à l'évaluation de mes travaux de thèse, ainsi que Daniel Bellet pour sa participation à mon jury et à Mario Maglione de l'avoir présidé. Je les remercie sincèrement pour l'intérêt qu'ils ont manifesté envers ces travaux.

Je souhaite maintenant remercier mes directeurs de thèse, Mona Tréguer-Delapierre et Laurent Servant, de m'avoir fait confiance en me proposant de faire partie de ce projet international. Leur encadrement m'a permis de progresser tout au long de ma thèse. Je remercie particulièrement Mona Tréguer-Delapierre qui a contribué à plus que 100% au déroulement de ce projet. Ses conseils et son soutien ont été précieux et m'ont m'aidé à garder un esprit optimiste.

Je souhaite remercier toutes les personnes avec qui j'ai pu collaborer durant ces années de thèse : David Talaga, Sebastien Bonhommeau, Christophe Pradère, Marta Romano, Daniel Bellet, Dorina Papanastasiou, Sara Aghazadehchors, François Weill et Marion Gayot.

Je remercie tout particulièrement Daniel, Dorina et Sara pour leur accueil exceptionnel durant la semaine que j'ai pu passer au LMPG à Grenoble !

Je remercie l'ensemble du laboratoire ICMCB et tout particulièrement mes collègues du groupe V avec qui j'ai passé d'excellents moments. Bon courage à tous les nouveaux thésards et profitez à fond de ces 3 ans de thèse !

Je remercie tous mes amis pour leur présence et support : Clicli, Obesa, Elodie, Arni le président, Belette, Simsim, Mathieu, Magda, Petra, Kat, Alberto, Noe, Cintia, Laura, Sergio et Maria, Manette et Paulette, Cora, Camille, Coline, Sonia… et tous les copains !

Je remercie ma famille pour leur soutien tout au long de ma thèse. Je remercie mon Miguel, d'avoir supporté mes angoisses quand les expériences ne fonctionnaient pas… et pour tous ses nombreux conseils.

Rr

Table of Contents

List of Figures

List of Abreviations

AgNW: Silver nanowire

ITO: Indium tin oxide

LCDs: liquid crystal displays

LED: light-emitting diode

CVD: Chemical vapor deposition

PECVD: Plasma-enhanced chemical vapor deposition

RGO: Reduced graphene oxide

SWNTs: Single walled nanotubes

CNT: Carbon nanotube

GO: Graphene oxide

LED: Light emitting diode

OLED: Organic light emitting diode

LCD: Liquid crystal display

PET: Polyethylene terephthalate

PEN: Polyethylene-naphthalate

PVP: Polyvinylpyrrolidone

SEM: Scanning electron microscope

TEM: Transmission electron microscope

MPT: Multiply-twinned seed/particle

SERS: Surface enhanced Raman spectroscopy

MuA: 11-mercaptoundecanoic acid

FCC: Face centered cubic

GA: Glycoaldehyde

GC: Gas chromatography

EG: Ethylene glycol

1.2-Pdol: 1.2 propanediol

HDD: Hexadecanediol

HDA: Hexadecylamine

DPE: Diphenyl ether

CTAB: Hexadecyltrimethylammonium bromide

ODT: 1-Octadecanethiol

MTP: Multiply twinned particle

HRTEM: High-resolution transmission electron microscopy

EDX: Energy Dispersive X-Ray Analysis

HR-SEM: High-resolution scanning electron microscopy

STEM: Scanning transmission electron microscopy

ICP-AES: Inductively Coupled Plasma – Atomic Emission Spectroscopy

XRD: X-ray diffraction

XPS: X-ray photoelectron microscopy

HOPG: highly oriented pyrolytic graphite

DRIFT: Diffuse reflectance infrared Fourier transform

LB: Langmuir–Blodgett

JCPDS: Joint Committee on Powder Diffraction Standards

NMR: Nuclear Magnetic Resonance

General Introduction

The topic of this thesis is focused on the development of transparent conductive materials which play a large role in electronic displays, transparent heaters, solar cells, light emitting diodes, touch screens and many other technologies.[1] These types of materials are continuing to attract growing interest due to the high demand for personal devices. Currently, indium tin oxide (ITO), and more generally transparent conductive oxides dominate the market as the most mature technology showing excellent transparency (above 80%) combined with low resistivity (of the order of 10-4 Ω/cm). However, they are prone to cracking when mechanically bent, are costly, and require high-temperature fabrication processing to reach the best performance. Recent discoveries in nanomaterials have opened up an important opportunity to develop a new class of transparent electrodes suitable for optoelectronic devices, generating alternative materials to ITO. Of the various candidates, films consisting of random networks of solution-synthesized silver nanowires have emerged as a leading candidate. Silver nanowire films have transparency and conductivity values better than competing new technologies (e.g. graphene[2], carbon nanotubes films[3], conductive polymers[4]) and comparable to ITO[7],[8]. And silver nanowire films are cheap, mechanically flexible, and compatible with roll-to-roll deposition techniques. Although these nanomaterials have strong potential to replace ITO, they are not yet used in commercial devices. The purpose of this research is to study and solve current limitations hindering their widespread use so that these electrodes become a viable alternative to ITO.

Key problems this research addresses. The demand for devices that use ITO, the most common of which are liquid crystal displays (LCDs) and touch screens, continue to increase. ITO accounts for the majority of global indium consumption, however, the price of indium is high and volatile, and has various supply concerns. This is the first major problem spurring the need for an alternative transparent conductor. The second major problem is that ITO

electrodes crack upon bending and are thus not suitable for flexible displays, flexible solar cells, and other up-and-coming mechanically flexible devices. The third problem is the deposition process: ITO is deposited by sputtering which means it cannot be deposited on top of organic layers. Moreover, high deposition temperatures are also required which are not compatible with polymeric substrates. Silver nanowire electrodes do not contain indium, and although silver is an expensive material, so little of it is used such that the material costs of the nanowire electrodes are less than half that of ITO. Because nanowires can endure higher elastic strains than thin-films, silver nanowire networks are very mechanically flexible. Furthermore, nanowire networks can be deposited as a solution at room temperature without the requirement of processing under vacuum. Even with all these advantages, nanowire electrodes are not yet attractive enough to replace ITO. To make nanowire electrodes a more viable alternative this project will (i) improve their conductivity and transparency and (ii) tackle their lifetime and stability issues. Silver nanowires can be synthesized inexpensively in solution by the polyol method. To improve nanowire electrode conductivity and transparency, we explore the possibility to synthesize nanowires with sizes, shapes and architectures that are different than those of the materials that are commercially available. Longer nanowires will lead to less nanowire-nanowire junctions in a connected network and thus a lower resistance will be attained. Similarly, 2D branched nanowires, rather than 1D nanowires will also lead to less inter-nanowire junctions.

The lifetime of nanowire electrodes is currently shorter than ITO. To improve nanowire stability, we will investigate the possibility of passivating the surface of the silver nanowires with short organic molecules to protect silver against oxidation. To assess thermal stability and the lifetime of an electrode consisting of passivated nanowires, a DC power supply is used to pass a current across the electrode for an extended period of time and the sheet resistance of the electrodes will be measured in real-time. A 2D thermal mapping of the

films is obtained using an infrared thermal imaging camera to assess the amount of Joule heating and temperature variation across the film.

Overall, this research is focused on developing nanowire-based electrodes as a more viable alternative to ITO. In this manner, the non-ITO transparent conductor market is predicted to grow from $206 million in 2013 to $4 billion by 2020. Such extraordinary evolution highlights the enormous economic impact that this approach may have. Furthermore, many companies in France and Canada develop devices that require inexpensive, high performing transparent electrodes. Therefore, nanowire electrode materials will enable the development of new devices, particularly mechanically flexible electronic and optoelectronic devices, resulting in direct economic benefits for those companies involved.

This thesis project is part of the IDS-FunMat program (International Doctoral School in Functional Materials) and involves two universities: the University of Waterloo in Canada and the University of Bordeaux in France. The synthesis of inorganic nanoparticles has been widely investigated in the research group "Chimie des Nanomatériaux" in ICMCB (Institut de la Chimie de la Matière Condensée de Bordeaux). On the other hand, the expertise of integrating these particles into materials, their electrical characterization and the testing of these devices for evaluation have been developed in the group of Irene Goldthorpe in WIN (Waterloo Institute for Nanotechnology). Finally, the vibrational spectroscopy and imagery techniques have been developed in the research group GSM (Groupe Spectroscopie Moléculaire) in ISM (Institut des Sciences Moléculaires). Along these lines, such a collaboration enabled us to take a combinatory approach using knowledge and techniques from materials science, chemistry, electrical engineering and spectroscopy.

This thesis consists of four chapters. **Chapter 1** can be considered a literature review and provides the context of the thesis as well as discussion of many of the works that have already been undertaken by other groups. It is focused on the possible applications of the

transparent conductive electrodes and the impetus behind the drive to replace indium tin oxide by silver nanowires thin films. In **Chapter 2**, we report how to achieve ultra-long nanowires and discuss the electro-optical properties of electrodes based on these long and thin Ag nanowire networks prepared by methods that are scalable to industrial manufacturing levels. **Chapter 3** discusses the synthesis of novel architectures different from the classical 1D nanowires. **Chapter 4** provides an in-depth description of the thermal and chemical stability issues of the silver nanowire networks presented throughout this work. Finally, this thesis concludes with a summary of the work and a discussion of which directions future researchers in the field should be oriented to.

Chapter 1: Introduction to transparent conductive materials

In this first chapter, I give a brief introduction of transparent conductive materials emphasizing the importance of using silver nanowire electrodes as an alternative material. Aside from providing general considerations and a review of the state of the art of electrode properties like sheet resistance and optical transmittance, I will highlight some of the current challenges of electrodes based on metal-nanowires that have to be overcome. The synthesis of silver nanowires will be then described through an explanation of the parameters that significantly affect their formation and their dimensions. This work will further highlight the current efforts to produce ultrahigh aspect-ratio nanowires as well as architectures other than one dimensional metal nanostructures. Moreover, a range of practical post-treatments to increase the chemical and thermal stability of the electrodes will also be discussed.

1.1. Transparent Conductive Electrodes

Transparent conductive materials are crucial components in numerous optoelectronic devices such as thin film solar cells, touchscreens, electromagnetic shielding, light emitting diodes and many other display technologies.[4] They are often used in these optoelectronic devices as electrodes and their characteristics are application dependent (Figure 1). For instance, touch screen displays need an electrode sheet resistance in the range of 50-500 Ω/Sq; however, a sheet resistance as small as 10 Ω/Sq is required for solar cells.[5]
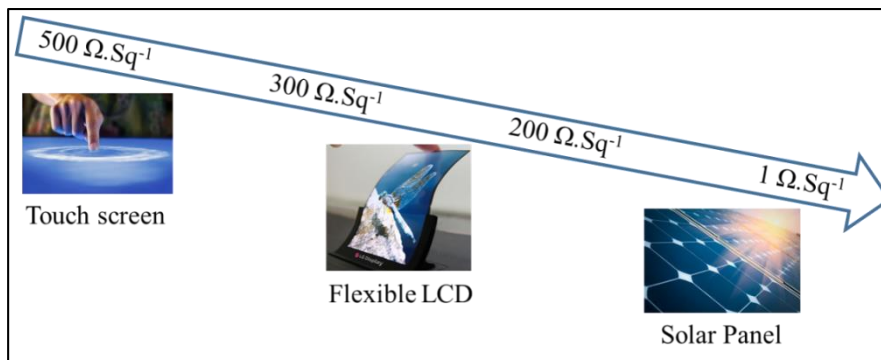
Figure 1: Sheet resistance requirements for transparent electrodes, depending on the application.

Doped metal oxides are the most commonly used materials in the electronic industry for transparent electrodes, in particular indium tin oxide.[4,6],[7],[8] The later has a low resistivity (R_{sheet} < 20 Ω/Sq), a high transparency (Transmittance > 80%) and allows a precise control of its thickness and doping concentration.[6] However, the price of ITO tends to increase over time due to the scarcity of indium and its high cost of manufacturing (high vacuum and high-temperature processing (T > 300°C) is required). Further, the elevated processing temperature severely limits the choice of substrate materials. While ITO electrodes on glass typically provide a sheet resistance in the range of 8 - 15 Ω/Sq, for ITO on plastic substrates, e.g. Polyethylene terephthalate (PET) or polyethylene naphthalate (PEN), which do not allow heat treatments higher than 150°C, the sheet resistance is significantly higher (on the order of 60 - 300 Ω/Sq).[9],[10] Moreover, the optical transparency of ITO is limited for films with a low sheet resistance. Other metal oxides such as aluminium doped ZnO and fluorine doped SnO_2, in general come with similar issues.[8,11] After decades of research, ITO remains the most important transparent conductive oxide, as of yet. Aiming for mechanically flexible, large-area, high-throughput optoelectronic device manufacturing, alternative concepts for the realization of (ideally) vacuum-free, low-temperature processed, scalable, flexible, highly transparent and conductive coatings are needed. These potential alternatives are described in the next section.

1.1.1. The polyol process

Polyol synthesis of Ag NWs is the most promising synthetic approach in terms of yield, implementation, cost and shape control. In a typical silver nanowires synthesis, the polyol solvent ($HOCH_2[CH(OH)]nCH_2OH$) ,which also acts as the reducing agent of silver, allows the reduction of an inorganic salt precursor (for example $AgNO_3$) at high temperature.(Figure 2) Polyvinylpyrrolidone (PVP) is added as a shape controller, promoting the anisotropic growth of the wires. The silver nanowires obtained through this self-seeding

protocol generally have diameters on the order of a few tens of nm and lengths of several μm. Moreover, the yield is about 60-70% and the co-products (i.e. nanocubes, spheres etc) have to be removed by purification. A few grams of Ag NWs can be obtained in a single experiment, allowing large area film deposition since only a few tens of mg are deposited per m^2 to obtain a ~90% transparency.
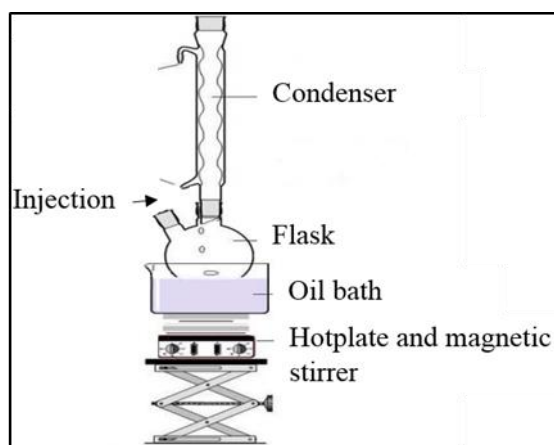
Figure 2: Schematic representation of the AgNWs synthesis set-up.

Even if the mechanism is still not fully understood, the synthesis of silver nanowires is believed to occur in two main steps: (i) the formation of tiny Ag seeds of 3-4 nm followed by (ii) the anisotropic growth of the seeds. The tiny seeds are produced from the aldehyde resulting from the dehydratation of the solvent. Along these lines, the most frequently used polyol is ethylene glycol (EG): OHCH$_2$-CH$_2$OH. The glycoaldehyde (GA) derived from the dehydration of the EG reduces the silver precursor into atoms at an elevated temperature (100-200 °C).[12]

In the initial stage of the reduction process, Ag atoms form small clusters of fluctuating structures. As the clusters grow larger, they become more stable and emerge into tiny seeds of 2-3 nm diameter. These seeds adopt one of three predominant structures: single crystalline, single twinned or multiply twinned structures (Figure 3.a). According to Xia et al., the nanowires are derived from the multiply twinned seeds (Figure 3.b). Most reported procedures use (PVP (polyvinylpyrrolidone) as a stabilizer, while other capping agents such

7

as cetyltrimethylammonium bromide (CTAB), sodium dodecyl sulfonate (SDS), vitamin B2 or polyethylene oxide have also been used to control the anisotropic growth of the seeds. Even though the interaction between PVP and the silver surface is not fully understood, this capping agent has proven to drive the elongated shape obtained at the end of the synthesis. In this manner, its binding affinity varies from one crystal face to another, hindering the grow of selective faces: PVP preferentially binds on lateral {100} silver-crystal facets rather than on the {111} facets facilitating the formation of silver nanowires.[13] There may be a region of optimal concentration out of which for too low of a PVP concentration, the sorption of PVP onto silver insignificantly affects the growth process whereas for too high concentrations (at which non-selective sorption prevails) the metal reduction is inhibited on all facets.
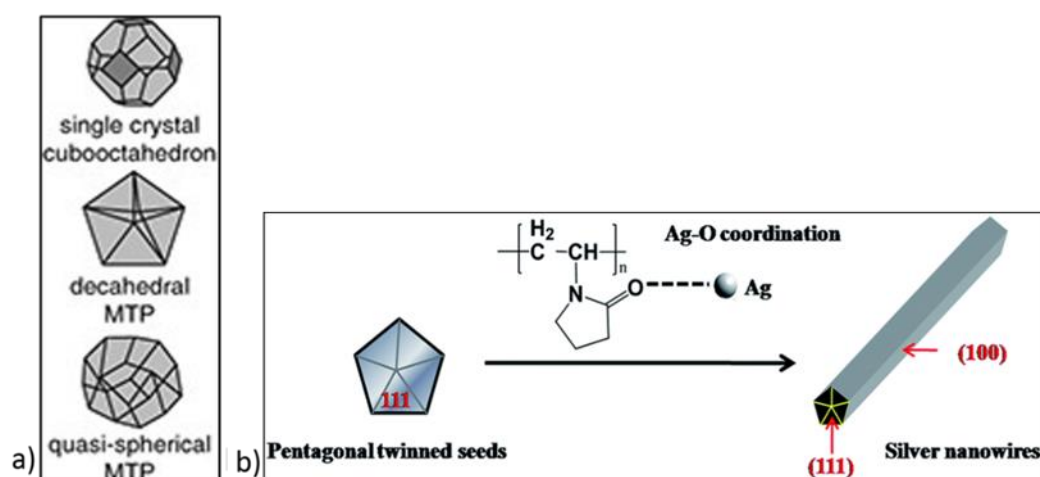
Figure 3: a) Ag_n seeds of different crystallinity, b) the evolution of the seeds into a rod. [182]

The morphology and size of nanowires substantially depend on the experimental conditions (temperature, silver salt concentration, PVP:silver salt ratio). By varying the reaction conditions such as the temperature, the stirring rate, the addition of heterogeneous seeds, the nature of the capping agent, the concentration of reagents, and the presence of trace amounts of ions, a certain degree of control over both the size and morphology distribution can be achieved.[13–16] In the next section, I summarize the impact of some of these key parameters on the dimensions of the silver nanostructures.

New types of materials that are future candidates for transparent electrodes include conductive polymers, graphene, carbon nanotubes (CNTs) and metallic nanowires based percolating networks (eg. copper nanowires (CuNWs), silver nanowires (AgNWs)) (Figures 4 and 5). [17][18] All these materials can be bent, stretched, compressed, twisted, and deformed into non planar shapes but maintain good conductive performance, reliability and integration. Figure 4 plots the transmittance versus the sheet resistance data of several transparent conducting materials including associated graphene, CNTs, AgNWs and ITO. It also shows the iso-values of the FoM (Figure of merit) that allows comparison of the overall performance of the transparent conductive materials. The classic FoM definition of Haacke is described by the following formula:

$$FoM = \frac{Tr^{10}}{Rs} \text{ (1-1)}$$

Tr is the optical transmittance measured at a wavelength of 550 nm and Rs is the sheet resistance. The larger the FoM value, the better the associated electro-optical properties (pink square in Figure 4).
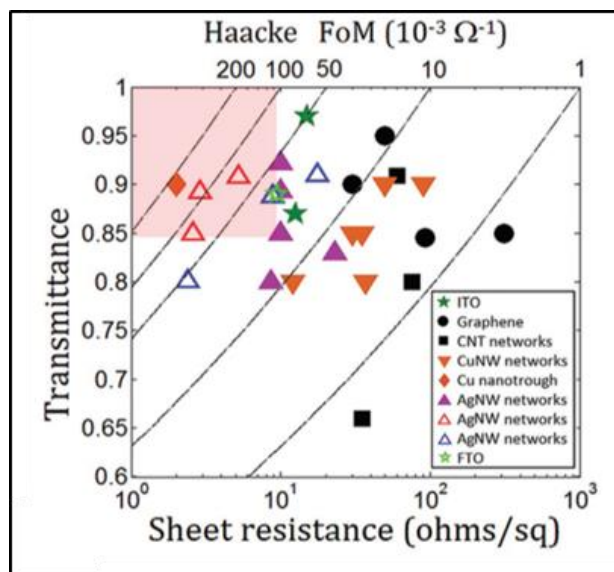
Figure 4: Transmittance (550 nm) plotted as a function of sheet resistance for various transparent conductive materials: Indium tin oxide (ITO), graphene, single-walled carbon nanotubes, copper nanowires, silver nanowires, and FTO. The solid lines are associated with iso-values of the Haacke FoM (Figure of Merit).[18]
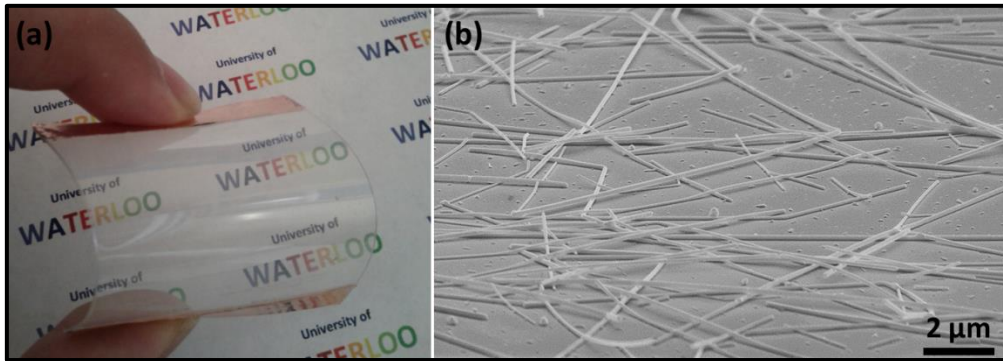
Figure 5: a) Example of an alternative transparent conductive material made of metal nanowire networks and b) SEM image of the Ag NW network.

The haze factor of the transparent conductive material is another parameter that needs to be considered for applications. This optical factor quantifies the percentage of transmitted light that is scattered, and is given by:

$$Haze\ Factor = \frac{Diffuse\ transmittance}{transmittance\ totale} x\ 100 \quad (1\text{-}2)$$

Diffuse transmittance is the scattered transmitted light while total transmittance is the sum of both the scattered and directly transmitted light. Depending on the application, haze is needed in higher or lower percentage.[19] For instance, touch panels place on windscreens need a low haze factor (< 3%) to ensure comfort for the human eye. On the other hand, solar cells need a high haze factor.

Other factors such as material preparation and processing, properties and limitations of the alternative materials are summarized in Table 1.1. Each material is discussed in more detail in the following subsections.

Table 1.1: General guide to the properties and fabrication methods of different transparent conductive materials.

Property	TCO$_s$	AgNWs	CNT	Graphene	Nanogrids
Rs (Ω/Sq)	5 – 100	1 – 50	25 – 300	30 – 5000	0,8
Transmittance (%) (at 550 nm)	80 – 97	80 – 96	80 – 91	80 – 96	90
Flexibility	+	+++	+++	+++	+++
Scability	+++	+++	+++	+++	+++
Chemical Vapor Deposition	+++	-	+	+++	+++
Sputtering	+++	-	-	-	+
Spray deposition	++	+++	+++	+	+++
Dip-Coating	++	+++	+++	+	-
Cost	++	+	+++	+++	++
Uniformity	+++	++	++	+++	+++

Conductive polymers

One alternative for transparent electrodes is based on films of conductive polymers. Poly(3,4-ethylenedioxythiophene) (PEDOT), encapsulated by poly(4-styrenesulfonate) (PSS), is most used thanks to its excellent mechanical flexibility, solution processability and high transparency.[20] In spite of its interesting characteristics, the sheet resistance of transparent electrodes based on PEDOT:PSS is much larger than that of ITO. Recently, thin films of highly ordered and densely packed PEDOT:PSS nanofibrils after acidic treatment have been reported. Such materials lead to a sheet resistance of 46 Ω/Sq at a transparency of 90%.[21]

Graphene

Graphene presents important advantages in terms of high electron mobility (200.000 cm^2/V·s [22] versus 10 and 70 cm^2/V.s for ITO) and high intrinsic in-plane conductivity.[23] Monolayers of graphene can be synthesized by chemical vapor deposition (CVD). [24],[25],[2],[26] Graphene can be doped with an acid to achieve a decent sheet resistance of 30 Ω/Sq at a transparency of 90%.[26] However, at this time, the cost of depositing graphene by CVD is too expensive to have values comparable (but not better) than the performance of ITO electrodes. On the other hand, the synthesis of graphene flakes is much cheaper, but the overlapping of flakes is very high, leading to high electrode resistance (95% of transparency

for a sheet resistance in the range of 200-1000 Ω/Sq).[27] Along these lines, graphene flakes-based transparent electrodes are still inferior to ITO, mostly due to their high sheet resistance and limited transmittance.[28,29],[30],[31]

<u>Carbon Nanotubes</u>

A random mesh of carbon nanotubes (CNTs) can be deposited as a film onto a substrate (Figure 7) in order to obtain a transparent conductive electrode. In this manner, current can flow from one tube in the network to the next, and like graphene, CNTs absorb only a small portion of the incoming light, making the film transparent. Moreover, the chirality of the nanotubes dictates whether the material has a semiconducting or metallic nature. In the metallic configuration, the electron mobility is comparable to the one of the graphene.[32] CNT-based electrodes have high thermal conductivity, high flexibility and good mechanical stability. The main problem of CNT electrodes is their low conductivity.[32] Although the conductivity of a single CNT is high, there is a high resistance at the junction of two overlapping CNTs[34] leading to a high resistance of the overall network. Another problem is that the synthesis of CNTs leads to both metallic and semiconducting species in the same batch. Even though the semiconducting tubes do not contribute much to conduction because of their higher resistance, they do decrease the transparency of the electrode.

<u>Metallic nanostructures</u>

The main metallic nanostructures considered for transparent electrodes are metal ultra-thin films (2D), metal nanogrids and metal nanowire networks (1D). Metal can be transparent when the thickness is below 10 nm.[35] However, due to surface electron scattering, the sheet resistance increases dramatically when the thickness decreases.[36] Thus, in turn, the transparencies required for applications at a given sheet resistance cannot be obtained. The sheet resistance of metal nanogrids could be close to bulk metals even when the line width is close to subwavelength and the period of the mesh is in submicrometer scale.[37] However, the

elaboration of silver meshes on flexible substrates is a complicated process involving several steps.[38] In the last decade, various metallic nanowire networks such as copper, gold and silver have been investigated as promising candidates for replacing ITO. The metallic NW transparent conductive film is typically obtained by a random arrangement (Figure 6). Contrary to carbon nanotubes, all conducting components conduct metallically. Furthermore, the junction of overlapping nanowires can be fused through sintering or mechanical pressure[39], which results in junction resistances significantly lower than carbon nanotube junctions.[40] Together, this results in lower electrode sheet resistances than carbon nanotube networks and comparable to ITO.
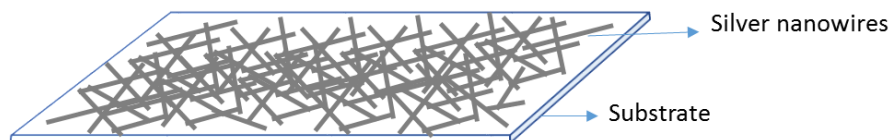
Figure 6: Schematic representation of a metallic NW network deposited randomly.

Numerous pathways have been developed to obtain metallic nanowires such as the polyol process, template-mediated synthesis using DNA or a porous material, the hydrothermal method, UV irradiation techniques and the microwave-assisted method.[41],[42] The nanowire networks can be deposited as a solution at room temperature using a number of different processes without the requirement of vacuum (Figure 7).[40,41,42,43] Many of these techniques such as spray coating and rod-coating are scalable, roll-to-roll compatible and processable at ambient temperature and atmospheric pressure.
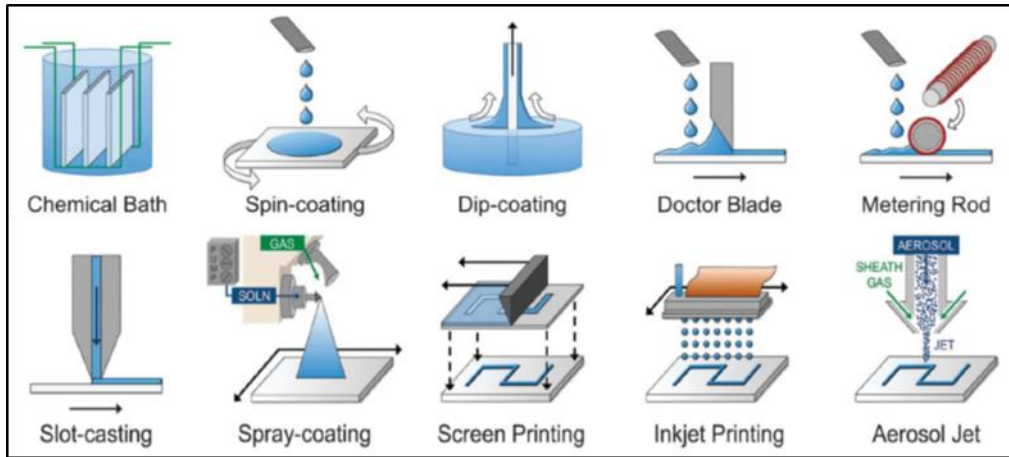
Figure 7: Schematic representation of common deposition processes.[33]

<u>Copper nanowires</u>

Due to its low material cost and the only marginally lower conductivity of copper compared to silver, Cu is also an excellent candidate for the mass production of opto-electronic devices. Cu nanowire electrodes have been mainly fabricated using two different approaches. The first one is based on an electrospinning process in which nanofibers of poly(vinyl alcohol) containing copper acetate are spun onto glass substrates. Subsequent calcination followed by hydrogen reduction leads to the formation of Cu fiber networks with high conductivity and optical transmittance (~50 Ω/sq at ~90% transmittance).[43] However, this method requires high processing temperatures (500 °C) and thus has limited applicability. The other approach is similar to the ones described for silver in the following section: solution processed Cu nanowires mesh electrodes.[24] With this second approach, an average transmittance of the network of Cu NWs of 85% with a sheet resistance of about 25 Ω/sq has been achieved.[44] Although different methods can synthesize CuNWs of various sizes and morphologies, there is still a lack of effective methods for the large-scale production of high-quality CuNWs with precise morphological control. More importantly, the low yield and complex process largely hinder the application of Cu NWs. A particular issue associated with Cu NWs is their susceptibility to corrosion, being far more severe than for Ag NWs.

14

Furthermore, the orange coloration of the electrode, due to their plasmonic band in centered between 560 and 590 nm, can be a major problem for several applications.[45]

Silver nanowires

Silver is the most conductive metal and thus an excellent choice to obtain a highly conductive NW film. Among the different methods to fabricate AgNWs, the polyol process is the most promising in terms of yield, implementation, cost and shape control.[42] Ag nanowires obtained with this approach have a mean diameter of tens of nanometers, a length of several tens of micrometers and an aspect ratio in the range of 50-500. Silver solutions are easily processed into transparent conductive films from a range of dispersions in water or alcohol. By controlling the concentration and the aspect ratio of the AgNWs, the sheet resistance and the transparency of the electrodes can reach low values. For instance, with a Ag nanowire diameter down to 20 nm, the sheet resistance reaches the level of ~10 Ω/sq at a transmittance of ~ 90%. Ag NW-based electrodes can be realized at a relatively low cost since the material costs of Ag nanowire electrodes are less than half that of ITO. To make a 50 Ω/sq electrode, the cost of the silver nanowires themselves is about 0.70 \$/m^2, while the price of the ITO will be 1.60 \$/m^2.[46] Furthermore, Ag NW networks are mechanically flexible while being transparent in the infrared (IR) range. Such properties make them more suitable for applications such as multi-junction solar cells and smart windows for the fenestration industry, capable of modulating heat dynamics (Figure 8). [47] Moreover, AgNW networks have been implemented for applications including transparent sensors,[48] transparent heaters[49] and medical devices.[50]
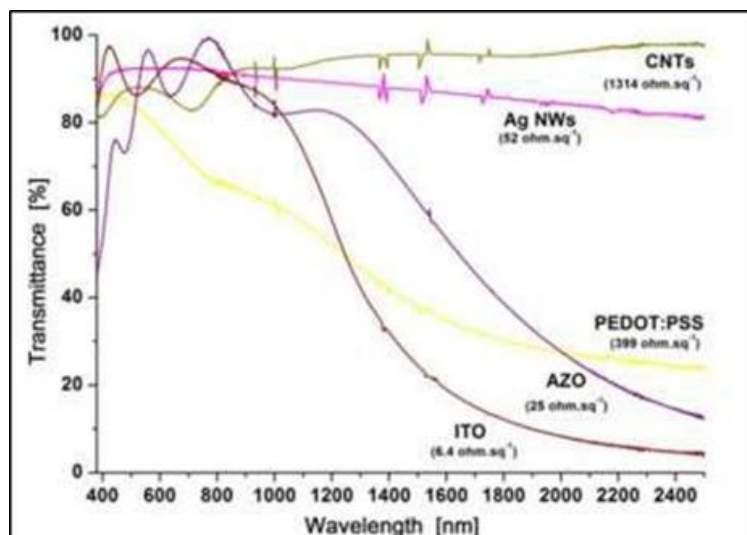
Figure 8: Transmittance versus wavelength of different electrode materials, showing their transparency in both the visible and the near infrared regions of the electromagnetic spectrum.[47]

However, silver is known to corrode in air and due their high surface-to-volume ratio, pure AgWs degrade even more rapidly than bulk silver, causing sheet resistance to increase over time.[51] Furthermore, the concomitant influence of humidity and illumination on the degradation has been unraveled by Jiu and al.[52]

1.1.3. General considerations on the performance of Ag NW electrodes

Several review articles on the different parameters that influence the electric properties of silver nanowire electrodes have been published in recent years.[47,53],[1,18,39,53–58],[59,60] Some of the fundamental trends are summarized below:

- Percolation theory allows one to better understand how AgNW networks achieve electrical conductivity. In this model, variables include the diameter, the length and the
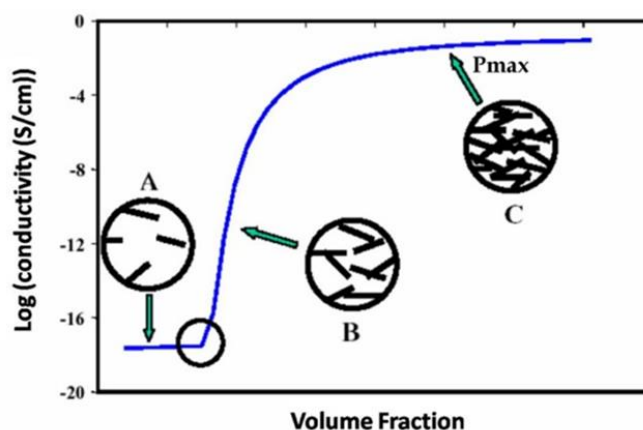
Figure 9: Log (conductivity) in function of the volume fraction of silver nanowires.

density of the Ag NW network. (Figure 9)

- By increasing the density of the network (number of silver nanowires per unit area), the number of percolation pathways increases and thus induces a higher conductivity of the electrical sheet.[54] According to theoretical and experimental investigations, the sheet resistance is indeed linked to the network density:

$$R_s \propto (n - n_c)^{-\gamma} \text{ (1-3)}$$

Where n_c is the critical network density, n the density network, and γ the percolation component.

- By increasing the length of the NWs, the percolation within a mesh at nominally identical density is statically improved, which leads to an overall lower sheet resistance.[57]

- Increasing the aspect ratio of the NWs leads to an increased transmittance at effectively the same areal mass density and at the same time the contribution of scattered transmittance to the total transmittance increases.[61] Good trade-off between length and diameter is important to favor a local conductivity, making it more uniformly distributed.

- Transparent electrodes made of curved silver nanowires could allow a better electromechanical stability of the electrodes under stretching in comparison to straight silver nanowires.[60]

- Nanowires with a thinner diameter lead to a more uniform conductivity across the surface, allowing for more electrons to be collected in solar cells and thus, a more uniform switching in displays. Thinner nanowires will also result in less scattering and thus less haze, an important factor for many applications.

- The junction resistance of two overlapping silver nanowires is higher than the resistance of the silver nanowire itself. For instance, Selzer recently determined that while the resistance of a single silver nanowire (d = 90 nm and L = 25 μm) is 0.2 Ω, the junction resistance of two overlapping silver nanowires is 529 Ω.[39] Treatments to lower this junction

resistance, such as removing the organics remaining on the NW surface, increasing the contact area between nanowires, and fusing the junctions, are very helpful. Similarly, obtaining networks with fewer junctions in the first place, as may be achieved through long NWs or branched NWs (to be discussed below), could result in lower film sheet resistance.

1.1.4. Limitations of AgNW networks and key problems to address

AgNW electrodes are promising because they have strong potential to replace ITO and they are available in various commercial devices.[62],[63],[64],[65,66] Lenovo, LG, and HP have all produced a PC/Tablet touch sensors based on silver nanowire networks. [62] C3Nano has developed a 55-inch silver nanowire-based touchscreen display. [63] However, Ag NW electrodes have not been used so far in applications such as solar cells and OLEDs.

The purpose of this project is to study and solve outstanding issues hindering the widespread use of silver nanowire based electrodes. Despite all the advantages of silver nanowire electrodes, they are not yet attractive enough to replace ITO. They are still challenges to overcome before Ag NWs could be fully integrated in commercial devices for applications such as solar cells where a sheet resistance approaching 10 $\Omega.Sq^{-1}$ is needed at a transparency higher than 90%.

Silver nanowires have also been found to be electrically and thermally unstable. When submitted to high temperature and/or current conditions, AgNW networks could have early features rates. For instance, Khaligh showed that silver nanowires broke up after two days when a constant current equivalent to that encountered in typical organic solar cells was passed through them. [67] Similar investigations were performed by Mayousse et al. and showed that the sheet resistance of Ag NW-based electrodes was insignificantly degraded after two years of storage in the dark and under air. [67–69] Exposure to natural light has also been found to be critical. [68,69] To make nanowire electrodes a viable alternative, it is important to tackle their lifetime and their thermal, electrical and chemical stability issues. As

mentioned previously, several studies show that silver nanowires corrode in ambient atmosphere. This is due to the presence of hydrogen sulfide gas in air. Such corrosion process leads to the formation of a non-uniform layer of Ag_2S onto the metal surface within 3 weeks. The combination of high relative humidity and illumination seems to be critical as well.[51] The degradation process yields to a sheet resistance increase by a factor of about 300% within 25 days. [70]

The purpose of this project is to study and solve outstanding issues hindering the widespread use of silver nanowire-based electrodes to become a viable alternative to ITO. To do so, this project will (i) improve their conductivity and transparency and (ii) tackle their lifetime, thermal and chemical stability issues.

To improve nanowire electrode conductivity and transparency, nanowires with sizes, shapes, and architectures that are different from what is commercially available will be elaborated. For example, longer nanowires will lead to less nanowire-nanowire junctions in a connected network and thus lower resistance.

To limit the corrosion of the silver nanowires, a passivation layer that will limit the exposure of Ag to the air/sulfur is needed. Robust silver nanowires will be then elaborated by a post-synthetic coating with a protecting material. Thermal instability of hybrid electrodes will also be analyzed thanks to infrared camera equipements.

In order to obtain a better understanding on how to tackle these challenges and give context and proper background for my work, I provide a brief overview of the latest metallic nanowires syntheses reported in the literature and highlight the developing prospects of silver nanowire passivation.

1.2. The synthesis of silver nanowires

As already mentioned, the most straightforward approach to produce inexpensive silver nanowires in solution is the polyol method. Such methodology was originally

introduced by Fievet et al. as an excellent manner to obtain submicrometer-sized metallic nanoparticles, and is now a widespread approach to the synthesis of metallic nanostructures.[71]

1.2.1. Key parameters for the control of NW dimension and yield

Influence of the nature of the seeds

Not only silver particles can serve as the seeds of nanowires. A two-step synthesis of nanowires in which platinum nanoparticles were used as the growth sites of silver crystals has been described (Figure 10.a).[15] In a first step, platinum chloride was reduced in ethylene glycol at 160°C after which PVP and silver nitrate were introduced in the medium. According to the data, the silver salt reduces at the surface of the Pt seeds and the core-shell seeds generated evolve into nanorods and silver nanowires with a yield of about 70%. This method of synthesis made possible a simple procedure for the formation of nanowires with the targeted morphology since it was believed that a nanowire evolves from one seed. For instance, it was shown that a decrease in the concentration of the primary platinum nuclei led to a decrease in the nanowire diameter. Note that most reports believed that the free chloride counter ion present in the reactional medium is the key element for the formation of the 1D nanostructure, prevailing over the role played by the presence of Pt seeds.[16],[72] Similarly, gold particles could also serve as seeds to produce silver nanowires. Since gold and silver have the same crystalline structures, and their lattice constants are similar, a seeded-growth process is clearly favored.[73] This report provides the first experimental evidence that the growth mechanism of silver from platinum or gold seeds previously proposed is valid. As can be seen in Figure 10.b, Au seeds could be evidenced in the middle of the nanowire.
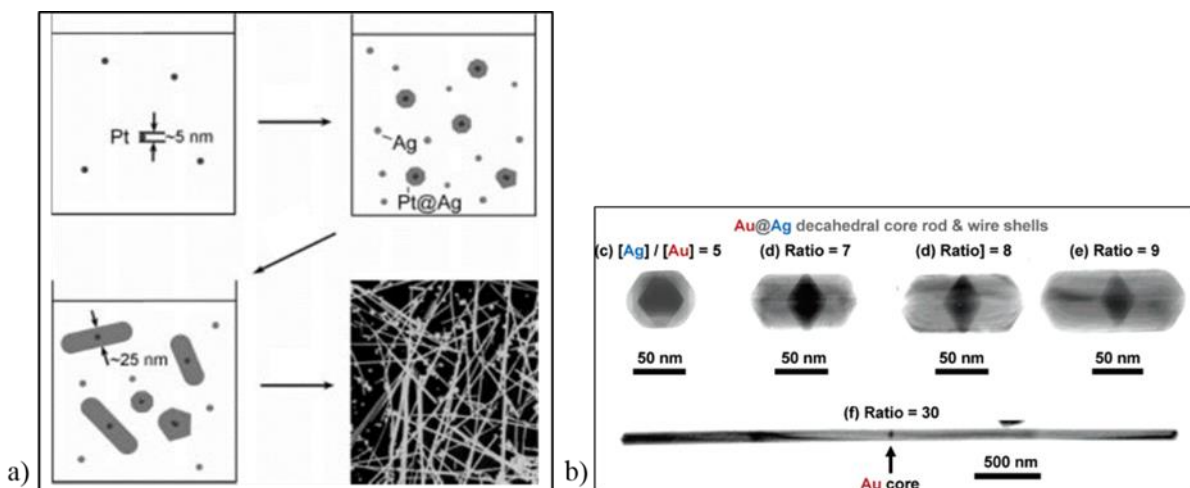
Figure 10: a) Schematic illustration of the formation of Ag nanowires using Pt,[15] b) TEM images of silver rod and wire from gold seed.[73]

Silver halide seeds, in particular AgCl, give good results for the formation of silver nanowires. In this manner, the addition of NaCl leads to the formation of AgCl nano-crystallites, reducing the concentration of free silver ions in solution during the initial seed formation. These slow reaction conditions enable the formation of the thermodynamically more stable multiply twinned seeds required for nanowire growth. The synthesis of silver nanowires via this approach allows one to obtain wires that are homogeneous in length and diameter.[74] Moreover, by tailoring the ratio of [AgNO$_3$]/[NaCl], the diameter can be controlled. For instance, NaBr favors the formation of thin nanowires (d=20 nm).[75],[76],[77] The anisotropic growth mechanism from silver halide seeds may be somewhat different from the one from Pt or Au seeds as shown in the following scheme in Figure 11 since one AgCl seed gives birth to numerous Ag NWs.
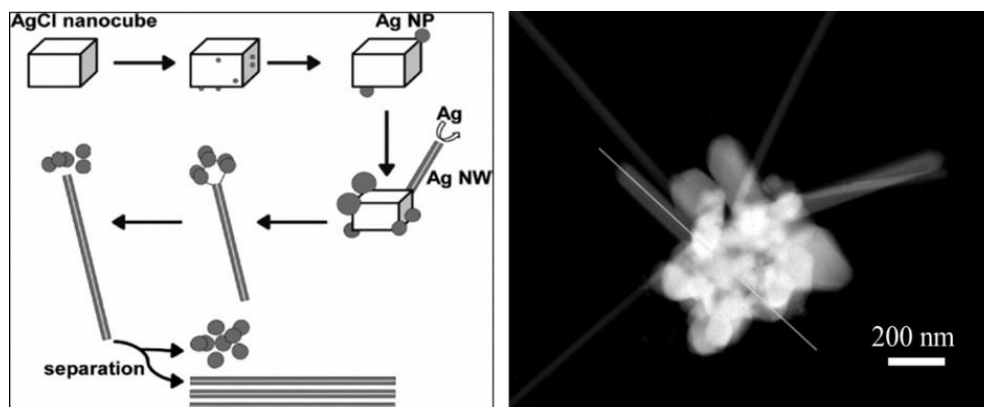
Figure 11: Schematic illustration of the formation of Ag nanowires using silver chloride seeds (left). SEM image of a AgCl nanocube initiating the growth of silver nanowires (right).[74],[183]

Influence of temperature

In the polyol process, the temperature at which the reaction is conducted is an important parameter for the synthesis of wire-like structures. Below a critical value of 110°C, no wires can be produced since no multiply twinned crystals are generated.[15,78] The reason for this is that a high temperature is crucial for the conversion of ethylene glycol into glycoaldehyde, reaction that initiates the nucleation step. This conversion occurs in general above 150 °C with the help of oxygen.[65],[79] The importance of temperature is also attributed to the deficiency of thermal energy in the formation of specific facets.[15],[80]

Presence of trace ions

It is difficult to freely obtain high-yield Ag NWs with the above-described seed-assisted process. In order to simplify the procedure and improve the quality of Ag NWs, different research groups have found that a very small amount of metal ions such as Fe^{2+}/Fe^{3+} and Cu^+/Cu^{2+} could drastically affect the yield and dimensions of Ag NWs. This is achieved by removing oxygen from the surface of the silver seeds (Figure 12) and preventing the dissolution of multiply twinned seeds. Different researchers have suggested that the low valence metal ions could react with the adsorbed atomic oxygen on the surface of silver and change into high-valence metal ions. This process prevents the multiply twinned seeds from being etched and the repeated process ensures the formation of Ag NWs. However, this oxygen-consuming mechanism was not completely responsible for the results attained since

anions such as Cl⁻ were also found to be crucial in the process. The oxidative etching happens when both couples Cl^-/Cl_2 and O_2/O_2^- are present in the reaction medium.[81],[82],[83]
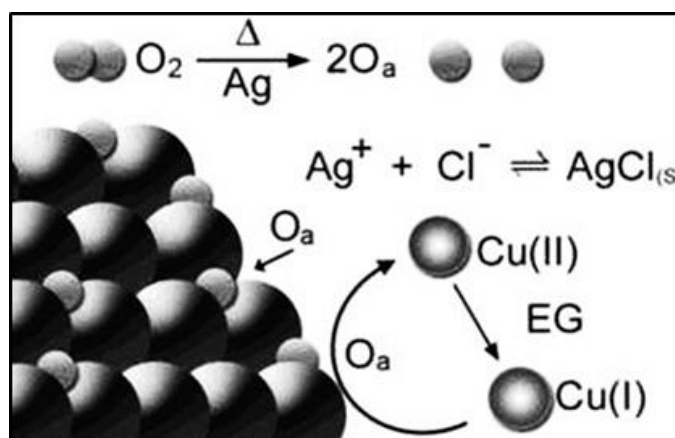
Figure 12: Role played by Cu(I) in the formation of AgNWs.[82]

Effect of the nature of the polyol

The nature of the polyol used also has an impact on the yield and the uniformity of AgNWs. The ICMCB group at the University of Bordeaux recently demonstrated that the synthesis of AgNWs performed in 1,2-propanediol instead of ethylene glycol increases the rate of AgNWs formation, the yield, as well as the size distribution of these 1D nanostructures.[84]

1.2.2. Ultra-long AgNWs

With the development of transparent and conductive films, the need for long and thin Ag NWs, i.e. with an aspect ratio higher than 500, has motivated scientists to further optimize the polyol process. Recently, different research groups have fabricated very long AgNWs with lengths larger than 100 μm and aspect ratios in the range of 1000-3000 by one-step or multistep methods.

The single step process

A low-temperature reaction, slow stirring speed, trace of halides, presence of transition metal ions, and PVP of high molecular weight have been reported to make ultra-long nanowires.[85–88] Jiu et al. have prepared very long Ag NWs at 130°C by stopping stirring and

keeping the solution in the stationary state. Nanowires with lengths between 20 and 100 μm (230 μm in for 12 hours of reaction) and average diameters of 91 nm have been reported.[65] Figure 13 illustrates the mechanism of growth of the silver nanowires in high and low stirring speed regimes.[65]
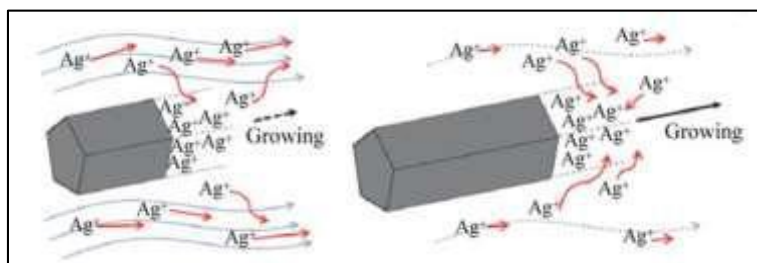
Figure 13: Scheme of the growth mechanism of a AgNW in high (left)
and low (right) stirring speeds.[65]

Ultra-long Ag NWs could also be obtained via the polyol process in hydrothermal conditions. Under these experimental conditions, Ag NWs with an average diameter of 45-65 nm and a length greater than 200 μm could be produced in about 22 h of reaction.[89,90]

The multistep repeating process

This approach is based on: (i) the synthesis of silver nanowires by a conventional polyol process and (ii) their sequential growth. Via this strategy, the lengths of nanowires were extended from 20-30 μm to over 500 μm.[91] The main disadvantage of this process is that it is time-consuming (12 h) and the diameter of the nanowires progressively increases after each additional step.

Table 1.2 summarizes the main characteristics of the high aspect ratio silver nanowires so far reported in the literature as well as the performances of the corresponding electrodes.

Table 1.2: Length and diameter of silver nanowires depending on the process used together with the sheet resistance and transparency of the resulting electrodes.

Year	Reference	Process	Time	T°C	Length	Diameter	Aspect ratio	Substrate	Rs	T%
2014	[69]	Polyol	12 h	130°C	65 μm	60 nm	1080	Glass	9 Ω/Sq	85 %
2014	[44]	Polyol	12 h	110°C	20-100 μm	91 nm	220-1100	Glass	24-109 Ω/Sq	94-97 %
2015	[67]	Polyol	30 min	170°C	110 μm	200 nm	550	PET	20 Ω/Sq	95 %
2016	[72]	Polyol-Hydrothermal	22 h	65°C	200 μm	65 nm	3080	Glass	7 Ω/Sq	90 %
2016	[71]	polyol	30 min	160°C	102 μm	140 nm	730	PET	14 Ω/Sq	87 %
2017	[73]	Polyol-Hydrothermal	8h	130°C	220 μm	55 nm	4000	PET	155 Ω/Sq	98 %
2017	[70]	Polyol	40 min	170°C	120 μm	30 nm	4000	PET	87 Ω/Sq	88 %

These data confirm that the use of high aspect ratio nanowires is of high interest since it allows one to obtain conductive films with maximum transparency. However, it has been reported that it is challenging to maintain the integrity of the very long NWs during the deposition process since they tend to break, in particular when ultrasounds are used. Fine-tuning synthesis to control the dimensions of the NWs with low standard deviation remains thus highly desirable because the properties of the networks, such as haziness or roughness, are application-dependent and rely on their constitutive building blocks.

1.2.3. Toward branched silver nanowires

Architectures different than 1D silver nanowires are also interesting nano-building blocks as they may decrease resistance through decreasing the number of highly resistive junctions where nanowires overlap. Importantly, such structures have not been explored for transparent electrodes by other groups. Along these lines, only three synthetic strategies have been reported in the literature to achieve such morphologies. Among them, the modification of the temperature during the synthesis of Ag NWs (160°C -> 100°C -> 135°C -> 100°C) induces branch formation.[92] In this manner, the diameter of the as-obtained nanowires is about 300 nm, the length of the main branch is about 6 μm; and the minor one 2 μm. Here, the growth of branches may be favored by the defects points induced by the change of

temperature. The authors also demonstrated that the molecular weight of the PVP played an important role in the branch formation during growth.

The addition of a transition metal ions with an oxidation state of +3,+4, +5, or +6 in the colloidal suspension during the growth process has been reported to drastically modify the shape of the nanowires and induce the formation of 'Y-type nanowires'.[81] The diameters of the branches are typically between 10 nm and 500 nm, and their aspect ratio is between 50 and 10000. For example, Ru^{3+} (from ruthenium chloride) was used for the production of Y type nanowires. In this case the ionic species may disturb the growth of silver nanowires by creating nucleation sites at their surface.

Finally, the input of microwave irradiation during synthesis generates nanowires with a 'V-shape' morphology. The irradiation of the colloidal suspension during the growth process induces the formation of branched silver nanowires with a yield of 40% (Figure 14).[93]
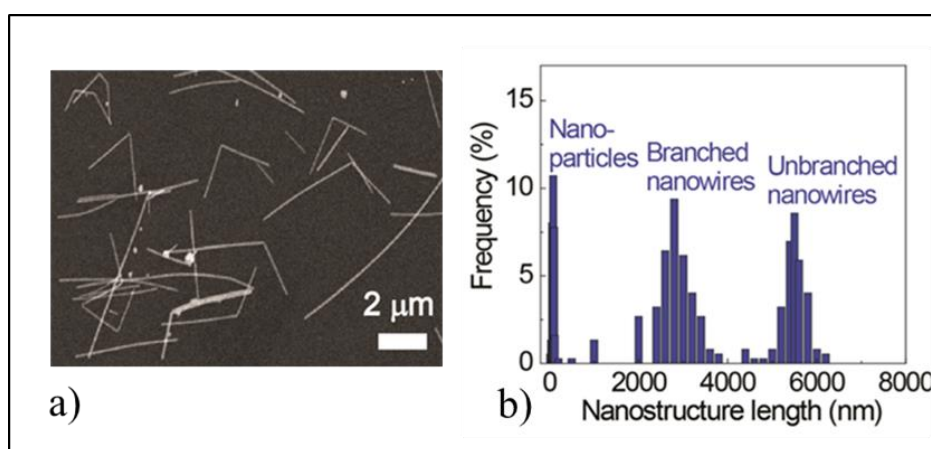
Figure 14: Nanostructures produced upon microwave irradiation of the colloidal suspension during the growth process (a) SEM image of 'V-type' nanowires, (b) distribution in morphology of the nanostructures.[93]

Though a plethora of metallic morphologies are accessible by the polyol approach today, the chemical synthesis of nanowires with a good control over the number and dimension of branches remains a challenge.

1.3. Robust silver nanowire networks

As already outlined, chemical stability issues remain a major limitation for the use of silver nanowire in commercial devices. Furthermore, metallic nanowires are thermally unstable materials. Along these lines, the requirements for a nanowire transparent electrode passivation are stringent. For devices such as solar cells and LEDs, current needs to flow between the nanowire electrode and the active part of the device. Therefore, the nanowire electrode cannot be fully encapsulated in a non-conductive layer. Rather, the passivation layer needs to be both transparent and allow current to flow across it, as well as be able to block gas diffusion and be inexpensive. Moreover, it should also be mechanically flexible and ideally be deposited from solution in a roll-to-roll compatible, low temperature process to maintain the advantages of silver nanowire electrodes.

Different strategies to improve the chemical and/or thermal stability of AgNWs have been implemented this last decade. For instance, by encapsulating the NWs by a polymer or by chemically modifying their surface with a layer of inorganic or organic material (metal oxide, graphene or polymer). However, none of these approaches slow down sufficientlyfast the degradation of the NWs while having all the properties described in the paragraph above.

1.3.1. Passivation with metal oxides

There are a number of reports on composite electrodes in which metal NWs are combined with metal-oxides (for instance TiO_2 and ZnO). Since metal oxides are both conductive and transparent, they have been tested as passivation materials.[94–97] This approach offers good chemical and thermal stabilities of the nanowires and thus a protection against their degradation. Additionally, these materials induce a decrease of the sheet resistance. For example, the resistance of Ag NWs passivated with TiO_2 decreases from 1000 to 20 Ω/Sq when the thickness of the shell is equal to 50 nm. The shrinking of the TiO_2 shell during its formation induces pressure in the network and thus better connections between the nanowires. However it lowers the transparency by 6 percentage points since metal oxides

affect the optical properties of the NW electrodes.[98,99],[96] In addition, the mechanical properties of the hybrid electrodes are not good in flexible substrates due the unfavorable interface between TiO$_2$ and PET.[98] Corrosion test applied to the TiO$_2$ coated and neated Ag NWs by dipping into aggressive sulfur solution in dimethylformamide show that after 30 minutes the resistance of the Ag NW/TiO$_2$ hybrid doubles, whereas unprotected NWs exhibit a 6 orders of magnitude increase of sheet resistance. Similar work was performed by coating Ag NWs with Zinc Oxide (ZnO). In this case the combination of the Ag NW and the metal oxide increases the robustness of the electrode during the annealing process. Unfortunately, the conductivity decreases when activated under light. [94,97]

1.3.2. Passivation with conductive polymer and graphene coatings

Coating the silver nanowires networks with one layer of graphene or conductive polymers can also improve the chemical stability as well as the conductivity of the final devices. For example, conductive PEDOT: PSS increases the Ag NW film stability. However, due to the acidic nature and intrinsic structural inhomogeneity, it has been associated with several degradation mechanisms and a limited device lifetime.[100],[101] Furthermore, it has been shown that upon prolonged contact with PEDOT:PSS the electrical properties of the Ag NWs deteriorate.[102] Another example demonstrated that transferring graphene monolayers and graphene flakes onto a transparent electrode of Ag NWs allowed to lower the contact resistance between wires and increase the lifetime of the electrode.[103],[104] However, the process of graphene deposition is costly and, in general, lowers the transparency of the electrodes.[105]

1.3.3. Passivation with short organic molecules

Rather than coat the Ag NWs with a passivation film, another approach consists in the customization of the surface of the Ag NWs themselves with short organic molecules prior to

NW deposition.[70],93 In one study, silver nanowires were coated with triphenylphosphine (PPh$_3$) in solution and then deposited as electrodes onto PET. Unlike the passivation approaches described above, neither the initial transparency nor the conductivity was decreased after coating with PPh$_3$. After 110 days at room temperature and under ambient conditions, the resistance of the PPh$_3$-passivated electrode only increased from 10 Ω/Sq to 60 Ω/Sq, while the bare AgNW electrode increased from 25 to 580 Ω/Sq. This result implies significant encapsulation of the NWs by the PPh$_3$ coating. Very recently, a similar study described the passivation of silver nanowires electrodes with ODT (octadecanethiol). Lifetime studies were performed over a period of 30 days in humid atmosphere at 85°C. In this case a 18% resistance increase for passivated electrodes was measured versus 169% for the unpassivated ones.[106]

In summary, for enhanced thermal and chemical stability, Ag NWs can be embedded into a conductive matrix of a metal oxide or an organic conductive medium. However, these approaches affect the intrinsic properties of the silver network, particularly they all decrease the electrode transparency. Care has to be taken to avoid the detrimental chemical attack of the silver due to corrosive precursors or their decomposition compounds. Alternative passivation strategies based on the surface modification of silver nanowire by short organic molecules is in its infancy. However, this approach seems to be a promising alternative since the molecules do not negatively affect the conductivity, mechanical flexibility or transparency of the electrode. Moreover this method is very inexpensive, thus contributing to its commercial viability.

1.4. Outlines

In this chapter, I have given a brief introduction to the context of this study and provided information on why silver nanowires are such promising materials to replace ITO. Nanowire electrodes are ideal for flexible electronics, and their simple room temperature

coating processes can be easily scaled up to a roll to roll industrial process. Further investigations of the growth mechanism should be devoted to understand and optimize the preparation process more precisely, thus contributing to further modifying and controlling the length, diameter and architectures in these nanowires. In the last part of this chapter, I have introduced the most important methods elaborated to coat silver nanowires in order to protect them against oxidation. Within all of these methods, the passivation with a short molecule such as trioctylphosphine seems to be the most interesting in terms of performance while no modification on the intrinsic properties of the material could be observed.

The most important results reported in this Thesis are divided in three parts: the first part of the project (Chapter 2) focuses on experiments I performed on the study of the mechanism of the synthesis of silver nanowires, the synthesis of ultra-long silver nanowires and the elaboration of the electrodes. Chapter 3 covers different methods developed on the possibility of making branched silver nanowires. To end the thesis, the passivation of the surface of the silver nanowires with graphene and MuA (11-Mercaptoundecanoic acid) has been performed in order to improve their chemical stabilities (Chapter 4). Additional investigations on the thermal stability performed in collaboration with Hadi Hosseinzadeh Khaligh are also introduced in the present manuscript.[107]

Chapter 2: Elaboration of Ultra-long Silver Nanowire electrodes

Silver nanowires can be synthesized inexpensively in solution by the polyol method. But it remains a great challenge to achieve control over the length and the width of Ag nanowires, leading to the formation of ultra high-aspect ratio Ag nanowires. Such materials would find an enormous niche of application in the development of transparent and conductive films. As outlined in the chapter 1, ultra-long nanowires, i.e nanostructures with an aspect ratio above 500, would improve nanowire electrode conductivity and transparency. They would lead to less nanowire-nanowire junctions in a connected network and thus to lower resistance.[57,61,88],[87] Some key parameters in the polyol process are known to yield nanostructures with long lengths: introduction of additives such as halide salts,[76] foreign ions such as Cu^{2+} or Fe^{3+},[87,88],[86] slow stirring speed or multistep repeating processes.[91] However, problems such as the uniformity of AgNW diameter remain elusive to the scientific community. Moreover, the output of long AgNWs is still relatively low for mass production and commercial applications. Here, we will introduce wet-chemical preparation methods for the synthesis of AgNWs with high aspect ratio and purity that we have developed. Moreover, the performance of thin films elaborated from these materials will be introduced. Along these lines, thin films were deposited on glass substrates using different methodologies that can scalable to industrial manufacturing levels. Finally, the properties reported herein will be compared with the state of the art.

2.1. Synthesis of long Ag nanowires in ethylene glycol in presence of halides and Cu^{2+}

We first explored the possibility to produce ultra-long nanowires in one step by optimizing a CuCl2-mediated synthesis developed by Shang Wang and coworkers.[108] In that work, CuCl2 was used as a chemical precursor for the elaboration of silver halide seeds, PVP with a molecular weight of 55K was the surfactant and silver nitrate was used as silver source.

This approach yields to the formation of relatively long silver nanowires, having an average length of 49.4 +/- 24.3 µm and a diameter of 75 +/- 13 nm, resulting in an aspect ratio (length/diameter ratio) of 686. By modifying some key parameters known in the literature to alter nanoparticle's size (temperature, molecular weight of the PVP, the CuCl2/AgNO3 ratio, the addition of Br-), we explored the possibility to produce longer NWs (Figure 15).
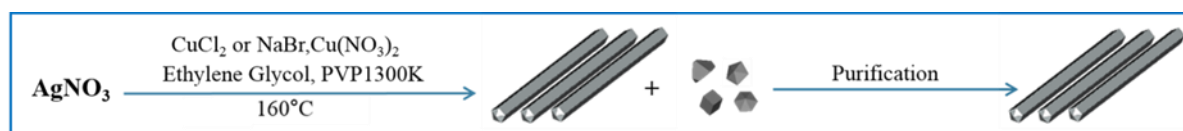
Figure 15: Scheme of the synthesis of ultra-long silver nanowires adopted.[108]

We summarize below some of the most interesting results.

2.1.1. Experimental section

Protocol 2.1: Ag NWs synthesized in presence of AgCl

In a 50 ml three-neck round-bottom flask, 20 ml of ethylene glycol (EG) were heated at 160 °C (temperature of the oil bath) for five minutes. 2 ml of a solution of $CuCl_2.H_2O$ in EG with a concentration of 4 mM were prepared and added to the previous one. After 10 min, 20 ml of the mixture of $AgNO_3$ (0.12 M) and PVP-1300K (0.36 M) were injected into the solution. The stirring rate was at 100 rpm during the entire growth process. After a given time (depending of the reaction conditions) the reaction medium turned from transparent yellowish to grey indicating the formation of the nanowires. Once this color change was observed, the mixture was refluxed for one additional hour. Then the flask was put in an ice bath for a few minutes in order to reach room temperature.

After the synthesis, the as-obtained product requires some purification. Indeed, a mixture of nanowires and nanoparticles was obtained. The colloidal suspension was purified according the following process: a slow addition of acetone (40 mL) into the reaction mixture (10 ml), in a 50 mL centrifugation tube, leaded to the aggregation of the wires and their deposition on the bottom of the flask. The supernatant containing nanoparticles was discarded

and the precipitated nanowires were redispersed in a solution of PVP-360K diluted in water (10 ml). This step was repeated 4 times.

Protocol 2.2: AgNWs synthesized in presence of AgBr

The experimental conditions were similar to the protocol 2.1 except that the initial reaction medium contained NaBr (0.28 mM) and Cu $(NO_3)_2$ (0.14 mM) instead of $CuCl_2$. The temperature was set at 150 °C.

2.1.2. Analysis of the morphology of the silver products

Dark field microscopy

200 µl of solution of silver nanowires was mixed with 1.5 ml of ethanol and a few drops of this mixture were deposited onto a glass substrate that was subsequently in an oven set at 70°C for 10 minutes. The substrate was then observed with a dark field microscope (LEICA DMI3000M) for visualization.

TEM analysis

Transmission electron microscopy (TEM) images were collected on a JEM-1400 Plus electron microscope JEOL operating at 120 kV. For this purpose, one drop of the solution used to perform the dark field analysis was deposited onto a carbon-coated copper grid.

Calculation of the mean diameter and length of the AgNWs

The analysis of the Dark-field and TEM images to obtain statistical information on the length and diameter of the nanowires was performed with the software Image J. The lengths of the nanowires have been measured on dark-field images (at least 150 nanowires were measured).

Calculation of the yield of silver nanowires

The calculation of the concentration in Ag^+ was performed by ICP analysis (Inductively Coupled Plasma Spectrometry). 10 ml of the solution were redispersed in 45 ml

of acetone. Once the silver nanowires precipitated, the supernatant was removed. The solid phase was then redispersed in a mixture of water/acetone (v/v 10/35) and centrifuged for 10 minutes at 4000 rpm. This step was reproduced three times and the silver nanowires were finally redispersed in 20 ml of ultra-pure water. A few milliliters of the previous solution were then redispersed in a mixture of HNO_3 and water for analysis.

UV-Vis absorption spectroscopy

Silver nanowires exhibit plasmon modes in the UV/visible range. Information regarding the size, shape and aggregation of nanoparticles could be extracted from UV-visible absorption spectra. The absorption spectra were recorded in the range of 350 -700 nm with an UV-3600 Shimadzu UV-Vis-NIR spectrophotometer. 200 µl of solution of silver nanowires were mixed with 1.5 ml of water in a ten-mm optical path length quartz cell. The data were recorded and treated with UVProbe software.

NMR (Nuclear Magnetic Resonance) Analysis

^1H (300 MHz) and ^{13}C-$\{^1H\}$ (75 MHz) NMR spectra were recorded on a Bruker DPX-300 spectrometer. ^1H and ^{13}C assignments were confirmed with the use of two dimensional ^1H-^1H COSY, ^1H-^{13}C-HSQC and ^1H-^{13}C-HMBC NMR experiments. All spectra were referenced internally to residual proto-solvent (^1H) or solvent (^{13}C) resonances, and are reported relative to trimethylsilane (d = 0 ppm). Chemical shifts are quoted in d(ppm), coupling constants in hertzs whilst "s" stands for singlet, "d" for doublet, "dd" for doublet of doublets, "t" for triplet and "m" for multiplet.

To identify the volatile species formed by polyol oxidation the "classical" polyol synthesis in presence of NaCl in 1,2-propanediol was performed. Instead of performing this process under reflux, the vapors were condensate into a cold trap to be analyzed by NMR.[109,110]

2.1.3. Results and discussion

A TEM image of the AgNWs synthesized according to protocol 2.1 is shown in Figure 16. As is typical with the polyol method, the synthesis yielded a mixture of nanowires and nanoparticles. After purification according the protocol 2.1, the nanowires could be isolated, having a length and diameter of 33 µm +/- 15 µm and 400 nm +/- 85 nm, respectively.
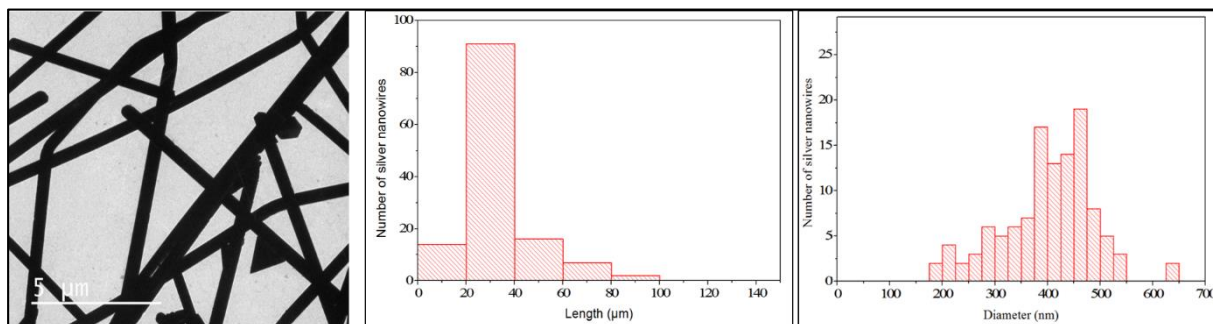
Figure 16: TEM image and size distribution of nanowires produced in the presence of $CuCl_2$ (160°C).

In the following experiments, we kept all the parameters constant (3:1 PVP:AgNO$_3$ molar ratio, 1:300 $CuCl_2$:AgNO$_3$, 160 °C growth temperature, ethylene glycol and 100 rpm stirring rate) except the parameter being investigated.

Effect of temperature

The temperature at which the reaction is conducted is known to be an important parameter for Ag nanowires synthesized via the polyol process in ethylene glycol. Experiments were performed at 140, 150, 155 and 160 °C. The change in nanowire length and diameter with respect to the growth temperature is plotted in Figure 17. When the temperature of the growth medium was reduced from 160 °C to 150 °C, the nanowires increased in length and decreased in diameter (Figure 17), both helping to improve the nanowire aspect ratio. At 150 °C, nanowires with an average length of 105 µm +/- 50 µm were synthesized but their average diameter was rather large: 245 nm +/- 80 nm. Further decrease in the reaction temperature (140 °C) increased the number of by-products.
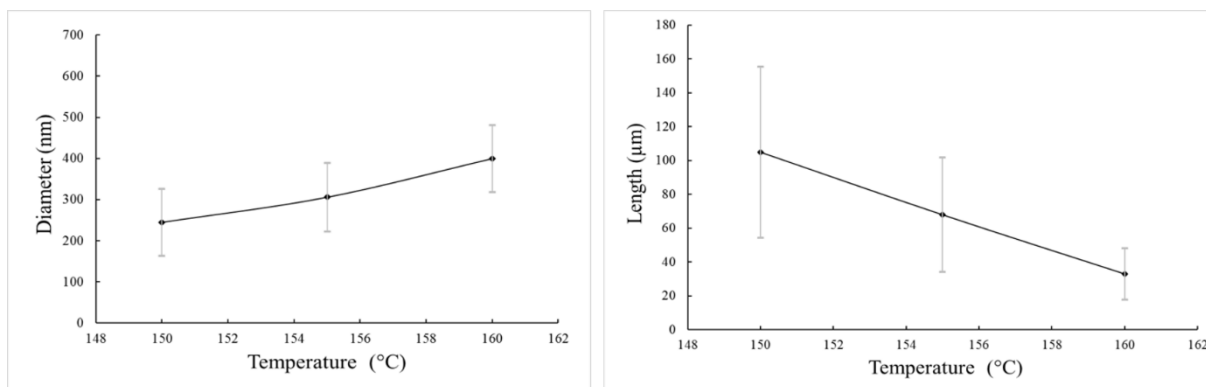
Figure 17: Evolution of the length (right) and the diameter (left) of the silver nanowires with the reaction temperature.

Effect of replacement of Cl⁻ by Br⁻

There are reports on the effects of bromide ions during the polyol process claiming that Br⁻ favors the formation of thinner silver nanowires.[75,77] Moreover, the AgBr precipitates that have been formed in the early stage of the reaction serve as seeds for multi-twinned particles (MTPs), decreasing the amount of free Ag^+ ions in solution. In this manner, the kinetics of the reduction process of AgNO₃ is slowed down and the difference in solubility between AgCl and AgBr favors the formation of more silver halide nuclei and thus the formation of thinner Ag NWs. By completely replacing Cl⁻ by Br⁻ in the polyol medium, we were not able to obtain silver nanowires. Thus, a controlled increase of the quantity of Br⁻ was necessary in order to promote the growth of silver nanowires. Figure 18 shows, nanowires with an aspect ratio of 870 that could be produced for a ratio [Br⁻] / [Ag] = 0.93. In this case the average length and diameter of the nanowires obtained are 120 μm +/- 55 μm and 138 nm +/- 56 nm, respectively (Figure 18). Some nanowires as long as 410 μm with the same diameter could also be observed under these experimental conditions. On the other hand, a further increase in the concentration of [Br⁻] allowed to reduce the diameter of the nanowires, effect accompanied by an important increase in the amount of by-products. On the other hand, by following protocol 2.2, where Cl⁻ is completely replaced with Br⁻ ([Br⁻] = 0.28 mM and

$[Cu^{2+}]$ = 0.14 mM), we observed the formation of a majority of silver nanospheres and a few wires.
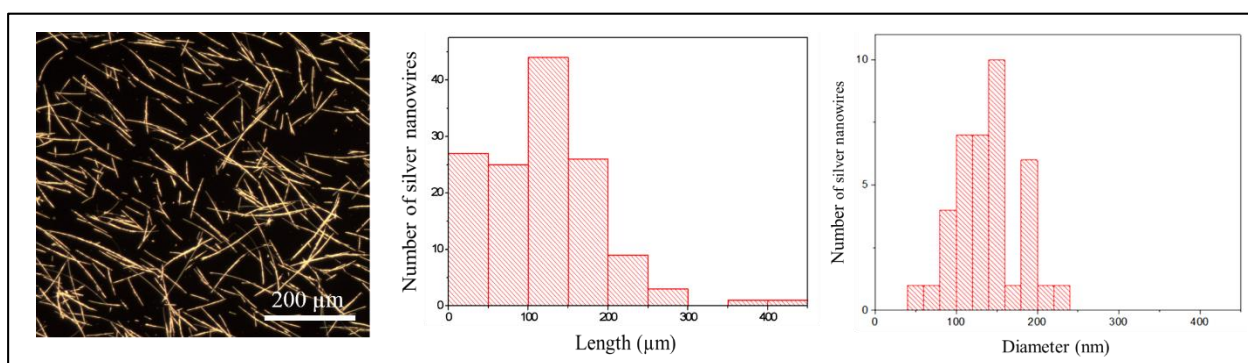
Figure 18: Dark field image of Ag nanowires produced in the presence of Cu^{2+} and Br^- at 150 °C together with their length and diameter size distributions.

2.1.4. Closing remarks

The synthesis of Ag nanowires performed in ethylene glycol medium in the presence of copper ions and halides (Cl^- and Br^-) yields the formation of relatively long and thin nanowires. By varying the reaction conditions such as temperature, reagent concentration, and presence of bromide ion, it was possible to achieve nanowires with an aspect ratio of 870. However, the above described synthesis yields to the formation of a large amount of by-products (spheres, cubes). Several stages of purification were thus necessary to obtain Ag NWs with a high-yield in morphology. Unfortunately, after the purification step the amount of silver NWs was so low that the quantity available was not enough for the fabrication of electrodes.

2.2. Synthesis of ultra-long Ag nanowires in 1,2 propanediol in the presence of halide

By exploring the possibilities of up-scaling the synthesis of Ag nanowires for industry (Solvay) during the post-doc of Marie Plissonneau in ICMCB (Université de Bordeaux), we discovered that we could successfully fabricate silver nanowires with uniform shape using $AgNO_3$ as the precursor, PVP as the capping agent, NaCl as the seeds and 1,2-propanediol as both the reducing agent and solvent (Figure 19).[84]
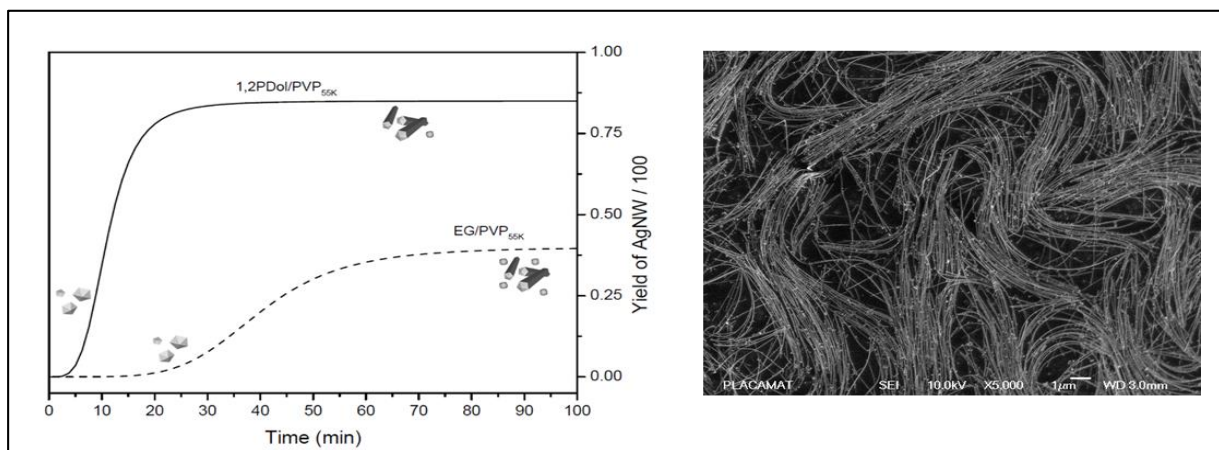
Figure 19: (Left) Comparison of the yield of silver nanowires in 1.2-propanediol vs ethylene glycol during the growth process. (Right) SEM image of Ag nanowires fabricated in 1,2 propanediol.

For the first time, it has been shown that using 1,2-propanediol instead of the typical ethylene glycol as the solvent allows for the fabrication of nanowires in higher yield (i.e. reduced number of non-nanowire products) and within a shorter period of time. Furthermore, it was observed that the amount of by-products was considerably reduced in these experimental conditions.[84]

The mechanism of formation of silver nanowires in ethylene glycol has been investigated by several research groups (Figure 20), but no attempt has been done to investigate the redox mechanism from alternative polyols such as 1,2-propanediol. We have tried to get further insight into this subject by performing a NMR analysis of 1.2-propanediol under relevant experimental conditions.
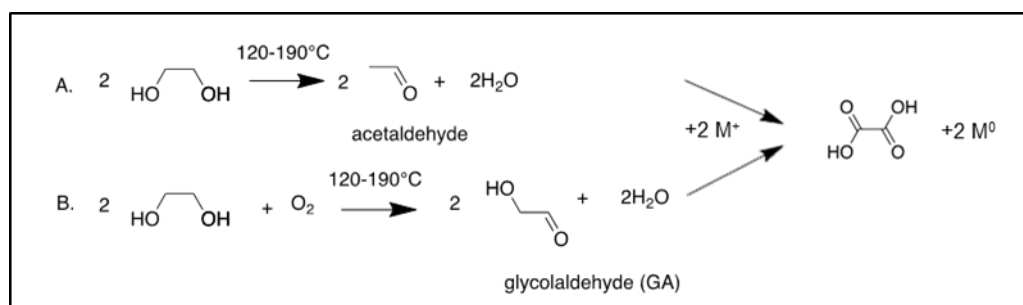
Figure 20: Reducing species upon dehydration of ethylene glycol. In the presence of oxygen, ethylene glycol can also form glycolaldehyde.

NMR investigations were conducted in order to determine the oxidation product of 1,2-propanediol. The volatile species were trapped in a cold trap before NMR analysis. Furthermore, 1D and 2D ^{1}H and ^{13}C NMR experiments reveal the formation of acetone, characterized by a singlet at 2.2 ppm (C$\underline{H_3}$) in ^{1}H NMR and resonances at 207.0 ppm ($\underline{C}$=O) and 30.9 ppm ($\underline{C}$H$_3$C=O) in ^{13}C NMR, and of 2,2,4-trimethyl-dioxolane, characterized in ^{1}H NMR by a doublet at 1.27 ppm (-CH(C$\underline{H_3}$)), two singlets at 1.36 and 1.41 ppm (-C(C$\underline{H_3}$)$_2$)), two doublet of doublets around 3.92 and 4.05 ppm (C$\underline{H_2}$) and a multiplet at 4.22 ppm (C$\underline{H}$). Moreover, the ^{13}C NMR spectrum showed typical resonances detected at 27.2 and 25.9 ppm ((-C($\underline{C}$H$_3$)$_2$)), 18.6 ppm (-CH($\underline{C}$H$_3$)), 72.0 ppm (-$\underline{C}$H(CH3)-O), 70.8 ppm (-$\underline{C}$H$_2$O) and 108.7 ppm (-O-$\underline{C}$(CH$_3$)$_2$-O) which is fully consistent with the formation of 2,2,4-trimethyl-dioxolane (Figure 21).
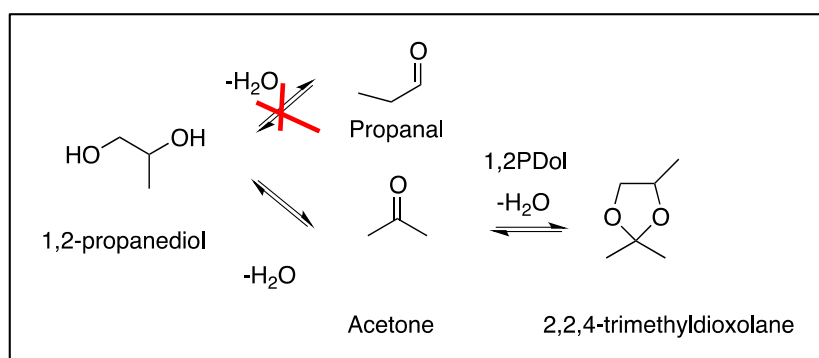
Figure 21: Mechanism of oxidation of 1,2-propanediol according to preliminary NMR investigations.

Acetone probably arises from the dehydration of 1,2-propanediol whereas it is postulated that 2,2,4-trimethyl-dioxolane forms by an acetalization reaction catalyzed with a Lewis acid (a silver cation) between acetone and 1,2-propanediol. Surprisingly, propanal, which is the most favorable kinetic product, was not produced during this process. The formation of acetone instead, which is harder to form but a more stable intermediate, was detected. Additional experiments need to be performed in the future in order to understand how the formation of acetone (in the case of 1,2-propanediol) leads to an improvement of the AgNW synthesis compared to acetaldehyde (in the case of EG). In particular, we plan to

perform gas chromatography (GC) "in situ" by directly injecting the volatile compound formed during the polyol process into the entry of the chromatograph.

Taking into account these interesting findings we have explored the possibility of generating ultra-long nanowires in 1,2-propanediol medium. In a typical process, the synthesis of silver nanowires consisted on the hot injection of both silver nitrate solution and PVP-1300 K in a reaction medium of 1.2-propanediol and Cl⁻ at 140 °C (Figure 22).
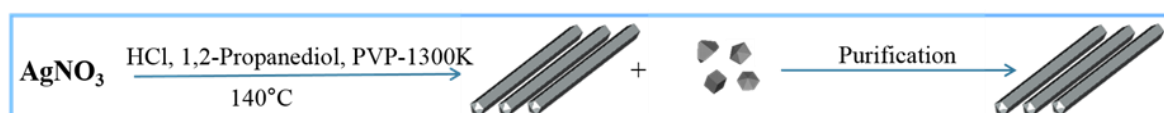
Figure 22: Scheme of the synthesis of silver nanowires in 1.2-propanediol.

2.2.1. Protocols:

Protocol 2.3

In a 100 ml three neck bottom flask, 30 ml of 1.2-propanediol (Pdol) were heated at 140 °C (oil bath temperature) for 45 minutes. Then, 5 ml of a solution of HCl diluted in 1.2-propanediol (3mM) was quickly added. After 10 min, 15 ml of $AgNO_3$ dissolved in 1.2-propanediol (94 mM) and PVP-1300K dissolved in 1.2-propanediol (147 mM) were injected drop-by-drop (45 ml per hour) into the solution. The stirring rate was set at 100 rpm during the entire process and the reaction time was set at 1 hour. Once the reaction is completed the flask is cooled down to room temperature with an ice bath. Finally, a single purification step was applied to the final solution and the product was redispersed in 20 ml of ethanol.

Protocol 2.4

Protocol 2.4 is the same as protocol 2.3 except the initial volume of 1,2-propanediol was increased to 32 ml, 35 ml or 40 ml.

2.2.2. Results and discussion

Figure 23 shows a dark field optical image as well as the size distributions of the silver nanowires synthesized following protocol 2.3. Under these experimental conditions, we could produce long nanowires with an average length of 112 μm +/- 58 μm in high yield but with a relatively thick diameter (≈275 nm).
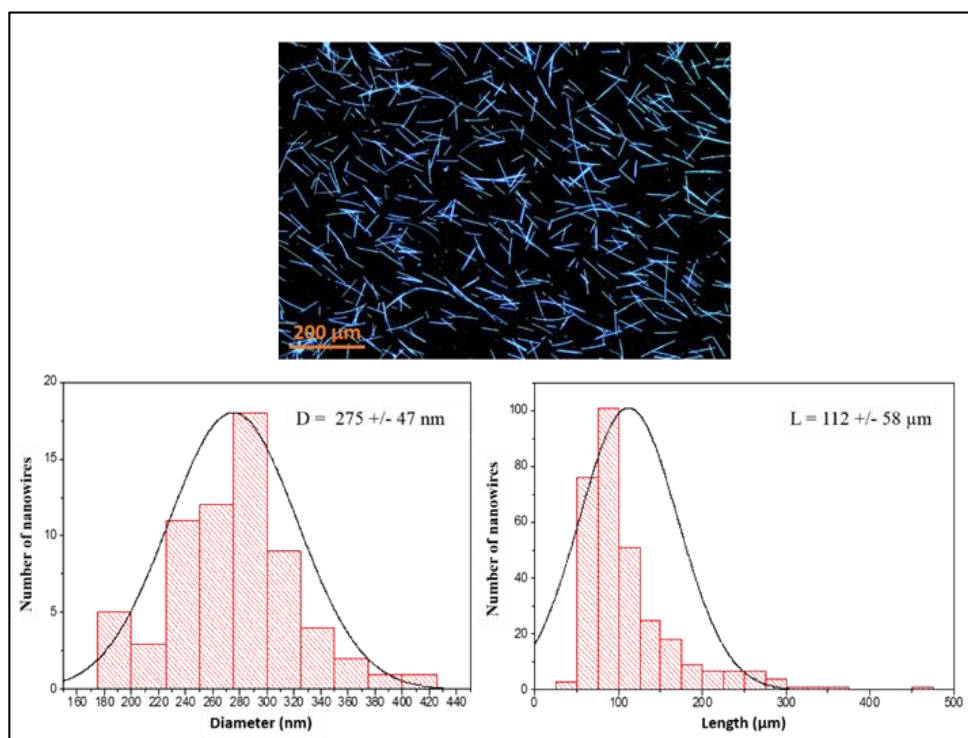
Figure 23: (Top) Dark field image of the silver nanowires produced in 1,2 propanediol (protocol 2.3) and their corresponding size distributions in diameter (Bottom left) and in length (Bottom right).

Even though the results obtained with Protocol 2.3 are not ideal, we realized that by simply varying the concentration of the reactants in the medium we could produce ultra-long nanowires with smaller diameter in high yield (protocol 2.4). The overall trend is that both the average length and diameter decrease when the concentration of Ag^+ is decreased in the reaction medium (Figure 24). Interestingly, for a certain concentration range, 19.3 mM < [Ag+] < 20.4 mM (highlighted in purple in Figure 24), the length is slightly higher than that of the original Ag^+ concentration (21.7 mM) while the diameter is reduced by a factor of two, thus resulting in a much higher aspect ratio.
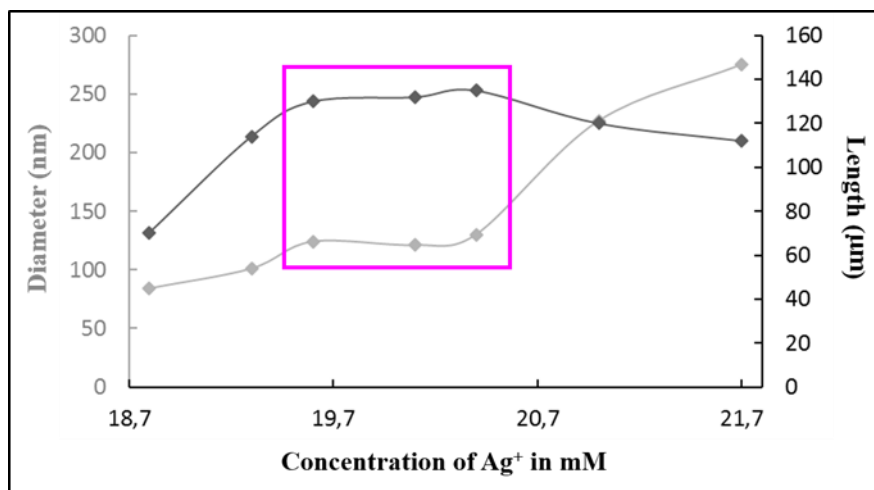
Figure 24: Plot of the diameter and length of the nanowires as a function of the initial concentration of Ag$^+$ developed following Protocol 2.4.

A selection of 3 batches produced with a silver concentration of 20.1 mM, 19.6 mM and 19.3 mM are shown in Figure 25. The silver nanowires not only become thinner but also more homogeneous in diameter than those synthesized with the protocol 2.3. Moreover, the number of ultra-long silver nanowires in the batch increases from 45% to 80%. In agreement with what we observe in Figure 24, the number of ultra-long silver nanowires is very high (86%) when the silver concentration is equal to 19.6 mM. However, a further decrease in silver concentration induces lower amount of ultra-long silver nanowires (57%). Importantly, the reaction (in 1.2-Pdol) typically proceeds for 80 minutes and the amount of the product obtained is 20 mg for a volume of 10 ml (whereas in ethylene glycol the amount obtained is 0.13 mg for a volume of 10 ml). Such concentration is high enough to fabricate several transparent electrode samples.
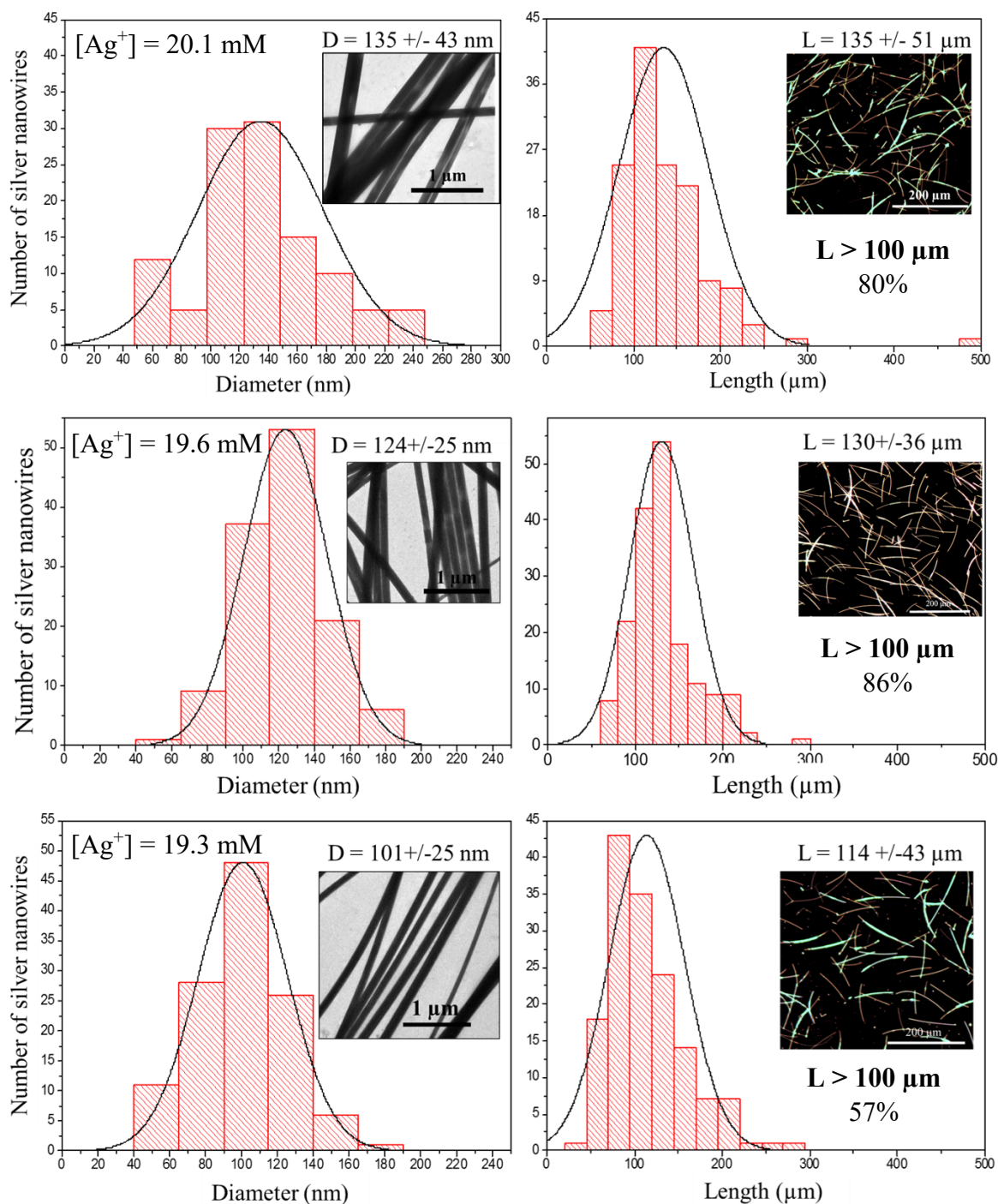
Figure 25: Dark field images and the corresponding size distribution of Ag NW produced for different [Ag⁺] in the reactional medium.

2.2.3. Closing remarks

Silver nanowires were developed in a single step process by using 1,2 propanediol as the solvent, without any addition of foreign ions, within 80 minutes. This approach allows the production of uniform nanowires in high yield (2 mg/ml), and with a high aspect ratio (from

1000 to 1130). Moreover, the proportion of synthesized nanowires that are "ultra-long" is also significantly increased (i.e. more than 80% of the wires obtained in one batch can have lengths > 100 μm). However, the diameters obtained are larger than 100 nm which is larger than desired and strategies to decrease diameters such as the addition of KBr in the medium have to be investigated in the future. Interestingly, Ag nanowires were developed in a single step process by using 1,2-propanediol as solvent, without any addition of foreign ions.

As already reviewed in Chapter 1, investigations on the elaboration of transparent electrodes based in ultra-long silver nanowires started in 2014.[85] The silver nanowires presented in this Thesis do not have the best aspect ratio of the literature but have higher length in comparison to previous ultra-long silver nanowires synthesized by the polyol process (see figure A). Very recently, ultra-long silver nanowires with an average length equal to 220 μm (aspect ratio more than 4000) synthesized via an hydrothermal process have been reported. Nevertheless, such approach involves a much longer reaction time (8 hours) than that presented here.[89] Other works reporting the formation of ultra-long silver nanowires do not lead to satisfactory yields in terms of inorganic nanowires.[88]
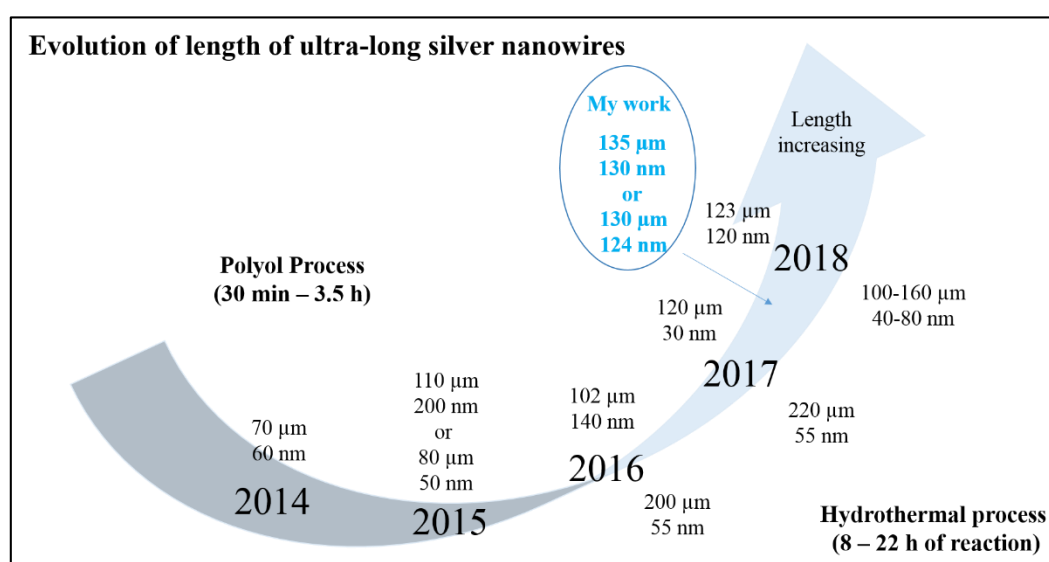
Figure A: Evolution of the length of the ultra-long silver nanowires published in the literature from 2014 to 2018.[65,86,87,89,90,108,111,112]

2.3. Fabrication of transparent electrodes based on ultra-long silver nanowires

This section focuses on the physical properties of silver nanowire networks based on the ultra-long nanowires produced above. Three different batches of Ag nanowires were used in order to elaborate thin films: Ag135 (d=135 +/- 43 nm and L = 135 +/- 51 μm), Ag124 (d=124 +/- 25 nm and L = 130 +/- 36 μm) and Ag101 (d=101 +/- 25 nm and L = 114 +/- 43 μm). Films were deposited on glass surfaces using three different deposition methods: Mayer rod coating, spin coating and spray coating (Figure 26).
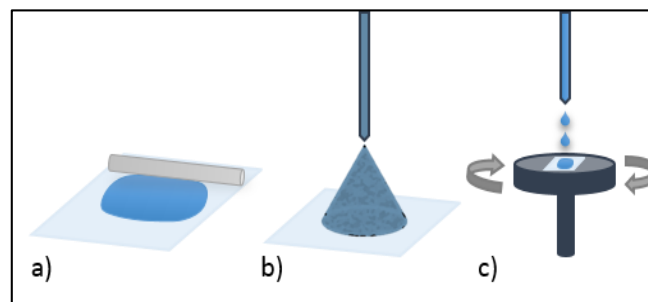
Figure 26: Schematic representation of the three techniques used here to deposit the nanowire film: a) Mayer rod, b) spray and c) spin coating.

Two types of glass substrates were used: Roth glass (2.4 cm x 3.2 cm and thickness of 0.17 mm) and Corning glass substrates (2 cm x 2 cm and thickness of 1 mm). The Mayer rod is the most widely used deposition process in the group of Prof. Irene Goldthorpe at the University of Waterloo. The spin coating and the spray coating deposition methods were investigated via a collaboration with the group of Daniel Bellet in LMGP (Laboratoire des Matériaux et du Genie Physique) in Grenoble, France. The experiments were performed with the help of Dorina Papanastasiou, a PhD student in the LMGP laboratory.

2.3.1. Film fabrication and characterization

Mayer Rod Coating

Mayer rod coating is a method that is scalable to industrial manufacturing levels. The method is easy to operate and allows one to get thin films of a desired thickness. The thickness of the thin film depends on diameter of the metal wires that wrap around the

rod. For instance, with a Mayer Rod RDS 10, the theoretical thickness of the deposited film is 25 µm.[113] The characteristics of the Mayer Rod used to fabricate the transparent networks in this work are detailed in Figure 27.
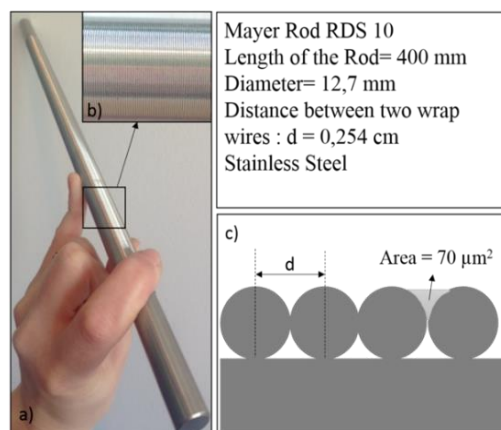
Figure 27: a) Picture of the Mayer Rod use in this study, b) Magnified image of the Mayer rod evidencing the wrapped wires, c) Schematic representation of the cross section of the Mayer Rod.

The solutions of silver nanowires were diluted to obtain different concentrations: 1.5 mg/ml, 1 mg/ml, 0.5 mg/ml and 0.25 mg/ml. A first series of deposition was performed on a Corning glass substrates. 4 coatings steps of 35 µl of AgNW suspension were developed on 2 cm x 2 cm glass substrates in 4 orthogonal directions (i.e. along the angles 0°, 90°, 180° and 270°) to obtain a random NW network. Moreover, another series of thin films were performed on Roth glass substrates: 4 coating steps of 50 µl of AgNW suspension were developed on 2.4 cm x 3.2 cm glass substrates in 4 orthogonal directions to obtain a random NW network. Finally, a thermal treatment of 1 hour at 200 °C for the thicker nanowires (Ag135 and Ag124) and 160 °C for the thinner ones (Ag101) was applied. These optimized annealing temperatures were chosen after a series of tests to minimize sheet resistance.

Spray Coating

Spray coating is a very interesting deposition method due to its ease of production at a large scale and the possibility of coating the large area substrates. This technique consists in forcing solutions of Ag nanowires through a nozzle while different parameters allow one to

get homogeneous thin films: distance between the nozzle and the substrate, the flow rate or the pressure and the temperature of the substrate.[114]

In LMGP, an automatic spray coater has been built. The solution of synthesized silver nanostructures was introduced into a spray head with a syringe. Note that this spray is not a classical spray coating with ultrasonic nozzle but a low-cost air-operated tool (Figure 28).
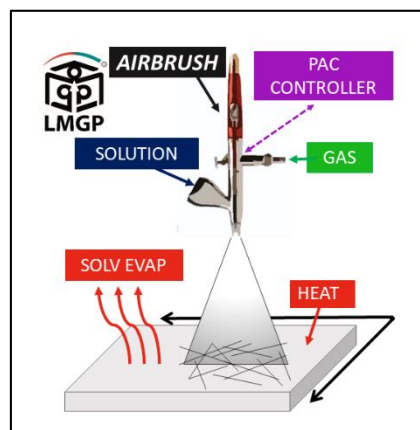
Figure 28: Schematic representation of an automatic spray coating deposition system built in LMGP, Grenoble.

Once the solution is converted into droplets, they are propelled onto a hot substrate. The movement of the spray is performed in both X and Y directions. The parameters of the deposition process used in the following work was determined by taking into account previous studies.[55] The temperature of the substrate was set at 90 °C, the distance between the spray head and the substrate at 4.5 cm, the solution concentration at 0.5 mg.ml^{-1}, the flow rate at 4 droplets / 20 seconds, the pressure at 3 bar and the aperture of the airbrush at 0.4 mm. Depending on the sheet resistance desired, 2 cycles of 2 PC (crossed passing) to 4 PC were applied to spread the solution. Deposition was performed on both Roth and Corning glasses.

Spin Coating

The spin coating deposition method involves the deposition of a drop of a solution onto a substrate in rotation. Thanks to centrifugal forces, the solution is spread over the surface of a given substrate, allowing the efficient preparation of homogeneous thin films.[115]

However, the spin coating process has some limitations: (i) it is a non-scalable process and (ii) the nanowires are often orientated radially from the middle of the electrode due to the centrifugal forces induced by the rotation of the substrate.[116] In this PhD study, the parameters of deposition were adjusted in order to get a random and homogeneous network. Two coating steps of 0.5 ml of a solution of AgNWs (0.1 mg/ml) were performed drop by drop. The speed of the rotation of the substrate was 1500 rpm and a period of drying of 30 s was necessary between each deposition step.[55] The initial solution of silver nanowires was diluted to 0.1 mg/ml and 2 times 0.5 ml of the solution was deposited onto the glass substrate in movement.

<u>SEM characterization of the networks</u>

The different thin films obtained were characterized using scanning electron microscopy (SEM). The SEM used was a FEI Quanta FEG 250 with a field emission electron source in LMGP in order to visualize the configuration of the network and to calculate the areal mass density. It has a spatial resolution of between 1.2 nm at 30 kV and 3 nm at 1 kV.

<u>Image processing</u>

SEM characterization allowed us to calculate the network density on a substrate. By using the software Image J, the areal mass density (Amd) of a given network could be evaluated. 2 processing steps of the SEM images were first necessary before the measurement of the area: (i) The SEM images are first smoothed (Process -> Smooth) and normalized (Process -> Enhance contrast), (ii) then the image is made binary (Process -> Binary -> Make binary) which converts all pixels into either white or black colors (Figure 29).
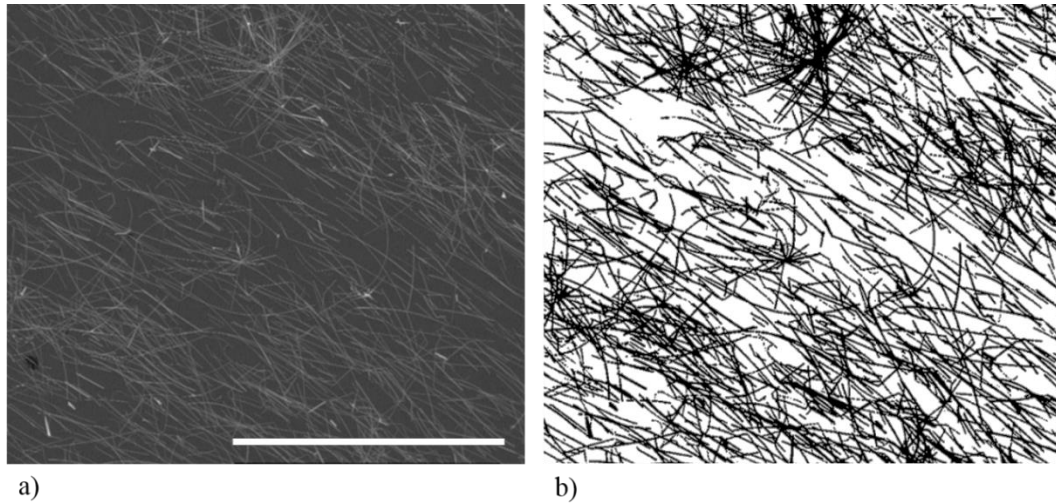
Figure 29: Example of image processing: (i) Smoothed SEM image and (ii) image after the binary process. Scale bar = 200 µm.

By using imageJ, the area covered by silver nanowires (black area) was measured. Furthermore, the calculations after processing of the SEM image consisted in calculating the equivalent total length. The value of the black area was divided by the value of the average diameter of the silver nanowires and the result is then divided by the value of the average length of the nanowires. After dividing by the area of the picture, we obtained the number of silver nanowires per unit area.

The pentagonal cross section was then calculated following the following expression (2-1):

$$A = \frac{5 \times D^2}{16 \times \sin 54^2 \times \tan 36} \quad (2\text{-}1)$$

The length of the silver nanowire multiplied by the cross-section allowed us to obtain the volume of one silver nanowire. By multiplying this volume by the silver density (1.049×10^{-8} mg.µm^{-3}), we obtained the mass of one silver nanowire. The number of silver nanowires per unit area was then multiplied by this mass leading to the areal mass density that could be extended to the whole sample.

Electrical characterizations

The electrical properties were evaluated by measuring the sheet resistance of the thin films by a 2 or a 4-point-probe system. Firstly, two paths of silver paint were deposited on the two opposite edges of the electrode and by making the contact with the multimeter, the resistance of the network was then evaluated. In the case of a thin film, the resistance R could be related to the sheet resistance R_s via the formula: $R = (L/W) \times R_s$ where L is the length of the film between the two silver conductive bars and W is the width of the film. The quality of the contact between the silver conductive bars, the silver network and the probes had to be
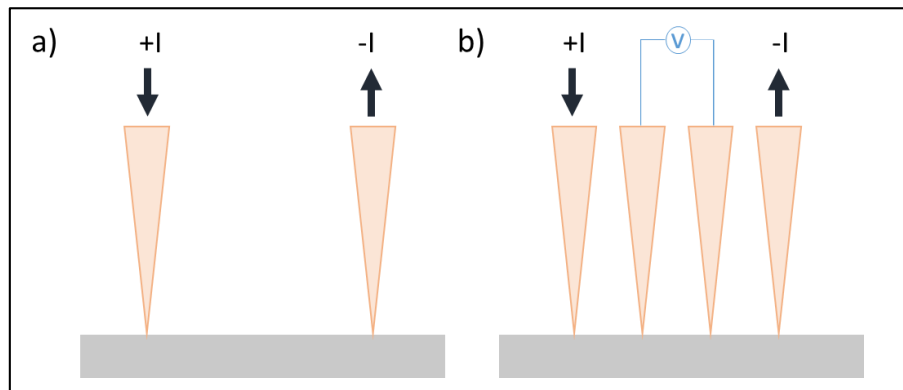
Figure 30: Schematic representation of the a) two-point probes and b) four-point ones.

very good to avoid losses and to have an accurate evaluation of the electrical resistance of the network.

The sheet resistance can be more accurately measured by using the four-point-probe method. This approach is better than the two-point-probe because it minimizes the contribution of contact resistance (Figure 30). However in the case of AgNW networks the probes can induce local damage at the contact location.

Optical Characterization

The transparency of the thin films was measured using a UV-Vis-NIR spectrophotometer (Perkin Elmer Lambda 950) equipped with an integrating sphere. The beam of photons illuminate the specimens at normal incidence (Figure 31). Either total

transmittance, which includes both unscattered and scattered transmitted light, or diffuse

transmittance, which includes only scattered light, could be measured.
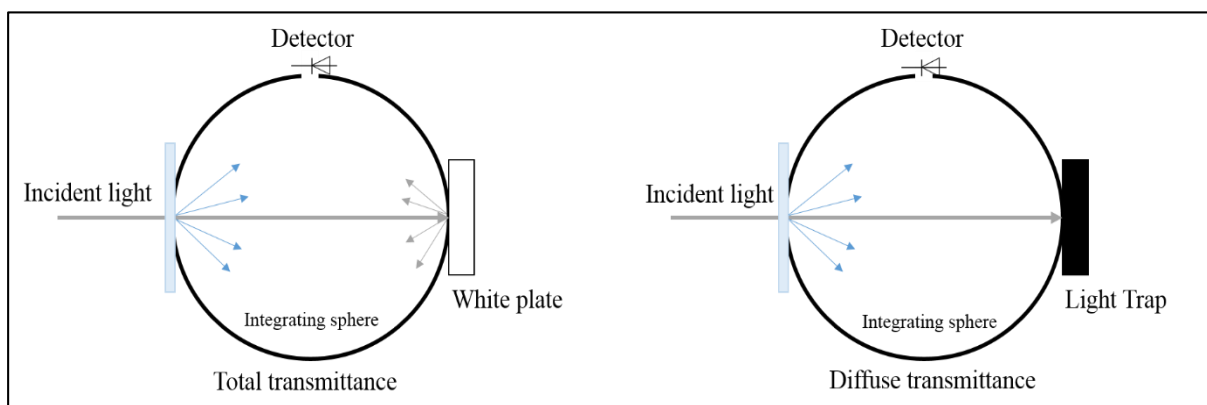
Figure 31: Schematic representation of the integrating sphere of a UV-Vis-NIR spectrophotometer. The set-up is equipped with a light trap in the case of measuring diffuse transmittance.[117]

In-situ thermal annealing

The impact of thermal annealing on silver nanowire networks produced in this work

was investigated by using an in situ set-up developed in LMGP in Grenoble (Figure 32). The

electrode was left on a hot plate connected to a temperature controller (Eutherm model: 3504

series) that allows the control of annealing ramp, time and temperature. Thanks to appropriate

software (LabView), the temperature of the hot plate could be collected. Moreover, two paths

of silver paint were needed to make the contact with the digital multimeter probes (Keithley

2400 source meter). The electrical resistance was then measured while the temperature was

varied: a ramp of 5 °C/min from room temperature (~20-22°C) to 400 °C was applied. In this

way, the temperature at which the resistance was a minimum could be found.
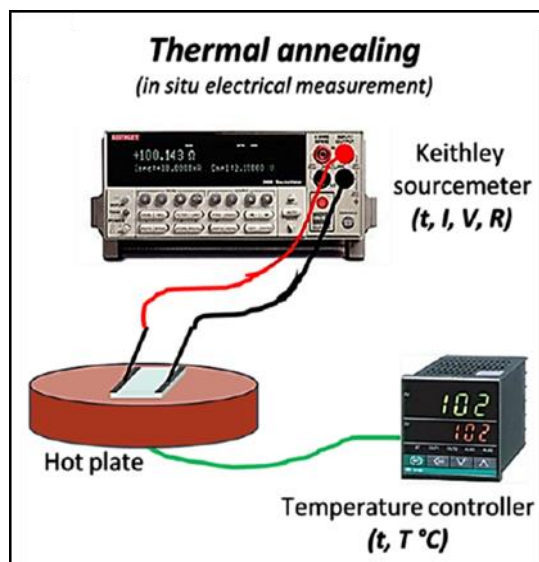
Figure 32: Schematic representation of the Thermal annealing set-up.

2.3.2. Impact of the deposition method on the network properties

Ultra-long nanowires were easily processed into transparent conductive films. Figure 33 shows the SEM images of the thin films of the same nanowire solution (Ag 124) deposited by the three different deposition methods (all of them performed on glass substrates).
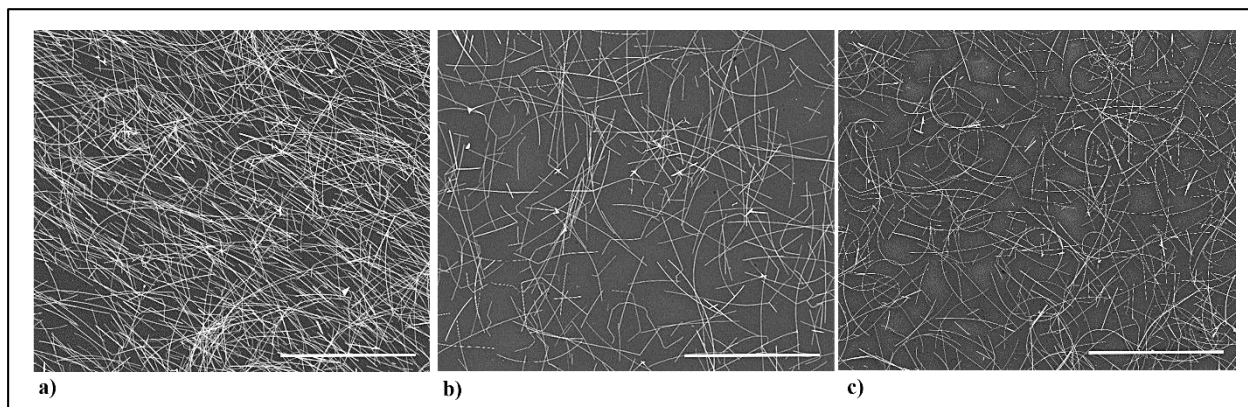
Figure 33: SEM images of a suspension of Ag124 deposited by a) spin Coating, b) Mayer rod coating and c) spray coating. Scale bar = 100 μm.

At first glance, there is a dependence of the deposition method used on the homogeneity and uniformity of the nanowire network. Some alignment of nanowires could be observed due the radial deposition when the solution was deposited by spin coating, whereas some circular silver nanowires are formed upon deposition via spray injection. Nevertheless,

this latter method appeared to form more uniform networks than the others. In addition, it did not appear to reduce the average length of the nanowires.

The areal mass densities (the metal mass per unit area) of the different films are reported in Table 2.1 and are in good agreement with the initial quantity of silver nanowires deposited.

Table 2.1: Areal mass density (amd) calculated for different deposition techniques.

Deposition process	Spin Coating	Rod Coating	Spray Coating
Concentration of solution	0.1 mg/ml	0.25 mg/ml	0.5 mg/ml
Volume of solution	1 ml	140 µl	1.17 ml*
Amd	249 +/- 71 mg/m^2	201 +/- 59 mg/m^2	261 +/- 34 mg/m^2

* The total volume used is about 7 ml but 6 electrodes can be elaborated, so the real volume necessary is about 1,17 ml

The comparison of the electro-optical properties of the different films is shown in table 2.2. Importantly, the network properties depend on how they were fabricated.

Table 2.2: Resistance, Sheet resistance, Total transmittance and Haacke FoM depending on the deposition process.

Deposition process	R (Ohm)	Rs (Ohm/Sq)	T_{tot} at 550 nm	Haacke FoM (Ω^{-1})
Spin Coating	104.5	60.0 +/- 16.0	91.0 %	6.5 x 10^{-3}
Mayer Rod	24.5	18.0 +/- 3.0	91.5 %	23 x 10^{-3}
Spray Coating	12.0	8.0 +/- 0.5	87.5 %	33 x 10^{-3}

*The Transmittance of the cleaned glass substrate is equal to 92 %.
* The Total Transmittance measured at 550 nm is relative to the glass substrate.

All three types of the Ag nanowire films exhibit at least 87% transmittance and sheet resistances of 8-60 Ω.Sq^{-1} depending on the deposition method. The spray coating method which yields coatings that are more homogeneous led to the best trade-off between the optical transparency and low electrical resistance. As presented in Figure 33, Mayer rod coating did not result in many curved nanowires, thus leading to more connections for a lower density network. Longer nanowires (that are not curved as by spray and more randomly distributed than by spin) lead to percolation with lower critical network density, as is shown from the 2D stick percolation theory.[118] Still, in that set of experiments, the Mayer rod coating does not allow the best performance of the electrodes. Note that it was difficult to roll over the fluid on corning glass substrates (2 cm x 2 cm; 1 mm of thickness) with the Mayer rod and thus it

could induce less homogeneous networks. The overall results demonstrate the importance of handling procedures for silver nanowire deposition.

2.3.3. Impact of the thermal annealing step on the electrical properties

As outlined in Chapter 1, post-processing treatments (thermal annealing, chemical treatments, laser sintering, mechanical pressing, etc…) of the silver nanowire networks, in general, lower the resistance. Many papers report that such methods can lead to a drastic decrease in sheet resistance from about 10^3 to about 10 $\Omega.Sq^{-1}$.[53],[18],[119],[1],[120] In the case of annealing post-treatment, elevated temperatures cause the overlapping nanowire junctions to sinter, lowering junction resistances which in turn lower the overall film resistance. However, excesive temperatures or annealing times may cause morphological modification of the silver nanowires (wire breaking into chains of nanospheres, i.e. Plateau-Rayleigh instability), thus preventing the network from percolating. Therefore, a minimum of sheet resistance is observed during a thermal annealing ramp, shown for a typical nanowire network from the literature (Figure 34).
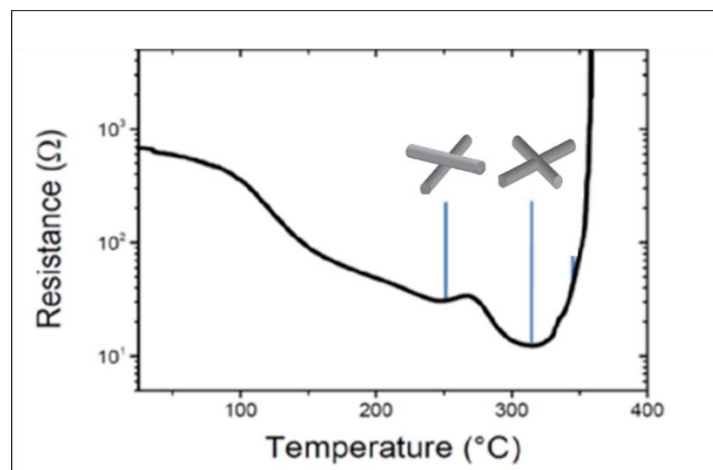
Figure 34: Resistance of electrodes as a function of temperature for commercial AgNWs (from Seashell company).[53]

Figure 35 shows the evolution of the electrical resistance of networks based on Ag124 with different nanowire densities, versus temperature during a thermal ramp of 5 °C/min in

air. Moreover, table 2.3 shows the resistance of the electrodes measured before and after annealing.
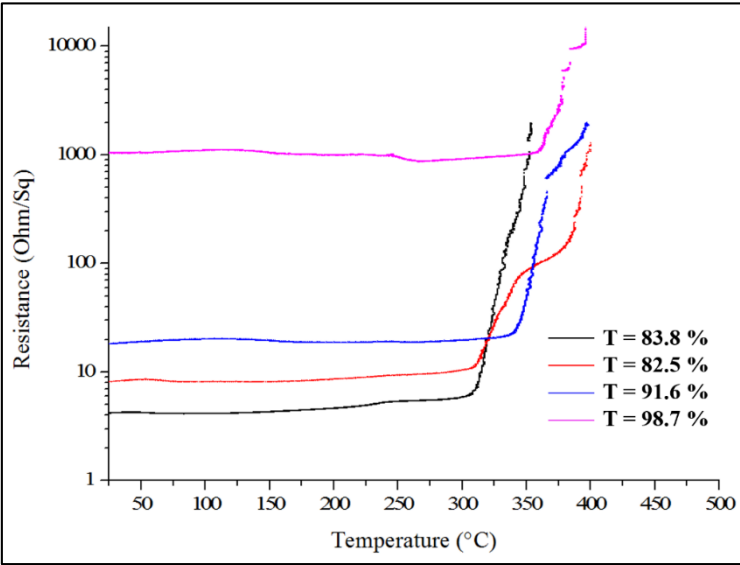
Figure 35: Plots of the resistance versus the temperature during the in-situ annealing treatment of Ag124 networks at different initial resistances and transparencies presented in table 2.3.

Table 2.3: Values of two-point probe resistance before annealing (22°C), minimum resistance reached during the anneal treatment (265°C), percentage of decrease of the resistance and transmittance of electrodes performed with Ag124.

Sample	Resistance (Ω) at 22°C	Minimum Resistance (Ω) during annealing treatment	Percentage of decrease	Transmittance (%)
Ag124	4.2	4.1	1%	83.8
	8.1	8.1	0%	82.5
	18.2	18.2	0%	91.6
	1044.0	877.0	16%	98.7

Unexpectedly, and unlike most silver nanowire electrodes report in the literature, the initial sheet resistance before annealing was low, and no strong variation of the resistance was observed upon thermal treatment until 300°C. Above this temperature, the resistance drastically increased suggesting the spheroidization of the AgNWs. The minimal reduction of resistance via thermal annealing (less than 1 Ohm/Sq of reduction) suggests that the contacts between the ultra-long nanowires were efficient even without thermal annealing. Along these lines, the low decrease was assigned to the evaporation of the residual solvents and PVP from the Ag NWs under thermal treatment. Note that the percentage of decrease has been calculated from the resistances measured at different temperatures (room temperature for the

initial resistance, and high temperature during the in-situ experiment). An additional experiment consisting in the anneal of the electrode until 265°C and the cool down to room temperature of this one should be performed. The slope of the curve corresponding to the cool down will allow calculating a factor β.[152],[53] Taking in account this factor, the percentage of decrease corresponding to the difference between the initial resistance and minimum resistance measured at room temperature will be much larger. However, the previous observation remains that the electrical resistance does not decrease much after thermal annealing, at the opposite of what was reported for industrial silver nanowires.[53]

Experiments were reproduced for lower network density. Decreasing the network density yielded to an increase of the initial sheet resistance, leading to a similar behavior for all the specimens studied upon the annealing treatment: limited drop in resistance of only a few ohms upon the increase of temperature and an increase starting from 300 °C. The critical temperature at which the increase in resistance occurs was slightly dependent on the density of the network. For dense networks, the increase was abrupt until breakdown of the electrode. On the other hand sparser ones led to an increase of the resistance in two steps: a first plateau was reached around 350 °C until 400 °C and the resistance increases again after this plateau. This phenomenon is more important when electrodes were performed with Ag135. The average diameter of Ag135 has a standard deviation that is higher than Ag124 or Ag101. Therefore, the origin of the plateau could then originate from the fact that at high temperature, thinner nanowires already reached the state of spheroidization removing connections between the wires that leads to an increase in resistance. On the other hand larger ones are still stable and connected allowing a constant resistance at higher temperatures until they break and induce a second increase of the resistance. In the case of a sparse network, the phenomenon is even more relevant since the number of percolation pathways is lower.

Figure 36 exhibits similar analysis for the electrodes based on Ag135 and Ag101. Table 2.4 shows the resistances of the different electrodes measured before annealing and the minimum resistance reached during the process. Similar trends than those presented in Figure 36 have been observed. This result was not surprising since the junction resistance is determined by the nature of the junction, which is dependent on how the nanowire were grown, purified and deposited. Since the chemistry is the same independently of the diameter, the results confirmed that the connections between nanowires were efficient even at room temperature. Additional measurements have been performed on Ag135 electrodes. After the thermal process the variation of the resistance was measured when the temperature was decreasing. In this case, the resistances are higher than the initial ones but the electrode did not break down. This result shows good thermal stability of the electrodes prepared with Ag135.
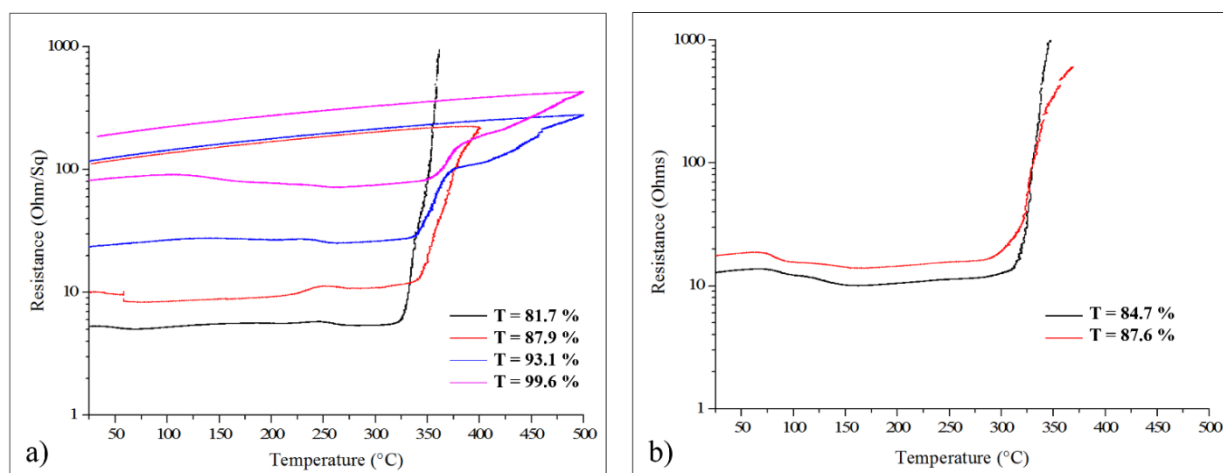
Figure 36: Plots of the resistance measured in-situ versus temperature during thermal ramp (5°C/min) of electrodes made with a) Ag135 and b) Ag101 at different initial resistances and transparency presented in table 2.4.

Table 2.4: Values of two-point probe resistance before annealing (22°C), minimum resistance reached during the anneal treatment (265°C for Ag135 and 175°C for Ag110), percentage of decrease of the resistance and transmittance of electrodes performed with Ag135 and Ag110.

Sample	Resistance (Ω) at 22°C	Minimum Resistance (Ω) during annealing treatment	Percentage of decrease	Transmittance (%)
Ag135	5.3	5.0	5%	81.7
	10.2	8.3	22%	87.9
	23.4	23.4	0%	93.1
	81.2	71.9	13%	99.6
Ag 110	6.2	6.1	2%	84.8
	12.9	10.1	22%	84.7
	17.5	14.0	20%	84.6

TEM and SEM observations of the junctions have to be performed in order to confirm these general observations and characterize the junctions upon annealing as well as the configuration changes of the nanowires above 300 °C. Interestingly, we do not need to apply any post-treatment to reach good performance of the electrodes, which makes this process compatible for the elaboration of flexible transparent electrodes. Along these lines, G. Deignan investigated the impact of the thermal anneal on the stability and lifetime of the electrodes and showed that electrodes which underwent a post-thermal treatment are less stable over time.[121]

2.3.4. Impact of the substrate on the network properties

The colloidal solution Ag124 was deposited as network on thinner substrates (Roth glass 0.17 nm vs Corning glass 1 mm). Since it was observed that nanowire networks prepared by spin coating showed spatial inhomogeneity and because it is a non-scalable process, networks were only prepared using Mayer rod and spray coatings. Films obtained were very homogeneous from one sample to another.

The following table 2.5 exposes the values of sheet resistances measured by a 4 point probe method.

Table 2.5: Resistance, Sheet resistance, Total transmittance, haze factor and Haacke FoM
of the films deposited by Mayer rod and Spray coating with a Ag124 solution.

		Rs (Ω/Sq)	T_{tot} at 550 nm	Haze factor at 550 nm	Haacke FoM (Ω^{-1})
Mayer Rod Coating	Sample 1	4.8 +/- 1.4	93.2%	11.8%	103 x 10^{-3}
	Sample 2	5.3 +/- 0.3	94.0%	11.4%	102 x 10^{-3}
	Sample 3	4.9 +/- 0.5	94.3%	11.9%	113 x 10^{-3}
Spray Coating	Sample 4	4.2 +/- 0.4	90.1%	16.5%	84 x 10^{-3}
	Sample 5	5.0 +/- 0.6	92.1%	14.6%	88 x 10^{-3}
	Sample 6	18.6 +/- 1.4	94.3%	12.4%	30 x 10^{-3}

- Total transmittance of the substrate at 550 nm is equal to 92,6 %
- Transmittance measured is relative to the transmittance of glass substrate

Both approaches yielded the formation of high-quality nanowire networks with sheet resistances that could be below 5 Ω/Sq. The standard deviation of the sheet resistance indicates better homogeneity of the network performed by Mayer rod coating. This technique also presents higher transparency and conductivity performance.

In Figure 37 are plotted the optical properties of both types of networks. Relative transmittance above 90% on thin substrates could be reached independently of the deposition method used. On the other hand, transparency is better for the samples elaborated by Mayer rod coating since the deposition method is more suitable for thinner substrates.
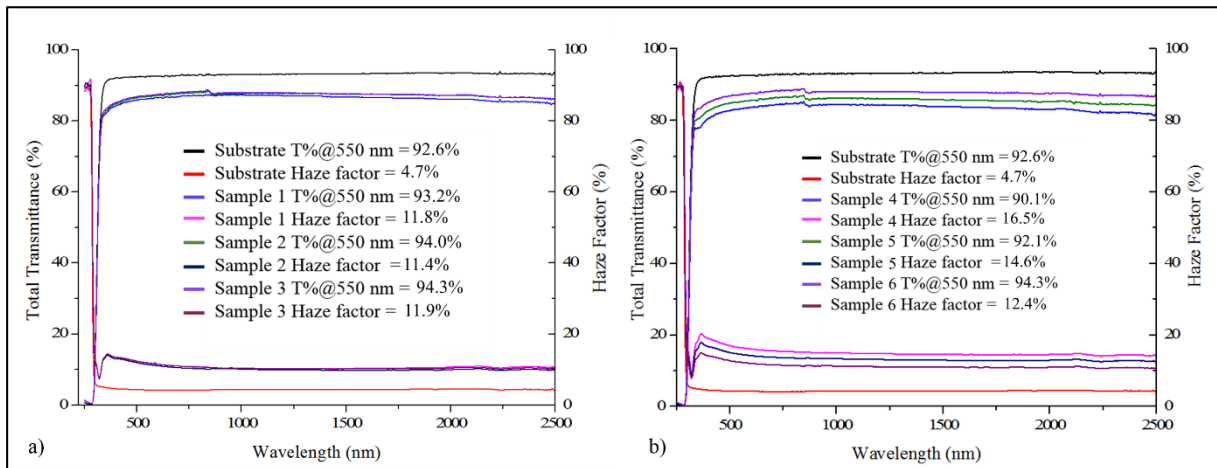
Figure 37: Transmittance and Haze Factor versus wavelength of the silver nanowire electrodes performed with a solution of Ag124 by a) rod coating and b) spray coating.

2.3.5. The haze factor

The ratio of diffuse transmission to total transmission of light (the haze factor) of the materials was determined since it can be considered as a critical factor for some applications. This parameter is strongly dependent on the experimental conditions and methods used for fabrication of the network. At 550 nm, the haze factor was equal to 12% for films prepared by rod coating and slightly higher for the ones produced by spray coating (about 14%). Note that these values were probably overestimated since the haze factor of the substrate itself was equal to 4.7% and should be much lower. The haze factor was relatively high because of their thick diameter, which limits their application in displays.

2.3.6. Conclusion

Figure 38 compares the performances of the electrodes elaborated in this study with those reported in the literature. This comparison indicates that we have successfully elaborated silver nanowire electrodes with the higher optical transmittance and lower sheet resistance than other electrodes developed from silver nanowires with smaller lengths. Moreover, this performance is achieved with a scalable process. The high aspect ratio of the nanowires is one of the main parameters responsible for such good performance. Moreover, the process developed in 1.2-propanediol leads to less by-products and thus, better optical properties of the final electrodes. Another important factor resides in the choice of the deposition process, allowing to tune the properties of the electrodes (i.e. Mayor rod coating is more suitable for thinner substrates). Moreover, the present work shows that excellent performance could be reached by using the spray coating protocol, in which the nanowires do not stuck in the aperture and are kept intact after their deposition. Another parameter that must be explored in more detail in the future is related with the surface of the silver nanowires. This characteristic could be engineered so that better connections between nanowires could be attained.
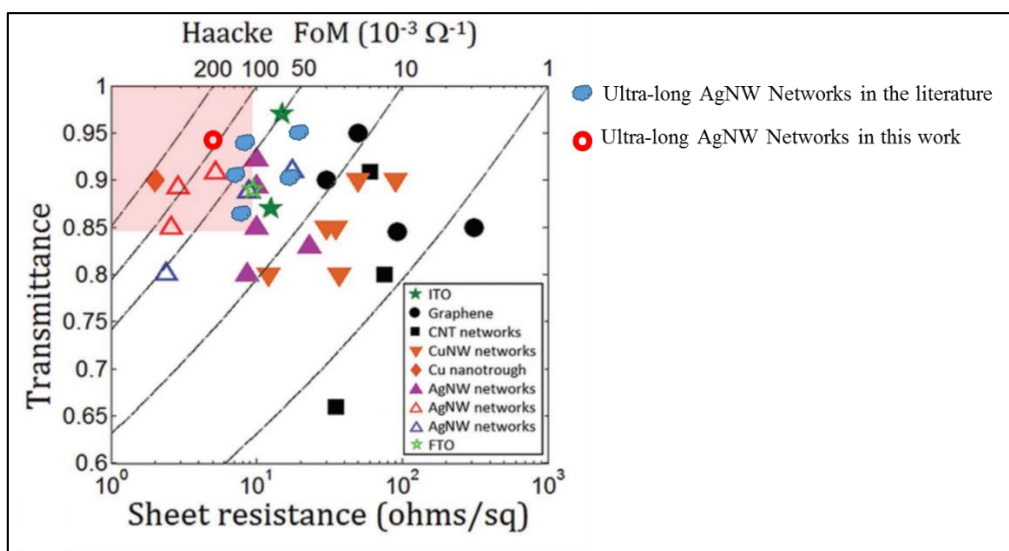
Figure 38: Transmittance (550 nm) plotted as a function of sheet resistance for various transparent conductive materials reported in the literature: ITO, graphene, single -walled carbon nanotubes, copper nanowires, silver nanowires, FTO and the present work.[18]

2.4. Conclusion

Fabrication of ultra-long silver nanowires has opened up exciting possibilities for electro-optical devices. This chapter evidenced that silver nanowires with an aspect ratio of 1050 and lengths higher than 100 µm were successfully synthesized in 1.2-propanediol and in presence of a high molecular weight PVP. The synthesis in these experimental conditions allows the fabrication of ultra-long nanostructures in high yield in one step and a very short reaction time (< 2 hours). Moreover, this process can be easily tuned to have access to a wide range of dimensions of silver nanowires.

High performance electrodes with sheet resistances lower than 5 Ω/Sq and transparency of 94 % could be elaborated. We also observed that thermal post treatment did not induce a significant decrease of the resistance, leading to the conclusion that the chemistry of the surface is different from commercial silver nanowires. Additional TEM analyses should be performed on these new types of junctions to know whether the nanowires are fused together at the junctions or not. Moreover, other post-synthetic treatments that may lead to better conductivities such as cold welding[111] or mechanical pressure[46] should be investigated. Therefore the combination of high-length silver nanowires and suitable post-

61

treatment mechanisms could open the way towards the formation of flexible electrodes with resistances approaching 1 Ω/Sq.

Chapter 3: Synthesis of Branched Nanowires

The objective of this chapter is twofold given that (i) branched nanowire networks would be original compared to standard silver nanowire networks available commercially and (ii) these novel architectures can be expected to form percolating networks at lower density. Since the networks used in devices require a density which is larger than the critical density (n_c, associated to the percolation threshold),[1] obtaining lower n_c values would lead to optimized networks of lower density and therefore higher transparency. The fact that branched nanowires with Y shapes could percolate with a lower network density compared to a stick-like network has never been reported (to the best of our knowledge). However, a group of physicists at Grenoble (LMGP, Grenoble INP) and Liège (Spin, Département de physique) has recently shown this feature thanks to Monte Carlo simulations [Aghazadehchors et al., unpublished results]. Results from one of their studies are reported in Figure 39. "Y metallic shape" network with branch length identical to a single silver nanowire appears to percolate at a lower density than a standard AgNW network. The associated total length of metal within networks appears nearly two times lower for Y branches than for straight nanowires: therefore, the Y shape networks should be more transparent. This constitutes a promising asset and therefore searching a way to fabricate these Y shapes appears interesting.
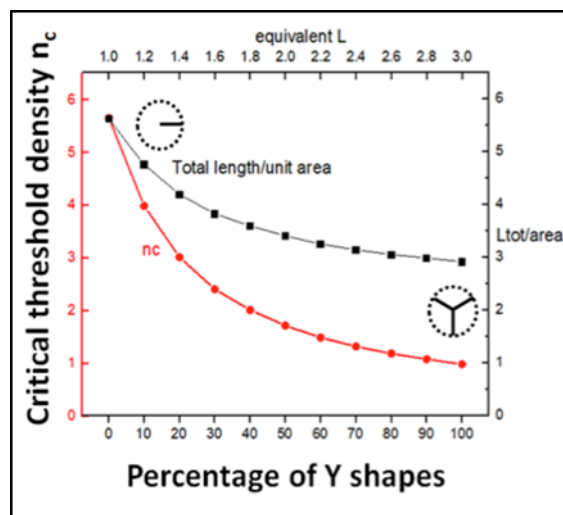
Figure 39 : Plot of the critical threshold density of a random mixture of nanowires and Y shapes, in function of the percentage of Y shapes.

As outlined in Chapter 1, architectures different than standard length 1D silver nanowires have not yet been explored in detail for transparent electrodes by other groups. Only three reports claim that by introducing some modifications to the polyol process, i.e. by
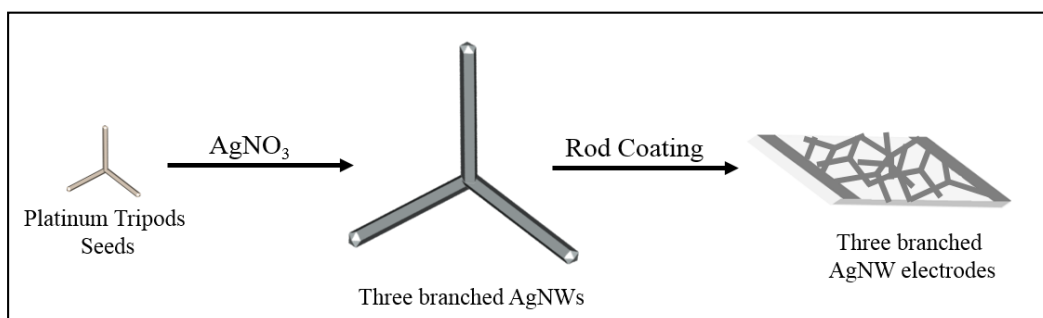
Figure 40: Schematic representation of the synthesis of branched silver nanowires.

varying the temperature of the growth process, adding transition metal ions or by introducing microwave radiations during the growth process, branched nanostructures could be formed.[81],[92],[93] In this chapter we have tried to develop a seeded-mediated approach based on tripod-like seeds in order to obtain nanowires with a "Y-shape". By using these 3D-anisotropic seeds, one can expect that the silver growth might occur more rapidly at preferential sites in the areas with a high radius of curvature (Figure 40).

A literature overview revealed that several candidate tripod seeds could be generated by wet chemical approaches: Pt, Au, Pd or PdCu (Figure 41).[122–125]
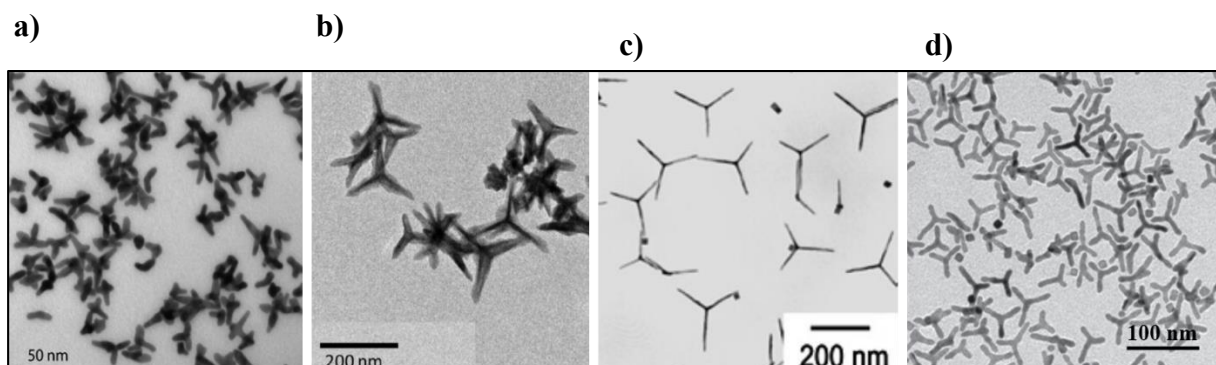
Figure 41: TEM images of a) gold, b) palladium, c) platinum and d) palladium/copper multipods.[122,126–128]

Since several investigations have demonstrated that silver nanowires could be prepared by the polyol method by using heterogeneous seeds such as Pt ones, we tested the possibility to produce branched nanowires from these seeds. Furthermore, these seeds have the longest branches reported so far.

3.1. 2D growth from anisotropic seeds

In this study, we monitored the polyol synthesis of Ag NWs employing anisotropic platinum seeds as the growth-promoting additive.

3.1.1. Experimental section

Protocol 3.1 Synthesis of platinum tripods.[129]

In a three neck round bottom flask of 25 ml, 100 mg of Platinum (II) acetylacetonate (Pt(acac)$_2$, Sigma-Aldrich), 135 mg of 1-Adamantanecarboxylic acid (ACA, Sigma Aldrich 99%), 1.6 g of Hexadecanediol (HDD, Sigma Aldrich 90%), 2 g of Hexadecylamine (HDA, Sigma Aldrich, 90%), and 1 ml of diphenyl ether (DPE, Sigma Aldrich, 99%) were mixed. The flask was immersed into an oil bath set at 130 °C for a few minutes under stirring until the liquid becomes yellow. Then, the flask was transferred into another oil bath set at 160°C, where the reaction took place for 2 hours. At the end of the reaction, the solution was mixed

with a solution of chloroform/ethanol v/v 40/10 and then centrifuged during 20 min and redispersed in 10 ml of chloroform. 5 ml of a solution of platinum tripod seeds were mixed with 20 ml of an aqueous solution of CTAB (cetyltrimethylammonium bromide) (10 mM). The solution was then stirred for one hour under an argon flow in order to remove the chloroform.

Protocol 3.2: Growth of silver on platinum seeds in polyol medium.[15]

The solution of platinum tripods elaborated in protocol 3.1 was centrifuged at 2000 rpm during 10 minutes and 2.5 ml of a solution of PVP in ethylene glycol (0.72 M) was added. The solution was centrifuged once at 5000 rpm in order to remove the excess of PVP and was redispersed in 0.6 ml of EG.

In a 50 ml three neck bottom flask, 5 ml of EG were heated at 175 °C (oil bath temperature) for one hour. Then 0.6 ml of the platinum tripods solution was poured into the hot EG. After 15 min, 2.5 ml of a solution of $AgNO_3$ (0.1 g dissolved in 5 ml of EG) and 5 ml of a solution of PVP-360K (0.4 g dissolved in 10 ml of EG) were added dropwise using a syringe pump over a period of 20 min. The stirring rate remains at 100 rpm during the entire process. The reaction time was set at 1h30. The flask was then put in an ice bath for a few minutes until it reached room temperature. A purification step with acetone was applied to the final solution (Protocol 2.2)

Protocol 3.3: Growth of silver on platinum tripod seeds in water.[130]

1 ml of Pt tripod seeds solution was then put in a vial and mixed with 4 ml of CTAB (10 mM), 100 µl of a solution of $AgNO_3$ (100 mM) and additional 5 ml of CTAB (10 mM). 400 µl of a solution of ascorbic acid (AA) (0.1 M) was then added. The pH was adjusted with NaOH and fixed at 4,5 in order to favor the reduction of silver. The reaction was then performed without any stirring for 5 hours at 60 °C. The suspension was then centrifuged at 2000 rpm during 10 min (three times) and finally redispersed in 5 ml of distilled water.

Protocol 3.4: Synthesis of palladium/copper tetrapods.[123]

A first solution was prepared by mixing 10.3 mg of $CuCl_2 \cdot 2H_2O$, 67.2 mg of AA (ascorbic acid), 116.2 mg of PVP-55K and 116.2 mg of KBr in distilled water (solution 1). A second solution was prepared by dissolving 19 mg of Na_2PdCl_4 (Sodium tetrachloropalladate) (solution 2). In a three neck round bottom flask of 25 ml, 3 ml of solution 1 was heated at 80 °C under magnetic stirring for 10 minutes. 1 ml of the solution 2 was then added. The reaction lasted 2h at 80 °C. At the end of the reaction, the mixture was centrifuged three times at 2000 rpm for 30 minutes. The black product was then redispersed in 10 ml of distilled water.

3.1.2. Results and discussion

The platinum tripod seeds were produced according to protocol 3.1 (Figure 42). The seeds have three branches of about 50 nm in length. They were produced with a yield of about 75 % and the by-products were cuboidal nanocrystals and two-branched nanostructures.
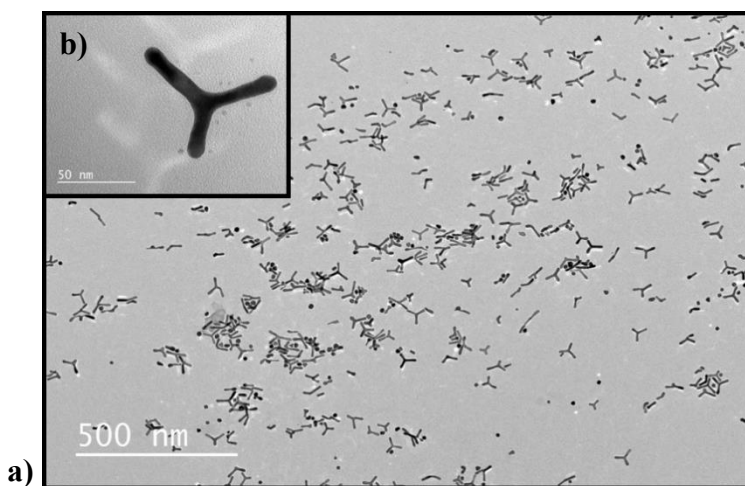
Figure 42: a) TEM image of the platinum tripod seeds (Protocol 3.1) and b) Zoom of one platinum tripod.

The Pt tripod seeds were then used to promote AgNW growth in a polyol synthesis (Protocol 3.2). In a typical procedure, a solution of ethylene glycol was heated to 175 °C prior to the addition of Pt tripod seeds. Solutions of $AgNO_3$ and PVP were then added to the hot solution, resulting in the instantaneous reduction of silver.

Figure 43 shows the products obtained adopting this experimental procedure. TEM analysis revealed that the polyol synthesis damaged the Pt tripods: the anisotropic seeds appeared partly dissolved. In certain specimens, the branches remained but their length was considerably reduced, suggesting a partial dissolution of Pt. Moreover, the silver nanoparticles nucleated through a homogeneous process and formed elongated structures with a large diameter ($\approx$150 nm).
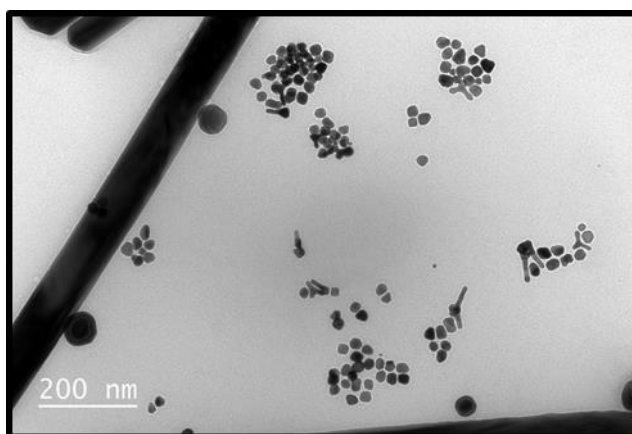
Figure 43: TEM image of silver nanowires synthesized with Pt tripods in polyol medium (Protocol 3.2).

In order to limit the dissolution of the platinum seeds, the experimental conditions used for the silver growth were modified. The synthesis was performed in an aqueous medium at lower temperature (60 °C) instead of in a polyol one (175 °C) according Protocol 3.3. Ascorbic acid was then used as soft reducing agent and CTAB (cetyltrimethylammonium bromide) as a micellar template. In this case, silver nanowires grow from platinum seeds (circled in red in the Figure 44). Dissolution of the platinum still occurred since it was observed that some of tripods presented only one branch or shorter branches at the end of the synthesis.
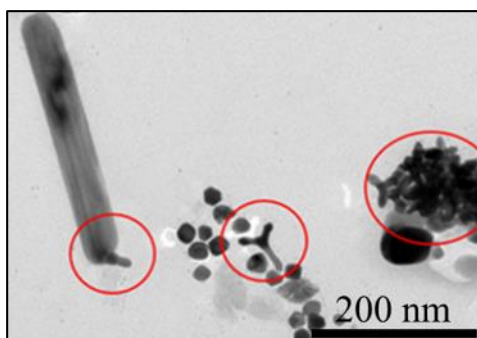
Figure 44: TEM image of silver nanowires synthesized with platinum tripods in aqueous medium at 60 °C.

Decreasing the temperature (from 60 °C to 40 °C) suppressed the problem of dissolution as shown in Figure 45.a, but no traces of silver could be observed at the tip of the branches. By modifying the experimental conditions (pH, temperature, amount of CTAB and ratio of silver precursor/seeds) we could promote the silver deposition on the lateral facets of the seeds (Figure 45.b) but no deposition could be observed on the tips of the Pt tripods. This preferential growth leads to the formation of heterogeneous nanoparticles with unexpected structures that could be interesting for plasmonic studies but not for the application targeted in the present study.
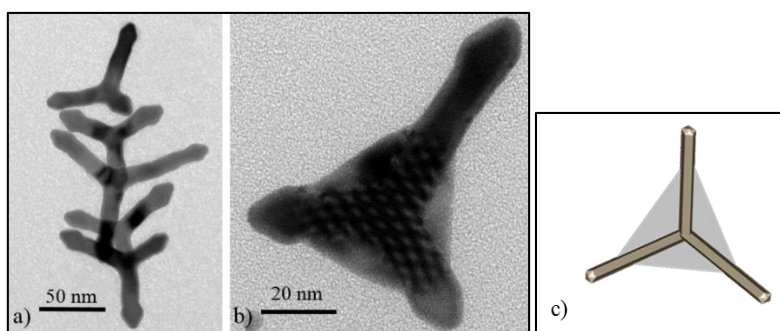
Figure 45: TEM image of silver nanostructures synthesized with platinum tripods in aqueous medium at a) 40 °C and b) at 60 °C with CTAB = 5 mM and c) schematic representation of the platinum tripods coated by silver.

Other tests of heterogeneous growth were performed by using PdCu tetrapods instead of Pt seeds. Palladium/copper tretrapods with a yield of about 90% were synthesized according the protocol 3.4. Their average length and diameter were equal to 30 +/- 5 nm and 5 +/- 1 nm, respectively (Figure 46.b and 46.c). We followed the same synthetic approach (Protocol 3.3) to extend the branches. Figures 46.e and 46.f show the TEM images and the size distribution in length and diameter of the nanostructures formed after silver deposition.
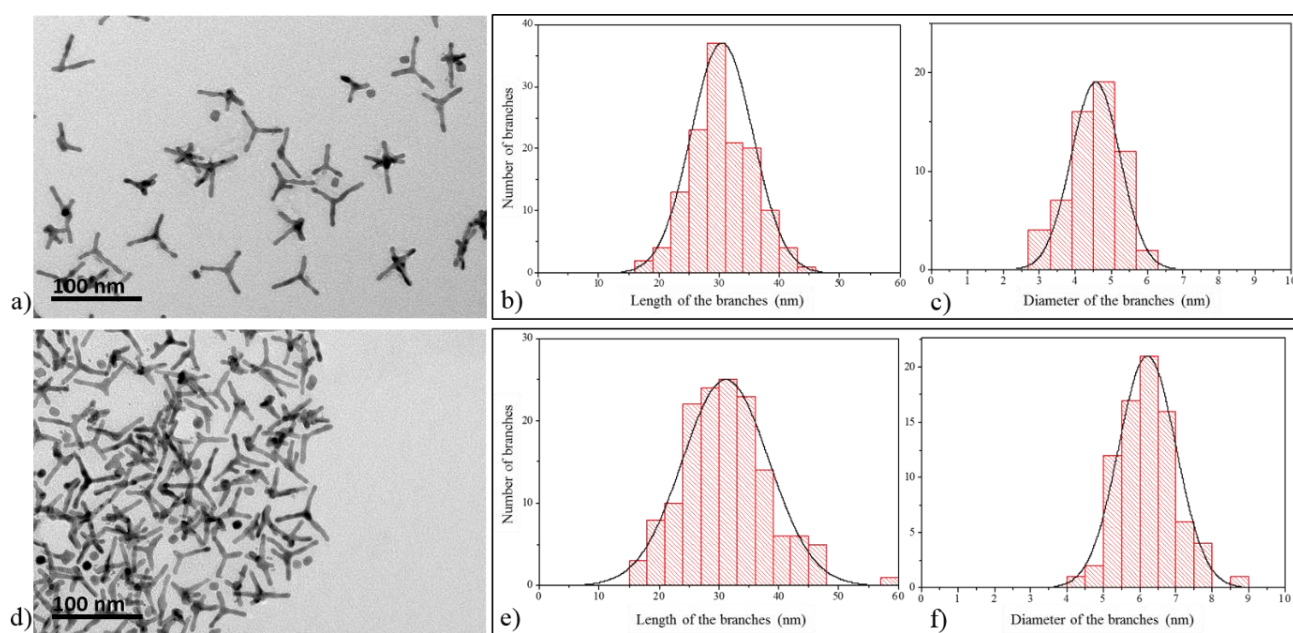
Figure 46: a) TEM images of Pd/Cu tetrapods and their size distributions in b) length and c) diameter. d) TEM images of Pd/Cu tetrapods after silver growth in aqueous medium and their size distributions in e) length and f) diameter.

The average length and diameter of the Pd/Cu@Ag tripods was equal to 31 nm +/- 7 nm and 6 nm +/- 1 nm, respectively. In this manner, silver extension onto the Pd/Cu tetrapods could not be successfully achieved.

Depending on the experimental conditions, silver deposition could also be favored on the lateral facets of the tetrapods. Such deposition leads to the formation of composite nanostructures with interesting features for plasmonic studies (i.e: triangular silver particles with tetrapod seeds, Figure 47).
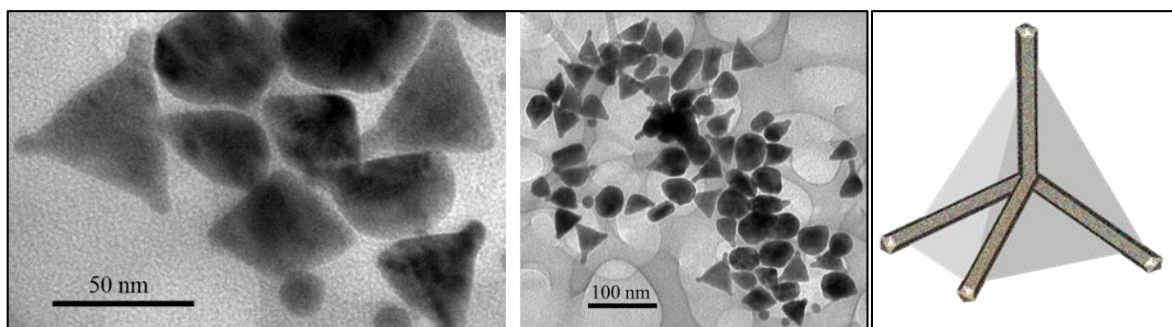
Figure 47: TEM images of silver nanowires synthesized with Pd/Cu tetrapods in aqueous medium at room temperature with CTAB = 1 mM and a schematic representation of the nanostructures.

Despite the lattice mismatch between the seeds and the deposited metal, it was surprising to have so many difficulties to achieve selective deposition of silver onto anisotropic Pt and Pd/Cu seeds. In order to obtain a better understanding on the heterogeneous growth process, in particular with the platinum seeds, we conducted a more detailed study on the real role that Pt seeds play on the formation of silver nanowires via the polyol process.

3.2. New insights in the growth of Ag nanowires from isotropic platinum seeds

Different groups have showed that AgNWs could be produced from pre-formed platinum nanocrystallites.[15] In the literature, it is believed that silver nanowire formation occurs from reduced silver atoms nucleating on multiply-twinned platinum seeds and that one seed gives birth to one nanowire. In a typical synthesis, solutions of PVP and $AgNO_3$ are added dropwise in a suspension of small Pt seeds with an average diameter of 5 nm. Moreover, in most reports studied the platinum seeds are grown from $PtCl_2$ precursor.

In order to understand the role of the Pt seeds over the nanowire growth, we used $Pt(acac)_2$ (platinum acetylacetonate) as the metallic precursor in the following study. This choice allowed us to separate the role of Pt from that of the halide. The AgNW synthesis mediated by the Pt seeds adopted is shown in Figure 48 below.
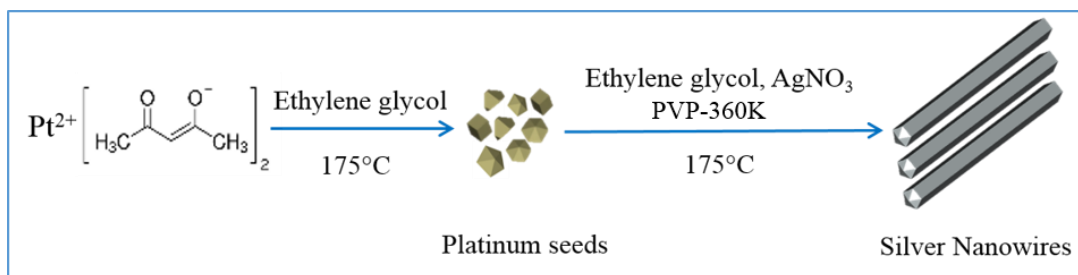
Figure 48: Scheme of the synthesis of silver nanowires from Pt seeds.

Protocol 3.5: **Synthesis of isotropic platinum seeds**

In a 100 ml three neck bottom flask, 0.0031 g of Pt(acac)$_2$ (Sigma Aldrich, assay > 99.98%), PVP (55K) and 50 ml of EG (Jt. Baker) were mixed. The flask was first immersed in an oil bath set at 130 °C for one hour. The flask was then transferred to another oil bath set at 175 °C and the solution in the flask was magnetically stirred (150 rpm) for several hours. After 4 hours, the flask was put in an ice bath for a few minutes to stop the reaction. The solution (Solution A) was then transferred to a tube and kept for several hours in the dark.

HRTEM-STEM-EDX analyses were performed with a JEOL 2200FS microscope operating at 200 kV at the "PLateforme Aquitaine des CAractérisations des MATériaux" (PLACAMAT, U.Bordeaux). For EDX analysis, a 1-nm probe was used in the bright field STEM mode and the Analysis program software from JEOL was used. For this purpose, one drop of the solution was deposited on carbon-coated copper grids.

Optical characterization

The absorption spectra of platinum seeds were recorded in the range of 200-400 nm with an UV-3600 Shimadzu UV-Vis-NIR spectrophotometer. 1 ml of the solution of platinum seeds was mixed with 2,5 ml of EG in ten-mm optical path length quartz cells. The data were recorded and treated with the UVProbe software.

Platinum seeds stabilized with PVP were produced using the protocol 3.5. The reduction process of the platinum precursor was followed by using UV-Vis absorption spectroscopy. Figure 49 shows the UV-Vis absorption spectra of the colloidal suspension

during the growth process and a TEM image of the final products. The metallic precursor exhibited a characteristic optical signature with four bands at 230, 250, 285 nm and 345 nm. Upon reduction, these bands decreased in intensity and the plasmon band characteristic of the Pt seeds of a few nanometers with a maximum in the UV was observed. TEM image confirmed the formation of the platinum seeds (Figure 49). The average diameter is equal to 9.8 +/- 1.2 nm.
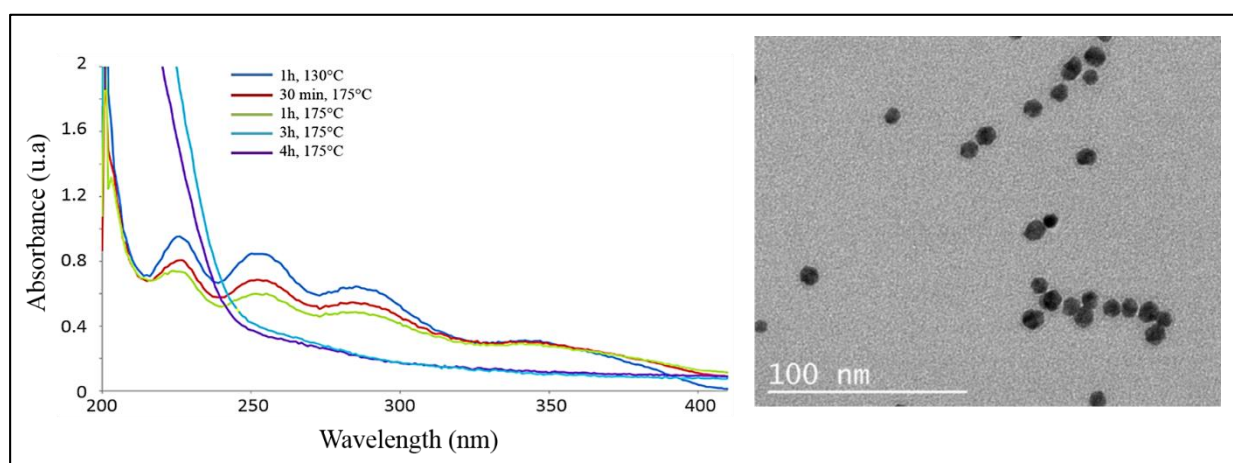
Figure 49: (Left) UV-Vis absorption spectra of the solution of platinum precursor upon reduction at different times. (Right)TEM image of the platinum seeds generated after 4 hours of reduction.

Silver nanowires were successfully synthesized from platinum seeds stabilized with PVP according the protocol 3.2. (Molar ratio n (Ag) / n (Pt) = 3110) Dark field and TEM images presented in Figure 50 show as-synthesized silver nanowires. Their average diameter and length were 61 +/- 10 nm and 37 +/- 23 μm, respectively.
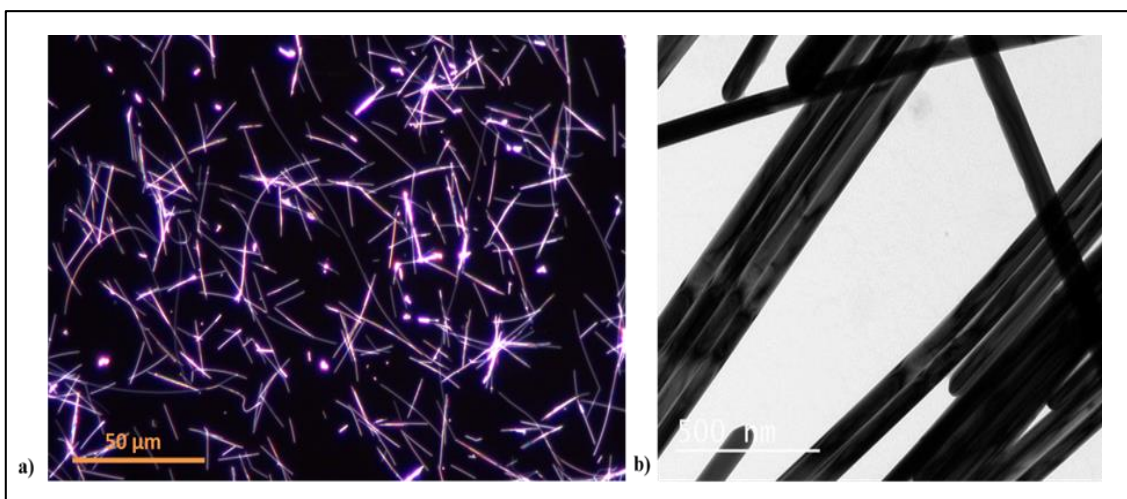
Figure 50: a) Dark field image and b) TEM image of the as-synthesized silver nanowires, respectively.

In order to understand if one seed formed one nanowire and where the Pt seed was located within the 1D particle (tip? center? other location?) different experiments and analyses via HRTEM-EDX, XPS and ICP-AES were performed. Figure 51 shows the elemental cartography of a short silver nanowire and the corresponding EDX spectrum. No trace of platinum within the elongated nanostructure could be observed.
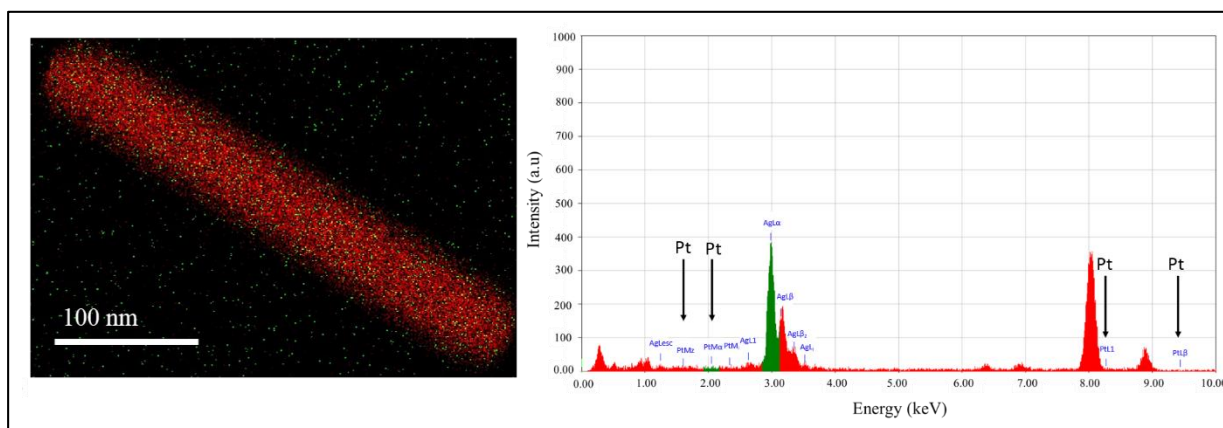
Figure 51: Elemental mapping of a silver nanowire and corresponding EDX analysis.

To investigate the role of Pt seeds stabilized with PVP in Ag NWs growth, a series of experiments were carried out. When Ag nanostructures were synthesized without Pt seeds (protocol 3.2), no wires were formed (Figure 52.a). In contrast, when the synthesis was performed without Pt seeds but with an amount of PVP equivalent to the one present upon addition the Pt seeds, we found that the nanowires could be prepared (Figure 52.b).
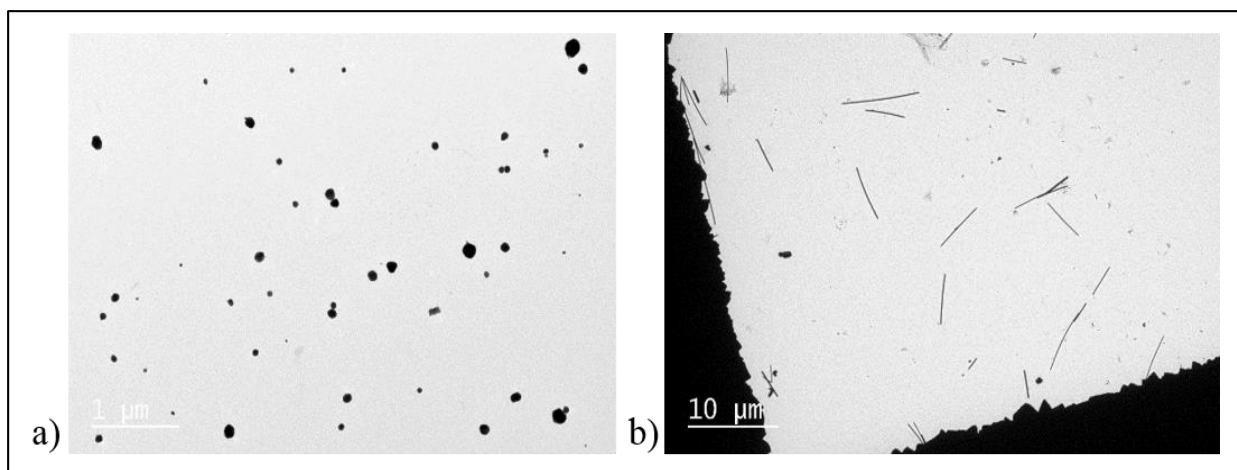
Figure 52: a) TEM images of the silver nanoparticles prepared without platinum seeds and PVP and (b) without platinum seed but with PVP.

In addition, we investigated the effect played by the concentration of platinum seeds in the growth medium on the dimension of the silver nanowires. We have found that by increasing the amount of platinum seeds until a certain threshold, 1D Ag nanostructures could be easily prepared and their yield increased (Figure 53).
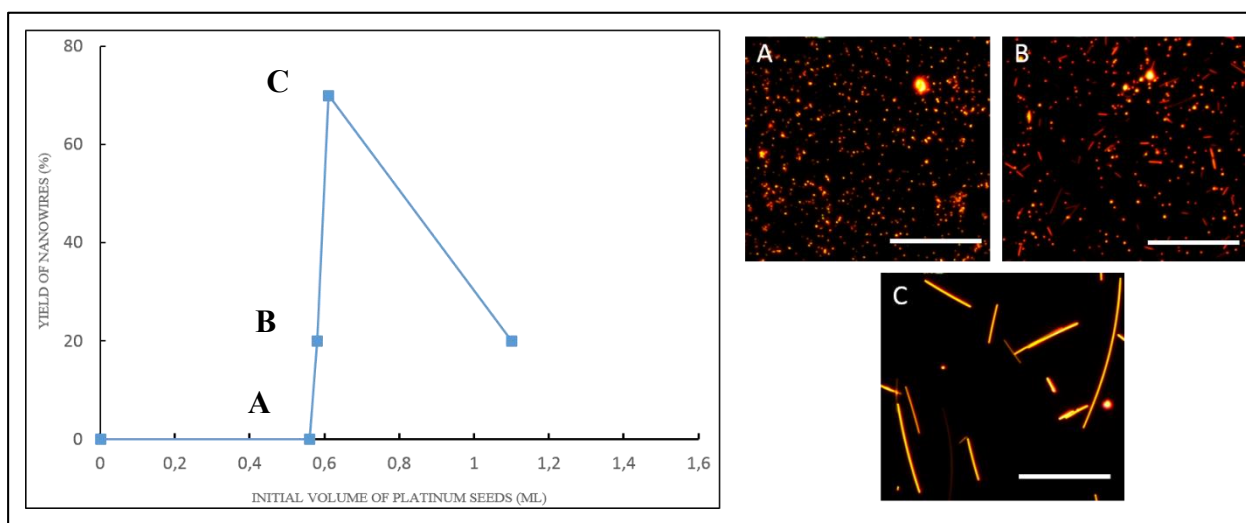
Figure 53: (Left) Plot of the evolution of the yield of silver nanowires as a function of the initial volume of platinum seeds: A) 0.56 ml, B) 0.58 ml and C) 0.6 ml. (Right) Corresponding dark field images. All scale bars correspond to 25 μm.

Our findings show that a low concentration of platinum seeds is in favor of the formation of spheres (Figure 53 A and B), whereas a higher concentration of Pt is the best condition for the formation of Ag nanowires (Figure 53.C). However, note that too high of a concentration of platinum seeds is not favorable for the formation of silver nanowires. In the

latter case, the anisotropic growth is considerably reduced. These experiments indicate that Pt nanoparticles probably do not act as seeds for the evolution of the 1D Ag nanostructures but act as catalysts. On the other hand, PVP may play an important role in assisting the formation of the 1D Ag nanostructures.

Elementary analysis of the silver nanostructures formed in the early stages of a nanowire synthesis were conducted by using a JEM-ARM-200F Cold FEG microscope (Plateforme Castaing, Toulouse). The growth medium was analyzed after 1 min, 3 min, 5 min, and 20 min of reaction. After 1 minute of reaction, organic preforms filled with metallic crystallites could be observed (Figure 54). Chemical analyses revealed that this pre-form was composed of silver nanostructures as well as numerous ultra-small Pt crystallites.
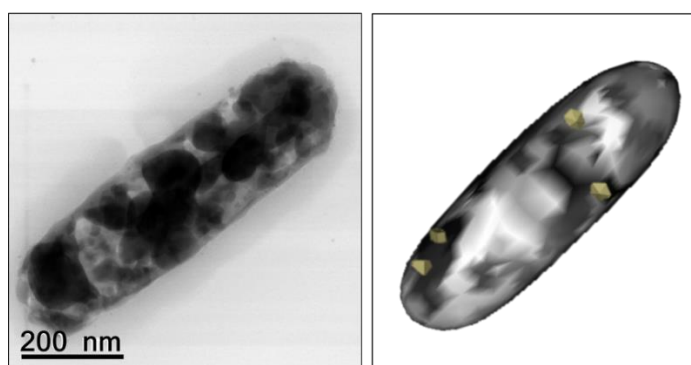
Figure 54: (Left) TEM image of the nanostructure obtained after 1 minute of reaction composed of both Pt and Ag crystallites. (Right) Schematic representation of the nanostructure.

Bright field and dark field HRTEM analyses are shown in the following table (Table 3.1). The first row of the table shows the evolution of the organic preform filled with Ag and Pt crystallites (after 1 minute of reaction) into nanorods (5 minutes) and finally into silver nanowires (20 minutes). In the second row, the corresponding dark field images allow to distinguish Pt seeds from silver nanocrystallites (the ultra-small Pt seeds appear brighter than the silver ones). The last row shows magnification areas of the corresponding nanostructures.

Table 3.1: Bright field and dark field images of the nanostructures synthesized after 1, 3, 5 and 20 minutes of reaction. Magnified images on the nanostructures.
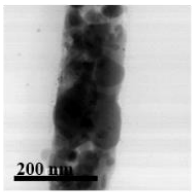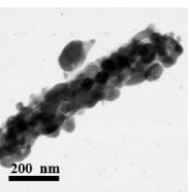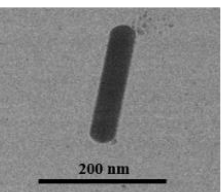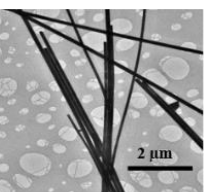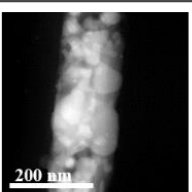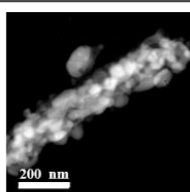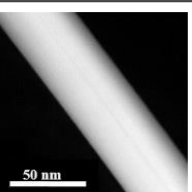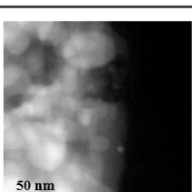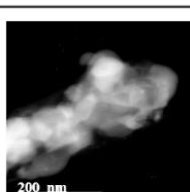
Reaction Time	1 minute	3 minutes	5 minutes	20 minutes
Bright field HRTEM Microscopy				
Dark field HRTEM Microscopy				
Magnification of the nanostructures				

Figure 55 exposes the images and the chemical analyses of the nanostructures formed after 1 minute (top) and 5 minutes (bottom). The small bright crystallites observed in the organic preform, obtained after 1 minute of reaction, were composed of silver and platinum while after 5 minutes, no more platinum could be detected within the silver nanowires.
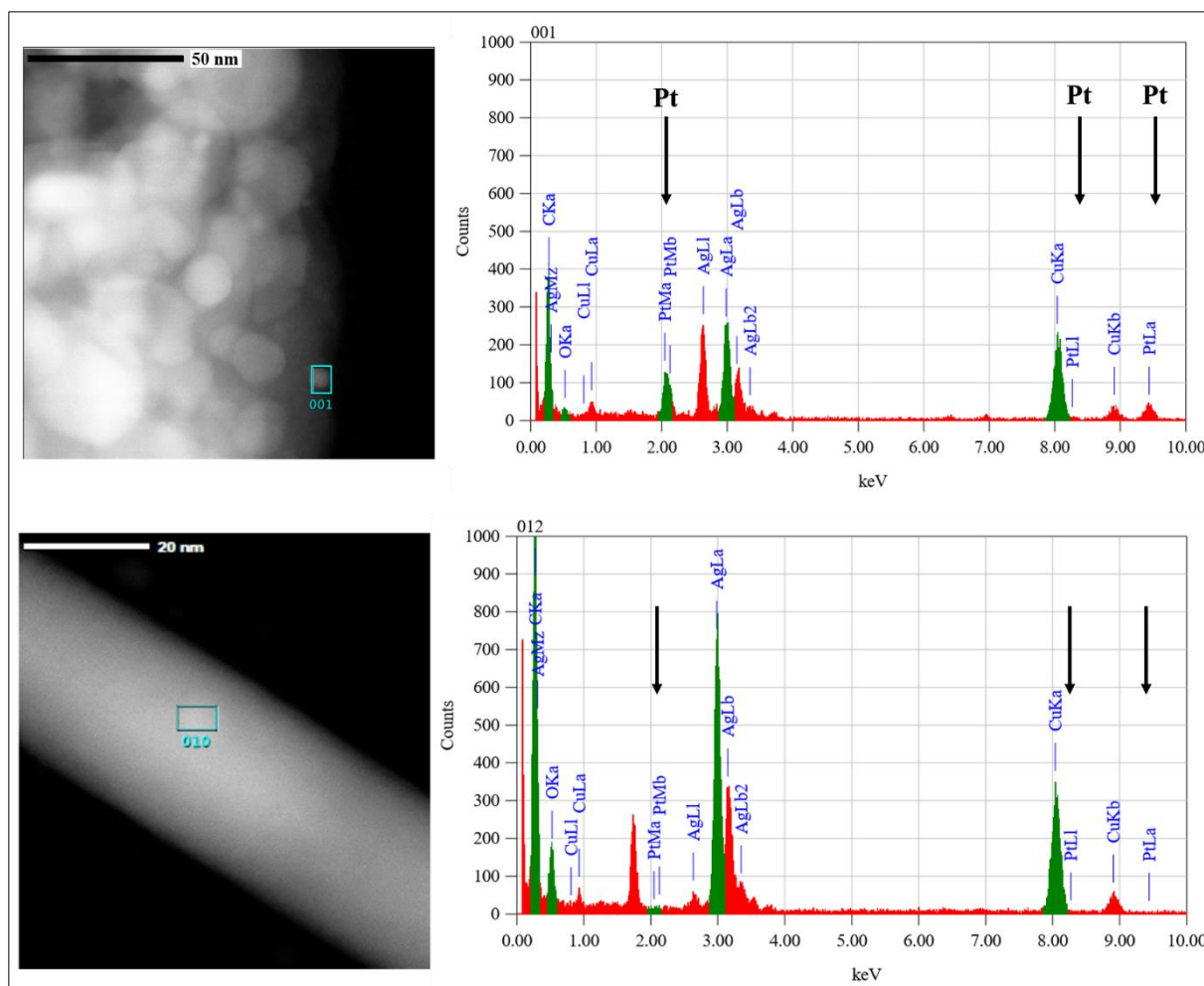
Figure 55: Magnified images and the corresponding chemical analysis of the nanostructures
formed after 1 min (top) and 5 min (bottom) of reaction.

All these observations revealed that under the experimental conditions adopted in our work, silver nanowires are not grown from one Pt seed but from several ones. The silver nanowire formation occurs from an organic preform, most probably generated by the PVP macromolecules (Figure 56). Moreover, the platinum seeds are present in the preform at the initial stages of the Ag nanowire formation but most probably dissolve during the growth process. In order to confirm this hypothesis of dissolution of platinum, an analysis of a colloidal suspension of nanowires was conducted by ICP. The colloidal suspension was centrifuged and both the supernatant and the precipitate were analyzed after their dissolution in nitric acid. The results show that platinum was found in the precipitate (0.435 +/- 0.029 mg/ml) and not in the supernatant. Even though we could not find the presence of Pt by

HRTEM-EDX characterization, this metal seems to be present in the dispersion. There are two possible scenarios to explain the presence of Pt: i) this metal is indeed present within the AgNWs or ii) Pt nanoparticles are formed again in solution after the total formation of the nanowires, given the reducing character of the polyol medium at high temperatures that could lead to the reduction of Pt^{2+} ions into Pt^0.
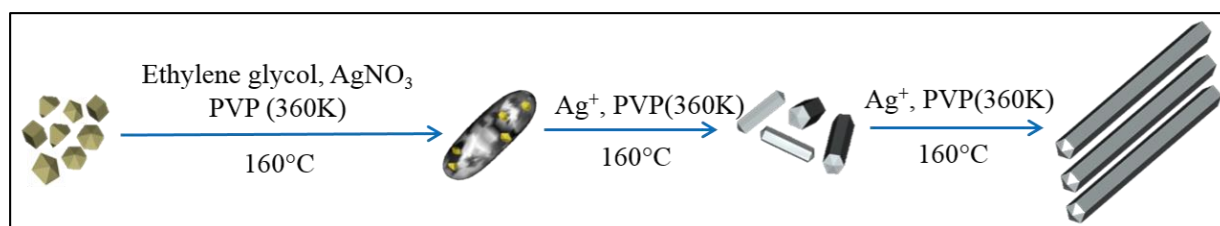
Figure 56: Scheme of the mechanism of silver nanowire formation from platinum seeds.

Closing remarks

To be able to grow novel silver nanostructure architectures, this study showed that it is important to obtain a good understanding of the growth mechanism of silver nanowires via the polyol process. Investigations revealed that the internal crystalline structure of the Pt seeds has no impact on the nanowire formation. These 1D structures form instead from a cavity generated by the PVP macromolecules. The Pt seeds catalyze the reduction of the silver precursor within the organic preform and accelerate the growth of the silver crystal. Nevertheless, if the concentration of Pt seeds is too important, the generation of silver atoms is too high and in these conditions, no anisotropic growth could be induced. These new insights on the growth mechanism of silver nanostructures from platinum seeds enabled us to understand why the extension of the branched seeds was not successful in polyol medium. Therefore, we decided to adopt other synthetic approaches to elaborate branched nanostructures.

3.3. Investigation of the modifications of the polyol process to induce branched nanowires

3.3.1. Primarily tests of anisotropic growth

To obtain branched NWs, one could imagine further experiments by modifying the growth conditions of the polyol process (described in protocol 3.6) during the formation of Ag NWs. The effects of an addition of a transition metal ion or a co-surfactant may induce branch formation as demonstrated in the literature.[81,92,93] A process involving the input of ultrasound irradiation during the growth process has been tested as well.

Protocol 3.6: Synthesis of 1D- silver nanowires

In a 50 ml three neck bottom flask, 8.6 ml of 1.2-Propanediol (Pdol) were mixed with 8.6 ml of a solution of PVP1300K in Pdol (233.4 mg dissolved in 10 ml). The mixture was under vigorous stirring for 10 minutes. 6 ml of a solution of $AgNO_3$ (110.4 mg dissolved in 6.5 ml) was injected into the previous one under vigorous stirring. 5 minutes later, 70 µl of a solution of NaCl in Pdol (0.1M) was slowly added to the medium under vigorous stirring. 5 minutes later, the flask was set into an oil bath for 1h15 with the stirring speed set at 100 rpm. At the end of the process, the flask was introduced in an ice bath for a few minutes in order to reach room temperature. A two-step purification with a successive addition of acetone and a solution of PVP360K diluted in water (0.1 M) was performed in order to precipitate/redisperse the silver nanowires.

Protocol 3.7: Modification of the protocol 3.6 by addition of RuCl₃

Same initial experimental conditions as protocol 3.6. 29 µl of a solution of NaCl in Pdol (0.1M) were introduced slowly instead of the 70 µl added in the previous case. Finally, 184 µl of a solution of $RuCl_3$ in Pdol (7.7 mM) were also slowly added to the medium under vigorous stirring (or added drop by drop at 0.75 ml/min after 40 minutes of reaction).

Protocol 3.8: Modification of the protocol 3.6 by an addition of a co-surfactant

Same initial experimental conditions as protocol 3.6. 8.6 ml of 1.2-Propanediol (Pdol) is mixed with 5 ml of a solution of PVP1300K in Pdol (233.4 mg dissolved in 10ml) and 3.6 ml of a solution of PEG-amine in Pdol (0.478g dissolved in 3.6 ml).

Protocol 3.9: Modification of the protocol 3.6 by the irradiation of the solution during the growth process

Same initial experimental conditions as protocol 3.6 but the initial precursor quantities have been divided by 3. After 30 minutes of reaction, the total volume was picked-up and ultra-sound was applied by using a sonicator Vibra-cell^{TM} 75042 (Bioblock scientif, 500W, 20 KHz) under the following conditions: time: 1 minute, amplitude: 20%, pulse: 0 on, 0 off). To avoid overload, the solution is introduced into an ice bath during the ultra-sound input.

Figure 57 shows a series of TEM images of the reaction products based on these different inputs. The control experiments led to the formation of conventional AgNWs with a mean diameter of 138 +/- 20 nm and a length of 50 µm (Figure 57.a). On the other hand, adding RuCl$_3$ in the reaction medium results in the formation of some Ag NWs with a 'V-like shape' in low yield and an abundance of spherical particles (Figure 57.b). Figure 57.c shows the products obtained when using a co-surfactant such as a PEG-amine, where only Ag nanoparticles and a small amount of nanowires with a 'Y-shape' can be observed. The most promising approach consisted in the ultrasonic irradiation of the colloidal suspension during the growth process (Figure 57.d). Interestingly, this approach could drastically modify the shape of the NWs and induce the formation of "V-like shape and Y-like shape nanowires" in high yield. In our opinion, the change in the geometry of the nanowires is an indication of irradiation-induced melting. This process will be further investigated in the following section.
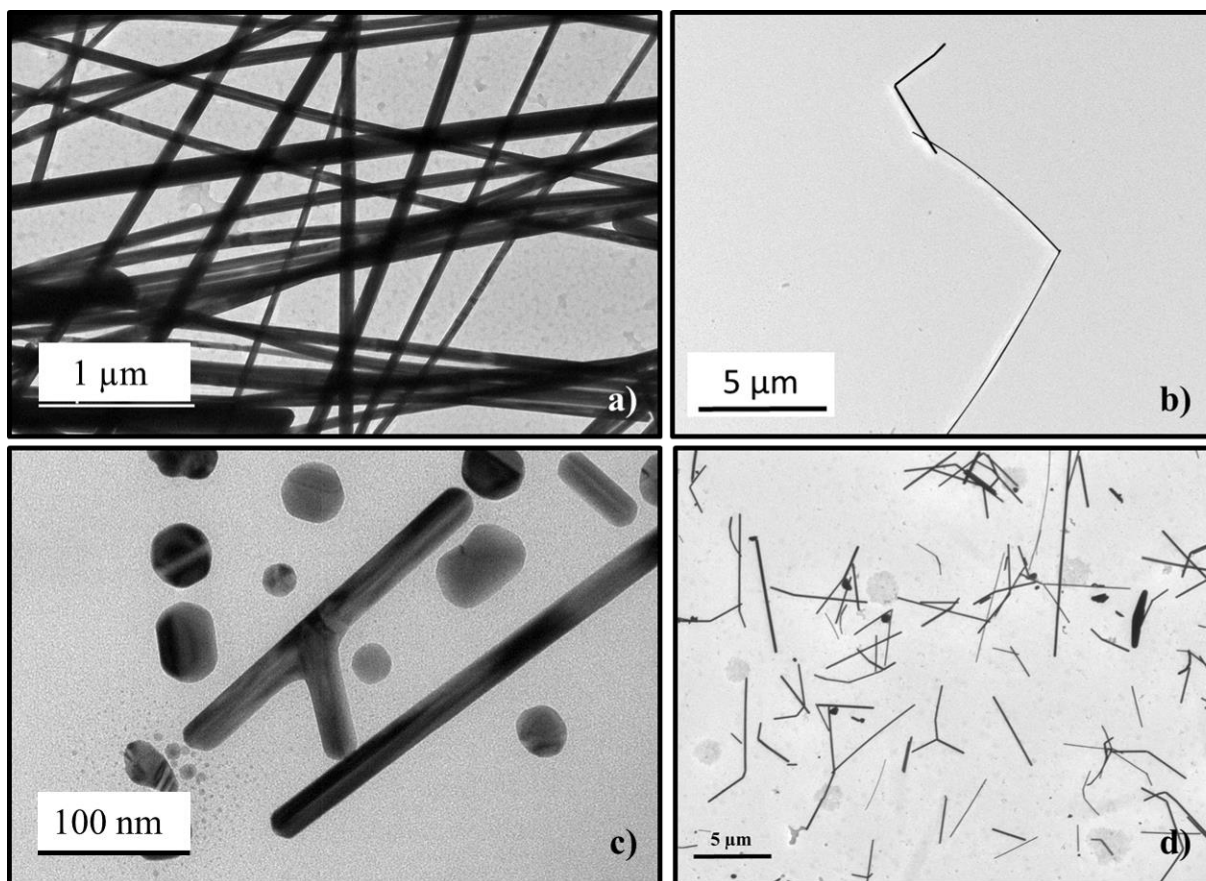
Figure 57: a) Conventional silver nanowires synthesized following the protocol 3.6, b) effect of the addition of RuCl₃, c) effect of the addition of a co-surfactant and d) effect of ultrasonic irradiation.

3.3.2. Input of ultra-sounds during the polyol synthesis

The change observed in the geometry of the nanowires upon ultrasonic irradiation of the growth medium according the scheme of the Figure 58 could be assigned to different possible mechanisms: (i) the ultrasonic irradiation may break the silver nanowires into small segments that are later welded in the growth medium or (ii) the ultrasonic irradiation may favor the formation of defects on the surface of the nanowires that could induce the growth of branches.
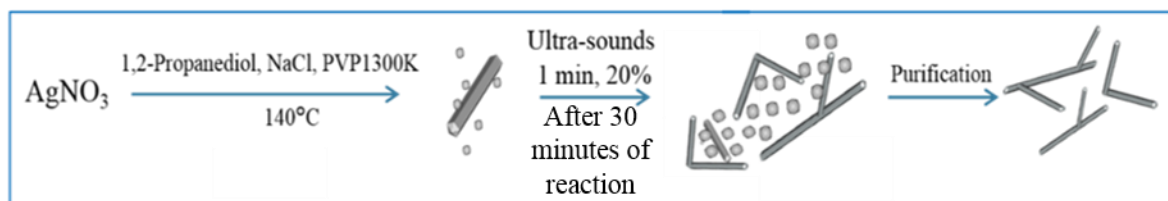
Figure 58: Scheme of the modification of the polyol process via the input of ultra-sound vibrations during the synthesis.

82

Since the first tests were successful, we investigated the effect of the irradiation time on the morphology of the products formed as well as the moment at which the ultrasonic treatment is performed. In a conventional synthesis of 1D silver nanowires (Protocol 3.6), the reaction medium turned from colorless to progressively yellow to dark orange. This coloration was due to the formation of small silver nanoparticles. Then, at a specific time, a 'colorimetric switch' corresponding to a grayish opaque coloration was observed, indicating the formation of the wires. In the specific condition of the protocol 3.6, the emergence of the first wires was observed approximately 20 minutes after the beginning of the heating process. To evaluate the effectiveness of the ultrasonic irradiation on the change of wire morphology, a series of experiments were performed by irradiating the solution during the growth process after 15, 20, 30 and 40 minutes. When ultrasonic irradiation was performed before 20 minutes, no silver nanowires were formed. On the other hand, when irradiation was performed after 30 minutes, the branched nanowires were observed. In this case, the silver nanowires are transformed from straight to a 'Y-shape' or a 'V shape' (a TEM overview image of the reaction product formed in this experimental condition is shown in the following image in Figure 59). The yield of boomerang-like silver nanowires (V shape) is about 75% while the one of 'Y' type nanostructures is 10%. Moreover, we performed a statistical analysis of the opening angle of the 'V-shape' structures, leading to a value in the range between 70° and 160°. Interestingly, no preferential bending angle could be observed.
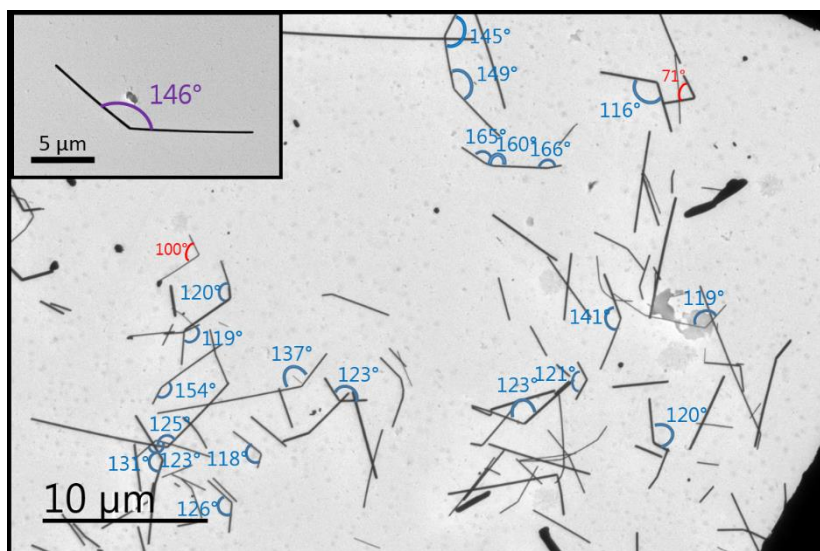
Figure 59: TEM image of nanostructures synthesized upon ultrasonic irradiation of the growth medium according to the experimental conditions of the protocol 3.9.

In addition to the previous data on the 'V-shape' structures, TEM images performed on the smaller population of 'Y-shape' wires (Figure 60) show that no specific opening angle could be detected in this case either.
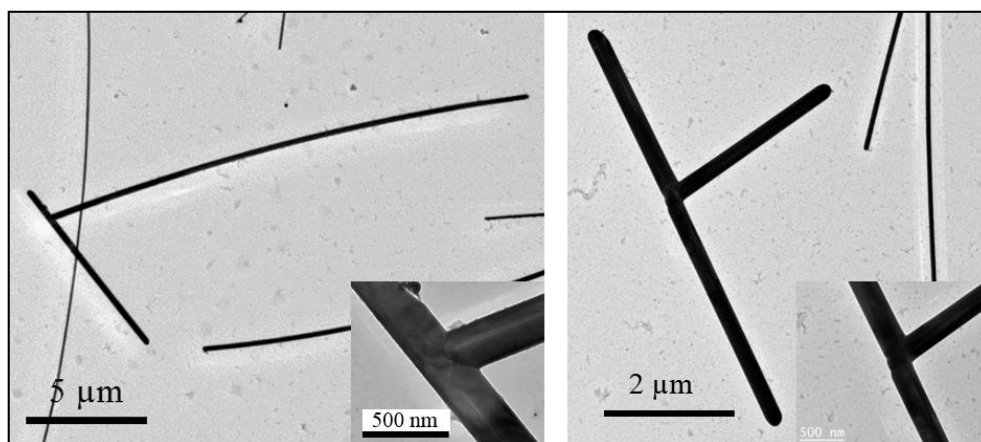
Figure 60: TEM images of the Y-shape nanowires produced when ultra-sound irradiation was applied during the growth process following Protocol 3.9.

By tuning the duration of the ultrasonic irradiation or its power density, it was not possible to generate nanowires with more than two branches. Along these lines, modifying the time of irradiation led to the formation of shorter segments as shown in Figure 61.
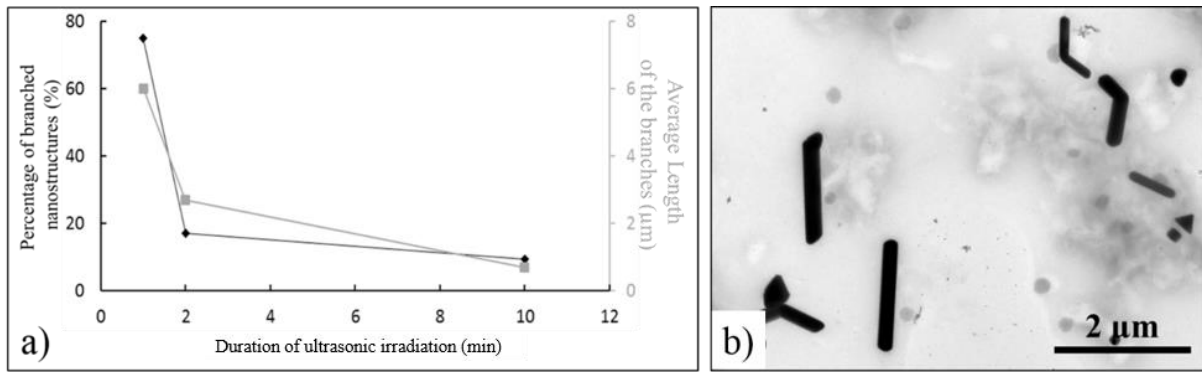
Figure 61: a) Percentage of branched silver nanowires as a function of the duration of ultrasonic irradiation and b) TEM images of the nanostructures obtained when ultra-sound was applied for 10 minutes.

In a different set of experiments, we found out that by gradually increasing the power of the ultrasonic irradiation, the nanowires could also be cut into shorter fragments, leading to the formation of small-unbranched nanostructures (Figure 62).
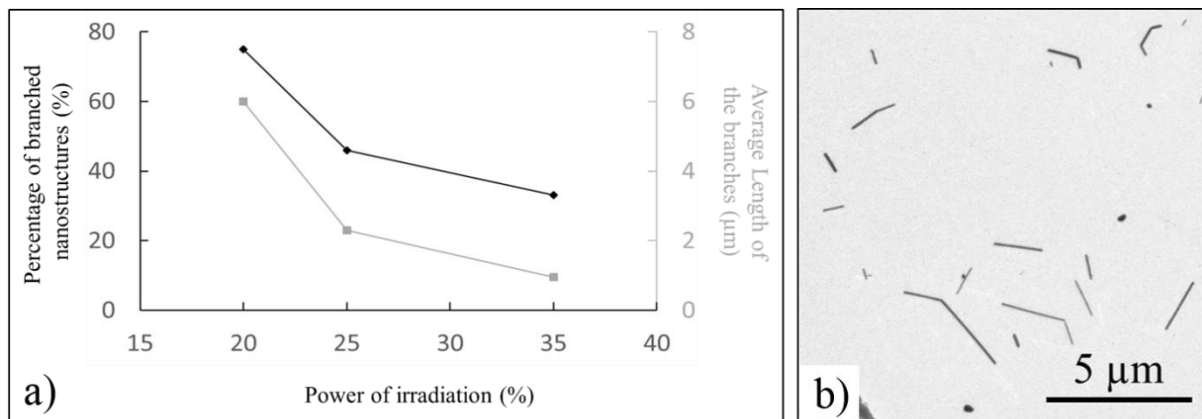
Figure 62: a) Percentage of branched silver nanowires in function of the power of irradiation and b) TEM images of the nanostructures obtained when the power of irradiation was about 35%.

We can conclude that the use of ultrasounds during the growth process allowed to induce branched nanotructures. Nevertheless, the length of such objects remains limited, thus reducing their interest for the fabrication of elecrodes.

3.3.3. Analysis of the crystalline structure of the branched nanowires

Two types of nanostructures could be observed: branched (Figure 63.a) and two welded silver nanowires (Figure 63.b).
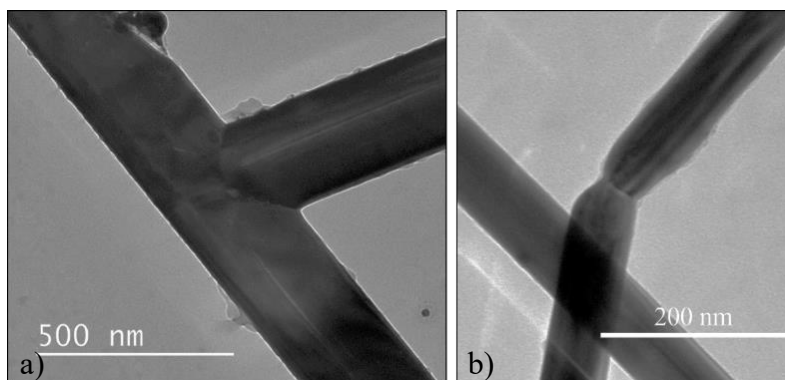
Figure 63: a) TEM image of a branched junction and b) TEM image of welded nanowires having a grain boundary junction.

Both types of junctions were analyzed by electron diffraction in order to understand the impact of the ultrasonic irradiation on the formation of these nanostructures. One would like to understand if the formation of a branch along a nanowire results from a melting of two segments or from the growth of a protrusion from the surface of a growing nanowire.

Electron diffraction analysis

5 µl of a diluted solution of branched nanostructures in ethanol was deposited onto a TEM grid. Analyses were performed with a JEOL 2100FS microscope operating at 200 kV at the "PLateforme Aquitaine des CAractérisations des MATériaux" (PLACAMAT, Pessac).

Procedure for the XRD analysis of the silver nanowires

Several drops of silver nanowires solution were dropped on a plate holder. Once the holder is full and the solution has dried, the sample is place into the X-ray diffractometer. (Goniometer = PW3050/60, Bragg Brentano Geometry). The anode material is the copper with a K-α1 = 1.54060 Å and K-α2 = 1.54443 Å and K-β = 1.39225Å. The ratio K-α2 /K-α1= 0.5.

Figure 64.a shows the selected area electron diffraction (SAED) pattern obtained by focusing the electron beam onto a conventional silver nanowire. It could be indexed to an FCC structure but the diffraction pattern clearly evidenced that the silver nanowire was not a single crystal. The diffraction spots could not be assigned to any particular simple pattern

86

associated with face-center cubic silver (FCC). The diffraction pattern is complex and some reflections are doubled.
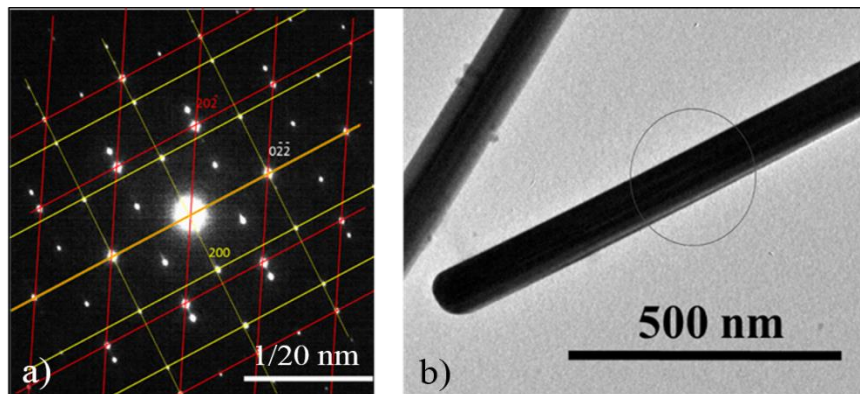
Figure 64: a) Indexed electron diffraction pattern of a silver nanowire and b) TEM image of the silver nanowire.

As shown in Figure 65, the pattern contained an interpenetrated set of two individual diffraction patterns corresponding to two different orientations ([1.1-1] and [0,1,-1]). The mutual orientation of these two zones induced the generation of a double diffraction, which accounted for the remaining spots. Each nanowire contains five single-crystalline sub-units. These assignments were consistent with results obtained for multiply twinned silver having the same pentagonal symmetry in the literature.[76,78]
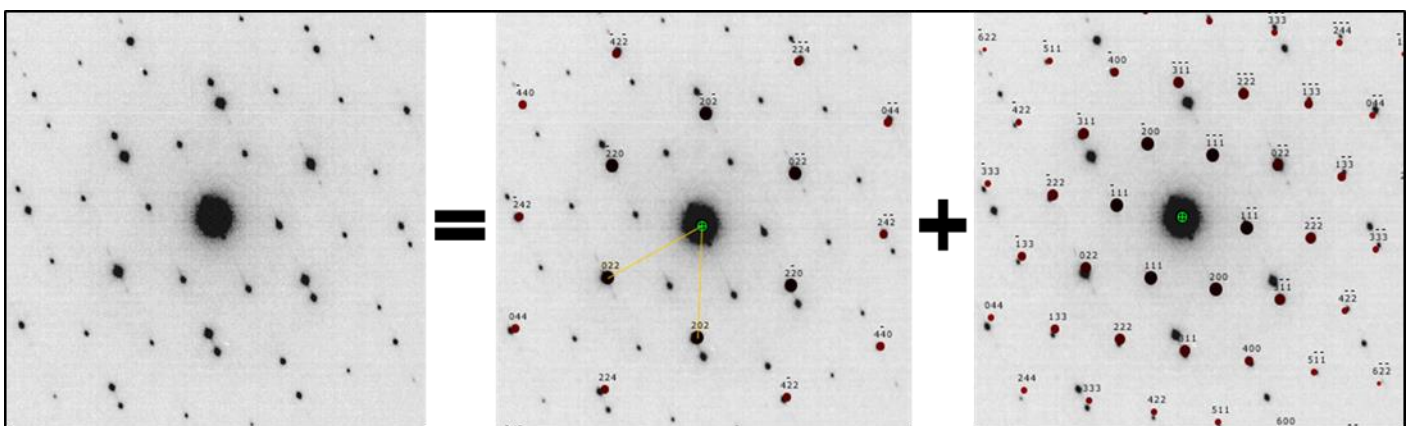
Figure 65: a) Electron diffraction pattern of the silver nanowire presented in Figure 64.b, b) and c) Indexation of the diffraction pattern in direction of the electron beam [1,1,-1] and [0.1.-1] respectively.

Several diffraction patterns were recorded along the axis of the nanowire with the orientation of the electron beam (Figure 66). One could observe that the diffraction pattern slightly changes from one area to another one. Some diffraction spots did not appear

depending on the zone analyzed, suggesting that the nanowire was not deposited on one of its five flat side surface on the substrate but was twisted along the entire longitudinal direction.
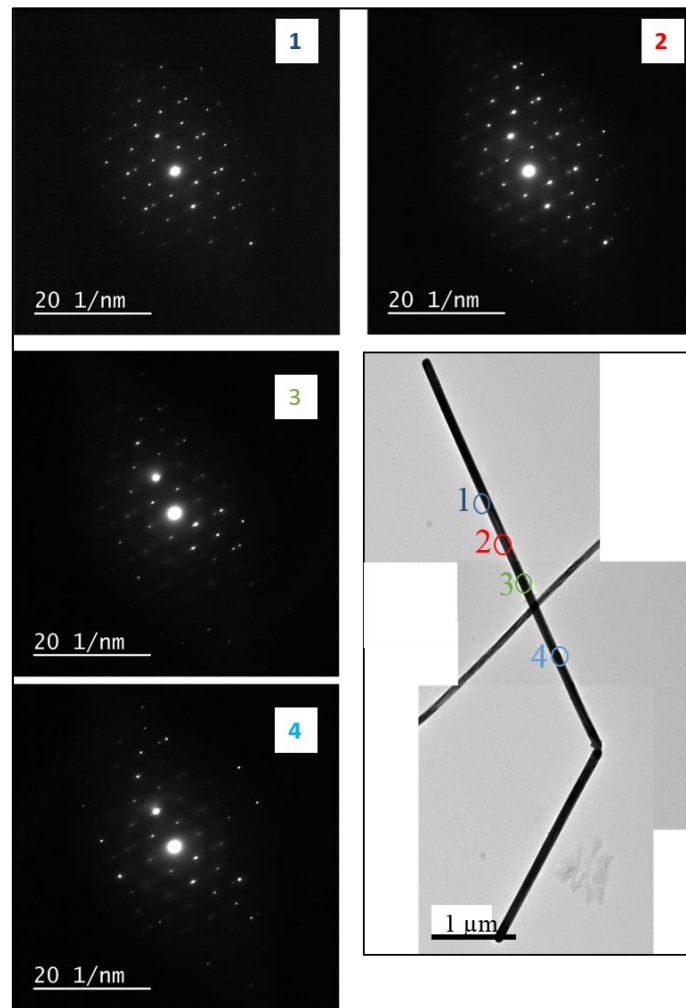
Figure 66: 1, 2, 3, 4 are the electron diffraction patterns of the different zones along the AgNW presented in the TEM image.

In the case of a grain boundary junction of two welded silver nanowires, the crystallographic orientation between the two segments was the same (Figure 67). However, one observed a difference in the macroscopic orientation. The orientation being at the atomic scale involves the connection of the whole structure. The angle measured in the diffraction pattern in Figure 67 is good agreement with the angle measured in the TEM image.
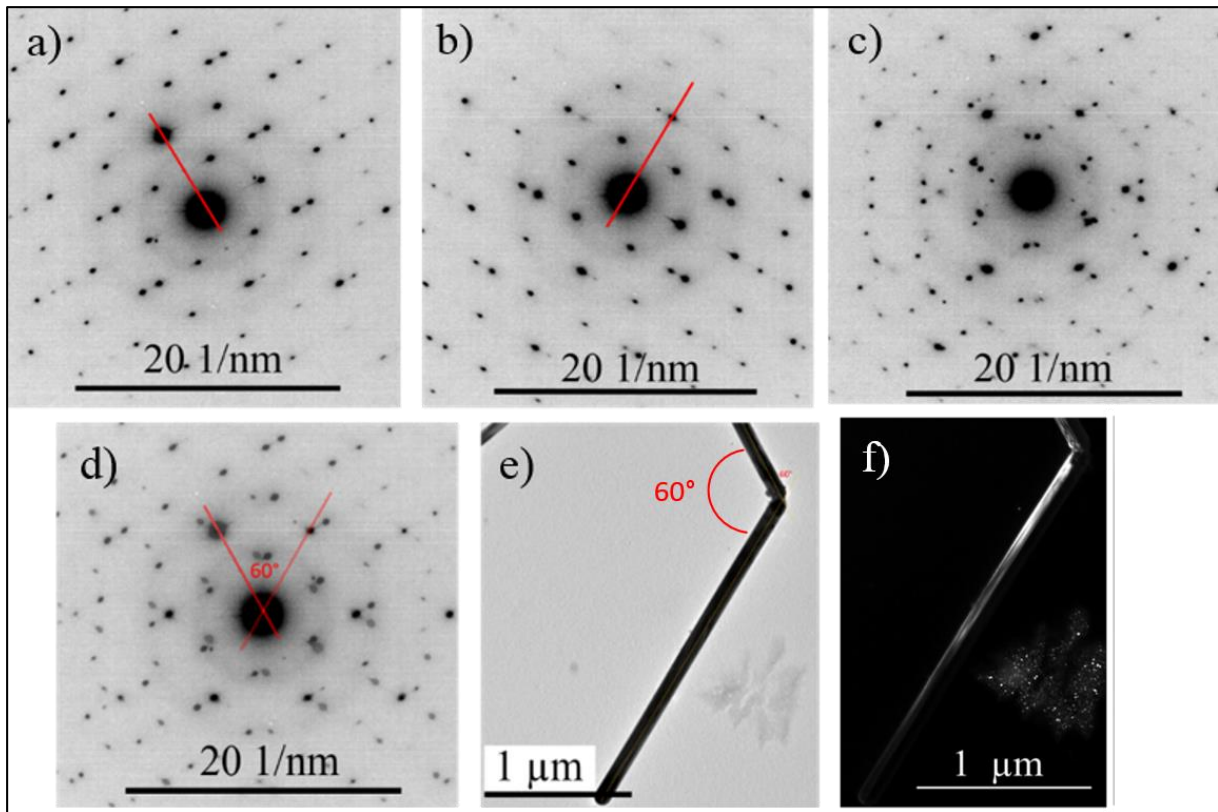
Figure 67: Diffraction patterns of the upper branch a) and the lower branch b) of the nanostructure, c) Superposition of the two diffraction patterns, d) Experimental diffraction pattern of the junction, e) Bright field and f) Dark field TEM images of the branched nanostructure.

Dark field TEM image of the same nanostructure confirms the previous observation of a twisting along the longitudinal direction of the nanowire (Figure 67.f). In the case of a "branched junction" (Figure 68), no difference in the diffraction pattern was observed. The diffraction patterns of the different branches were similar to those of the wires with a "grain boundary" junction. The nanostructure presents the same twinning along the branch. Therefore, the electron diffraction can not allow to get information on the mechanism of the formation of the branch.
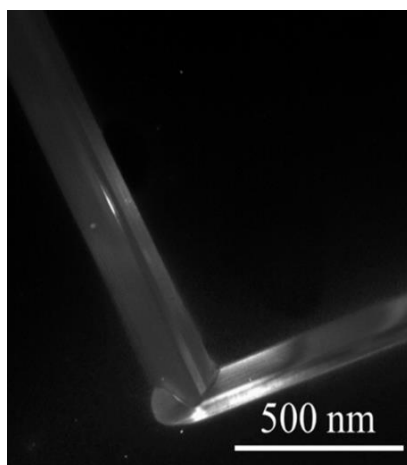
Figure 68: Dark field image evidencing the twin in a branched nanostructure.

Figure 69.a and b show the XRD pattern of branched silver nanostructures generated via ultrasonic irradiation (Figure 59) and the one of conventional silver nanowires (Figure 57.a) respectively. The 4 peaks correspond to (111), (200), (220) and (311) planes of Ag (FCC crystal structure, JCPDS card 04-0783). Note that the 3 peaks (200), (220) and (311) at high angles are broadened and asymmetric. This could be due to the presence of an impurity in the crystal lattice, microstrains or the decrease of the domains of consistencies. Traces of AgCl could be detected in the pattern. The peaks located at $2\Theta = 28°$ and $2\Theta = 32°$ with a very small intensity could be assigned to (111) and (200) reflections of the silver halide.
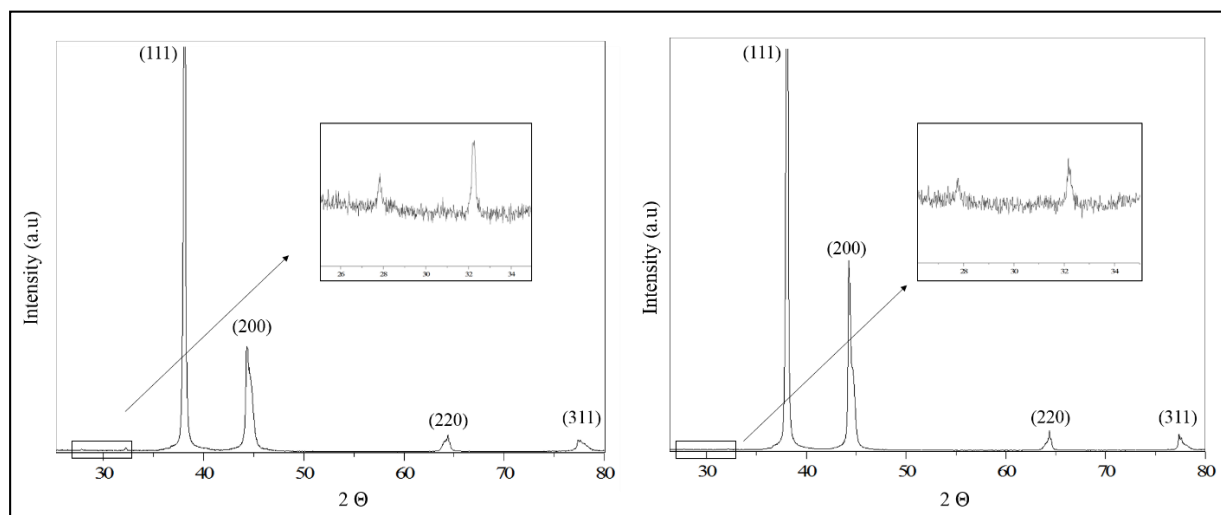
Figure 69: XRD pattern of the a) as-synthesized branched silver nanowires and b) 1D silver nanowires.

90

Further refinements of the XRD pattern evidenced that the crystal structure of the wire was distorted (Figure 70). The calculated curve could fit the broaden peaks when a monoclinic structure was considered (P 2/m space group).
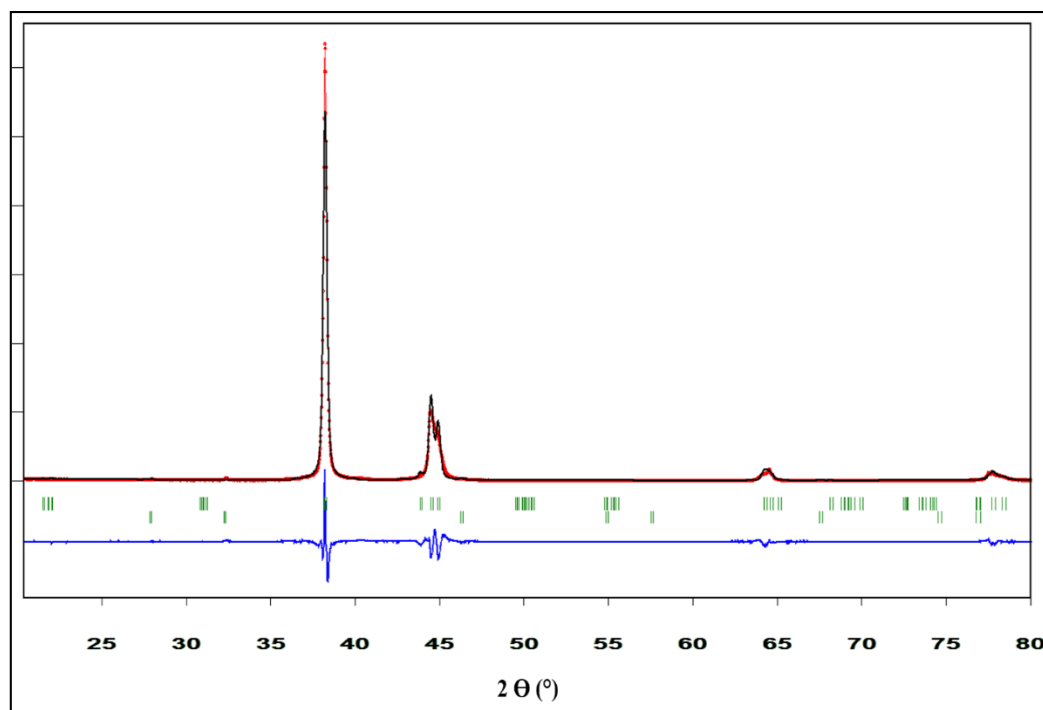
Figure 70: XRD pattern of the as-synthesized branched silver nanowires (black curve) and the refinement corresponding (red curve).

The lattice parameters of the branched nanostructures are the following: a = 4,07 Å, b = 4,03 Å and c = 4,12 Å and β = 89,88°. Knowing that the space group of silver is F m –3 m (a = b = c = 4,086 Å with a cubic crystal system), we believed that the structure underwent a monoclinic distortion of the cubic lattice. In order to confirm this hypothesis, the lattice parameters were measured by a detailed investigation of the electron diffraction patterns of the structure. The following Figure 71.a,b and c show the associations of the theoretical indexed reflections to the experimental one, considering the previous lattice parameters of P 2/m calculated by refinements. These indexations were performed in 3 different directions: [0,1,-1], [1,-1,0] and [-1,0,1]. The Figure 71.d shows the theoretical indexations of the reflections considering the lattice parameters of the silver FCC. The fit of the theoretical indexations is possible when the direction taken in account in [-1,0,1] and a slight shift

between the theoretical indexations and the experimental ones is noticed for the other theoretical indexations.
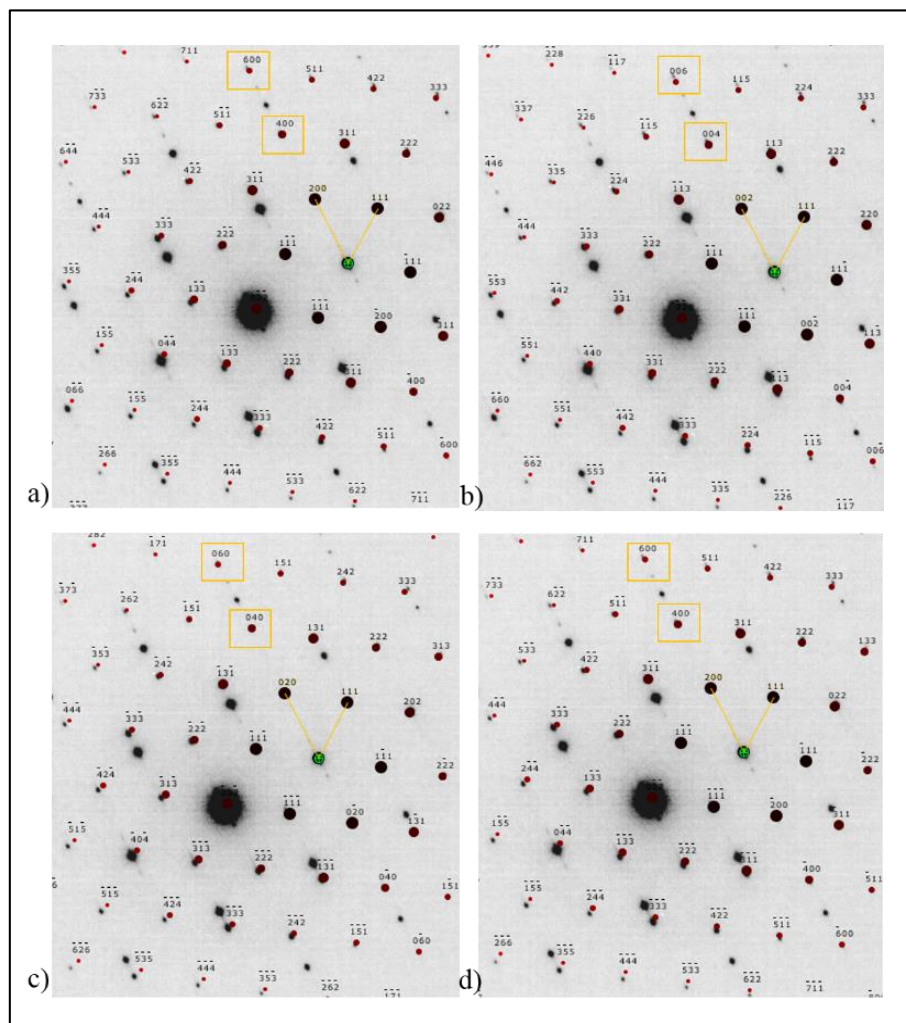
Figure 71: Theoretical P 2/m indexations of the reflections of the diffraction patterns following a) [0,1,-1], b) [1,-1,0], and c) [-1,0,1] directions. d) Theoretical F m -3 m indexations following the [0,1,-1] direction.

The electron diffraction analysis evidences that the crystal structure of the branched silver nanostructures was not cubic anymore. Further analysis should be performed to confirm the presence of the distortion of the crystal lattice. This one could be due to the presence of traces of Cl$^-$ in the interstitial positions or randomly spread within the crystal lattice of the metal.

3.4. Conclusion

Two strategies were adopted to generate branched nanowires: (i) Seed growth from anisotropic seeds and (ii) modifications of the conventional polyol process. Regarding the first approach, the different investigations showed that it was challenging to perform the growth of silver from anisotropic seeds. The dissolution of the platinum seeds being the major issue in this process. From this study, we explore the growth mechanism of silver nanowires from platinum evidencing the initial presence of an PVP preform and the number of seeds involved in the gowth of one nanowire. The second approach based on the input of ultrasonic vibrations during the growth process of silver nanowire was more successful. The irradiation induced the formation of numerous nanowires with a 'V' or a 'Y' shape. The branch formation mechanism has been investigated by varying the different parameters of the synthesis. Structural analyses of the branched nanowires revealed that the crystal lattice underwent a monoclinic deformation of their cubic (FCC) structure. This distortion may be due to the presence of microstrains or to the presence of traces of Cl^- within the crystal nanostructure. Even though the results are promising, the length of the branched nanowires limits their attractiveness to elaborate transparent electrodes having enhanced performance.

Chapter 4: Thermal and chemical instability of silver nanowire electrodes

Although silver nanowire networks have numerous advantages in comparison to ITO (mechanically flexible, cheap, and compatible with roll-to-roll deposition techniques, plastic substrates and deposition on top of organic layers), they are not yet attractive enough to replace the doped metal oxide material in commercial devices. One major reason for this is the instability of silver nanowires, which is the most stringent requirement of the electrodes in devices such as solar cells and LEDs. As will be discussed more in this chapter, because current is continuously flowing across the electrode in these latter devices, Joule heating leading to nanowire breakdown is a severe issue. Secondly, unlike in touch screens, where the nanowires can be protected from the air by full encapsulation in a non-conductive material, this cannot be done in solar cells and LEDs because current needs to flow between the electrode and the active part of the device.

In this chapter, we perform two studies to tackle the thermal and chemical stability of the electrodes. The main goal of the thermal investigations was to better understand the propensity of silver nanowire electrodes to self-heat during their operation. The electrodes were fabricated, characterized and modeled by Hadi Khaligh Hosseinzadeh, a Ph.D student at the University of Waterloo supervised by Prof. Irene Goldthorpe. Luzhu Xu (from Prof. Michael Pope's research group at the University of Waterloo) deposited and characterized the graphene oxide layer. Alireza Khosropour (from Prof. Andrei Sazonov's research group at the University of Waterloo) helped develop nanowires' network model. I experimentally characterized the Joule heating and the variation of temperature of the working electrode by using of a high quality infrared imaging camera at the University of Bordeaux. This equipment, along with the associated expertise of Dr M.Romano and Dr C.Pradère (TREFLE, U.Bordeaux) allowed us to study the behavior of nanowire electrodes under current flow. The first section of this chapter represents an expanded version of an article published in

Nanotechnology.[107] In the second part of this chapter, I report how to chemically modify the surface of the nanowires to limit their corrosion and the resulting electrode resistance over time which is a severe problem hindering their use in commercial devices.

4.1. Self-heating problems of silver nanowire electrodes

AgNW transparent electrodes are under development for use in commercial touchscreen applications. These touchscreens work by creating and changing an electric field between the nanowire electrode and a parallel electrode, with an active dielectric material in between that responds to the field. A current flows across the nanowire electrode only for a short time to change its potential during switching, with minimal current flowing otherwise. This is also true for other capacitive- type devices such as smart windows.[46] However, for devices such as solar cells, organic light emitting diodes (OLEDs), and transparent heaters, there are long periods of time when current continuously flows across the transparent electrode during device operation, resulting in Joule heating. Although not typically problematic for ITO electrodes, H.K. Hosseinzadeh has previously shown that the Joule heating created at the current levels typically encountered in organic solar cells causes nanowire electrodes to fail in a matter of days. The nanowires breakup and electrical discontinuities appear in the electrode.[67]

Multiple mechanisms can lead to silver nanowire degradation. Silver nanowires corrode in air, specifically due to the presence of trace amounts of sulfur, and this corrosion phenomenon is accelerated at elevated temperatures.[51,131] Additionally, silver nanowires are not morphologically stable owing, in part, to their high surface-area–volume ratio. They tend to break into small segments, a behavior usually attributed to the Rayleigh instability.[53,58] Like corrosion, this instability of metal nanowires is also worsened at higher temperatures.[132] In order to slow nanowire degradation and thus increase the lifetime of Ag NW electrodes, various passivation strategies have been developed that use an outer layer to protect the silver

nanowires from corrosion and other side reactions with the environment. The passivation layer must be optically transparent, and electrically conductive as well if it stands, for example, between the nanowire network and the active part of a solar cell. Several passivation materials such as TiO$_2$, ZnO, or graphene have been studied and were reviewed in chapter 1.[94,95,133,134]

In this subchapter, we investigate the Joule heating effect in Ag NW electrodes and RGO-passivated Ag NW electrodes under current flow. Reduced graphene oxide (RGO), in particular, is attractive since it can act as a barrier for both moisture and gases in air.[135] It can be deposited as films thinner than ZnO and TiO$_2$ ones, optimizing optical transparency. Furthermore, like AgNW films, RGO is mechanically flexible and can be deposited from solution. Several studies have demonstrated the utility of RGO as a passivation layer for AgNW electrodes. [103,133,136–138] For instance, whereas the sheet resistance of an unpassivated AgNW electrode more than tripled in less than a week while annealed at 70 °C in air, the resistance of the same nanowire electrode passivated with a uniformly dip-coated RGO layer increased by less than 50% over the same time.[104] If a layer of graphene is instead deposited on an AgNW electrode using chemical vapor deposition (CVD), it can stabilize the silver nanowires more effectively. A recent experiment revealed only a 10% increase of sheet resistance after one month while annealed at 70 °C.[139] However, this latter method is presently not economical for commercial manufacturing, especially since the graphene layer cannot be directly synthesized on the nanowires but rather needs to be first deposited on a substrate and then transferred onto the nanowire film. In the above studies, degradation of passivated and unpassivated silver nanowire electrodes were evaluated either at room temperature or when the electrode was annealed in an oven (or on a hotplate) to achieve an elevated temperature. In all cases, the temperature was the same at all points on the electrode. However, as we will show, the surface temperature profile across a nanowire electrode is not

uniform when it is used in a solar cell, OLED, or transparent heater. Unlike in a continuous conducting film (e.g. ITO) where current flows throughout the entire area of the film, in the case of nanowire electrodes current only flows through the thin metal pathways. Furthermore, there are variations in the nanowire density across the film and thus the current density flowing in some nanowire pathways is higher than in others. These factors combined result in a non-uniform temperature distribution in the electrode where the temperatures of some individual nanowires are significantly higher than the average surface temperature of the electrode.[18]

4.1.1. Experimental section

Protocol 4.1: Fabrication of the electrodes

Silver nanowires dispersed in ethanol were purchased from Blue Nano Inc. (Charlotte, NC) with an average diameter and length of 90 nm and 25 μm, respectively. Polyethylene terephthalate (PET) films (127 μm thick from Dupont Tianjin Inc.) were used as substrates for the electrodes (PET was used rather than glass since a distinct advantage of AgNW electrodes is their suitability for plastic substrates). The PET films were cleaned sequentially in a sonication bath of acetone, isopropanol alcohol, and distilled water each for 1 min, then dried with nitrogen gas. The nanowires were deposited on the PET films using the Mayer rod coating technique to obtain a random network of silver nanowires.[140] The active area of the deposited AgNW film was 2 cm × 2 cm with two strips of 0.5 cm wide copper tape installed at the two ends of the electrodes (2 cm apart) as current collectors. The transparency and conductivity of the silver nanowire electrodes can be controlled by changing the concentration of the nanowires in ethanol and the number of coating layers. The dependency of the transmittance and conductivity has been reported elsewhere.[141] The deposited films were dried in air for 5 min and mechanically pressed by rollers at room temperature to reduce the nanowire junction resistances.[142] ITO on PET with a sheet resistance of 60 ohms/sq was

purchased from Sigma Aldrich. Although lower sheet resistances are desired for solar cell applications, ITO on PET has higher resistance than on glass due to the need for lower deposition temperatures. To be able to compare with ITO, the AgNW electrodes were also made with a sheet resistance of 60 ± 10 % ohms/sq. AgNW electrodes with sheet resistances of 20 ohms/sq were prepared as well to see the effect of Joule heating in lower resistance networks.

Protocol 4.2: Reduced Graphene oxide monolayer fabrication

GO was first prepared using the Tour method.[143] A continuous, densely tiled, monolayer of the GO was then formed on the surface of water using a modified Langmuir–Blodgett (LB) trough technique.[144] Instead of using mechanical barriers to compress the film, as in the typical LB process, the spreading force of the solvent is used to compress the films against the edge of the trough. Thus, in principle, this approach has the potential to be adapted to a roll-to-roll manufacturing by withdrawing a substrate during material deposition. Such a system will be reported elsewhere. The as-prepared AgNW-coated PET samples were placed at the bottom of the trough prior to GO deposition, and the floating monolayer GO film was lowered onto the substrates by slowly draining the water. In addition to coating PET samples, mica and highly oriented pyrolytic graphite (HOPG) substrates were coated at the same time to verify film morphology and coverage using atomic force microscopy (AFM) and scanning electron microscopy (SEM). The GO was chemically reduced using $NaBH_4$. For more delails see [107].

4.1.2. Characterizations

Determining current value

The current density assumed in this study was 20 mA.cm^{-2}, which is the typical operating current of the best performing organic solar cells in the literature.[145],[146] Current densities in OLEDs can also reach values as high as 20 mA.cm^{-2}.[98] The maximum current is

usually incurred near the current collector bar in these devices. In common designs of organic solar cell modules the width of the active layer is around 1 cm, and the current flowing through the transparent electrode is collected at one end only.(Figure 72)[147–149] Therefore, with a current density of 20 mA .cm^{-2}, the current at the current collector bar will reach 20 mA per centimeter length (20 mA.cm^{-1}) of current collector. As this is the typical maximum current incurred in the transparent electrode, this is the value we used in the experiments.
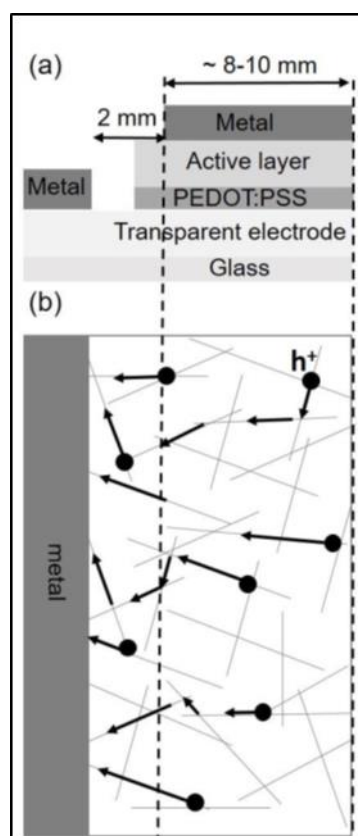
Figure 72: a) Schematic of a typical organic solar cell module. b) Planar view of the transparent electrode.

Surface analysis

Contact mode AFM was carried out on GO films deposited on atomically flat muscovite mica (SPI) substrates using NPSTT10 tips (Bruker) and a Nanoscope MultiMode AFM (Veeco). AFM images were analysed using Gwyddion software to extract height profiles between the atomically smooth substrate and the GO sheets, and a custom MATLAB code was used to estimate sheet thicknesses from the steps in the height profiles. The sheet resistance of the electrodes with and without the RGO layer was measured by either a

multimeter or a 4-point probe measurement system. UV–vis photospectroscopy with an integrating sphere was used to measure the transparency of the electrodes. SEM images were taken before and after failure of the electrodes. A DC power supply was connected to the current collectors to apply a constant current of 20 mA.cm^{-1} across the electrodes. A multimeter and a flat leaf-style thermocouple were used to continuously monitor the voltage across the electrode and its average surface temperature, respectively, during extended time experiments and PC link software was used to record the data. (Figure 73)
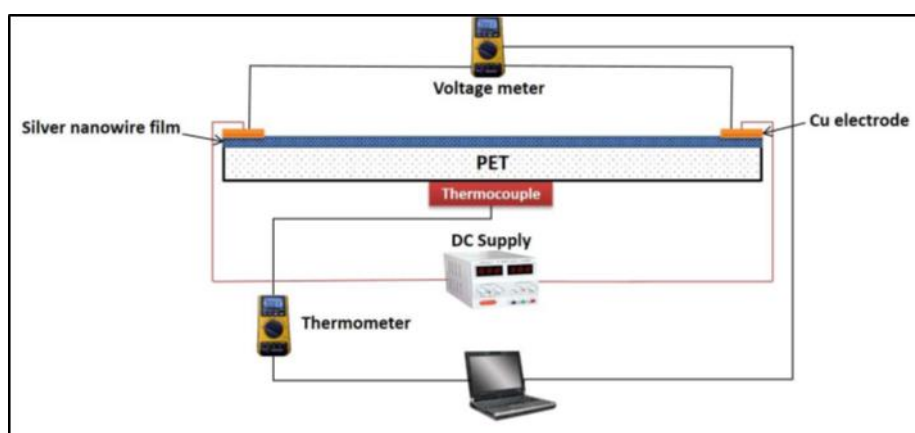
Figure 73: Schematic of the experimental setup to measure temperature and voltage across the electrode under a constant current.

In a separate measurement, an infrared (IR) camera was used to map the spatial temperature distribution over the electrode area while the electrode was conducting 20 mA.cm^{-1} of current. The IR camera (FLIR SC7000) had an indium–antimony detector composed of a focal plane array featuring 81 920 pixels (matrix 320 × 256), and a simultaneous measurement at all 81 920 spots could be performed using the snapshot mode. The camera was equipped with an IR lens with a focal length of 25 mm. The resulting spatial resolution per pixel is around 250 μm × 250 μm. A previously reported calibration method was used to retrieve the absolute temperature of the samples (semi-transparent samples) from the raw intensity data provided by the IR camera.[144,150]

A thin layer of black paint was deposited over the back of the electrodes in order to avoid reflections. Reference samples were warmed-up on a heating stage at several

temperatures ranging from room temperature to 45 °C. For each temperature, the digital signal level of each pixel of the images recorded by the IR camera was fitted to the imposed temperature in order to estimate the emissivity of the sample. From this calibration, the local absolute temperature could be determined during the experimental measurements of the electrodes.

Modelling

Random networks of silver nanowires were modelled in MATLAB and the electric current values retrieved from simulations were subsequently used to model Joule heating in individual nanowires using the Joule heating module of COMSOL Multiphysics software.[138],[151–154] See more details in [107].

4.1.3. Results and characterization

Characterization of the electrodes

Our first goal was to create a transparent barrier film of RGO to protect the Ag nanowires as illustrated schematically in Figure 74.a.
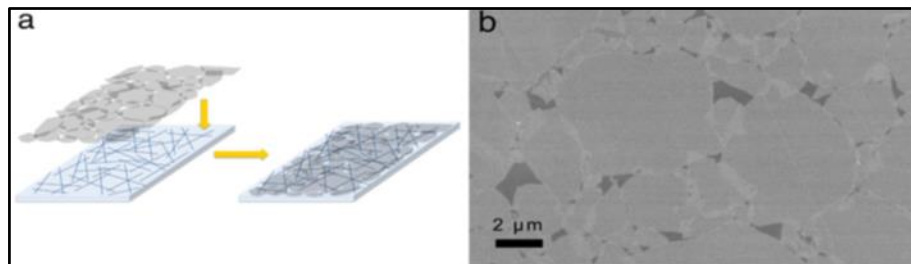
Figure 74: Reduced graphene oxide blocking layer. a) Schematic illustrating graphene oxide monolayer deposition on a silver nanowire/PETfilm. b) SEM image showing contrast between the graphene oxide film (light) and some pinholes exposing the HOPG substrate (dark).

The morphology and coverage of the RGO film, deposited by a modified LB technique, are shown in the SEM images in Figures 74.b. The analysis of the contrast in the SEM image sheets allowed the estimation of the film coverage at 95% (RGO film brighter and HOPG darker). The optical transparency of the 60 ohms/sq AgNW films (not including the PET substrate) at a wavelength of 550 nm were 94%. The transmittance of the AgNW

101

electrode dropped from 94% – 91% after the deposition of the RGO layer. The observed 3% transmittance decrease is consistent with the transmittance value of a single layer of graphene in the visible range.[155] The RGO sheets are electrically conductive, however, their electrical conductivity is significantly less than the conductivity of the nanowires, and the contact resistance between two overlapping RGO sheets is high.[156] Thus, the overall sheet resistance of the Ag NW electrodes did not decrease significantly after adding the RGO layer (only by 0% – 10%).

Annealing study

We first confirmed prior studies of the literature showing the effectiveness of RGO in protecting the nanowire films against degradation when annealed in a furnace. Both the Ag NW and Ag NW-RGO electrodes were annealed at 70 °C in air for 14 days. After 6 days, the sheet resistance of the Ag NW electrode increased by a factor of 180 compared to the initial sheet resistance of 60 ohms/sq, whereas the sheet resistance of the Ag NW-RGO electrode increased only by a factor of 1.5 after 14 days. This indicates that the RGO layer is quite successful in slowing down silver nanowire electrode degradation under annealing conditions, as concluded by many others.[104,137] However, testing its effectiveness under current flow is essential to mimic the stress faced by the Ag NW electrode during use in a solar cell or OLED.

Surface temperature distribution under current flow

A 20 mA DC current was passed across the electrodes per centimeter length of the current collectors (20 mA.cm^{-1}). Figure 75 shows the evolution of the surface temperature profiles obtained using thermal imaging for 60 ohms/sq ITO, Ag NW, and Ag NW-RGO electrodes.
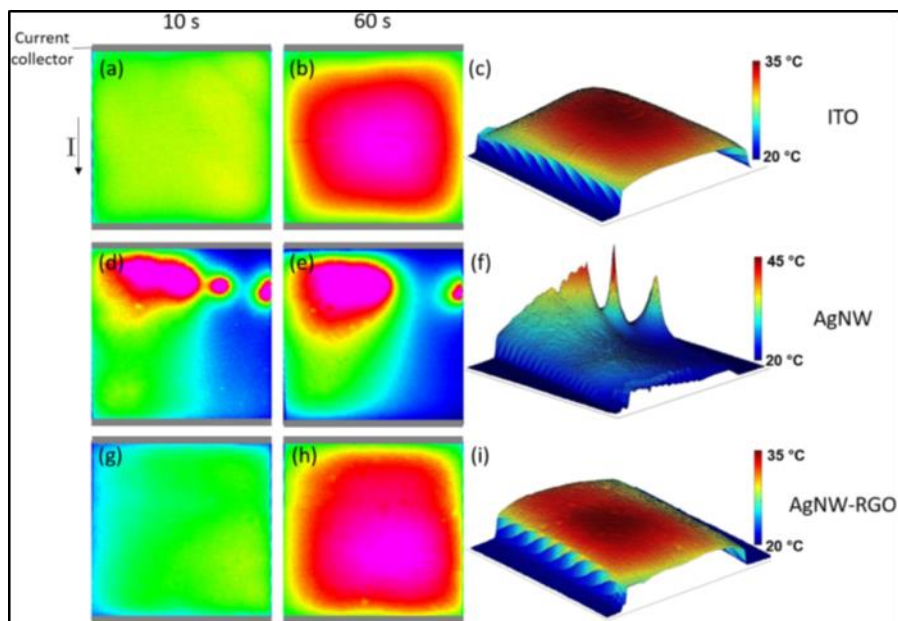
Figure 75: Temperature profiles of 2 cm × 2 cm electrodes, measured using a thermal imaging camera, when 20 mA cm^{-1} of current is applied from top to bottom. a), b) surface temperature of ITO, c) 3D temperature profile of ITO after 60 s. d), e) Surface temperature of the Ag NW electrode, f) 3D temperature profile of the Ag NW electrode after 10 s. g), h) Surface temperature of the Ag NW-RGO electrode, i) 3D temperature profile of the Ag NW-RGO electrode after 60 s.

Temperature images in Figures 75.a, d, g are shown 10 s after the current flow was applied whereas images in Figures 75.b, e, h are recorded after the temperature has stabilized (60 s). In these images, the current flows from top to bottom, as indicated schematically in Figure 75.a. As can be seen, the temperature appears uniform over the ITO electrode. However, local temperature variations greater than 20 °C are evidenced across the Ag NW electrode (Figures 75.d-f). The presence of such hot spots in nanowire electrodes has also been reported by others and may be due to the non-uniform density distribution of the nanowires across the electrode.[157,158] In bottleneck regions where there is a sparser nanowire concentration, individual nanowires must sustain high current densities and thus local Joule heating will be significantly higher than in denser nanowire regions. The hotspots observed in the unpassivated nanowire electrode exist along a line across the electrode parallel to the current collectors. We hypothesize that there are regions of sparse nanowires along this line and thus much of the current cannot re-route through denser locations. Thus Joule heating, equal to I^2R where I is current and R is resistance, is high along this line. The existence of hot

spots accelerates both corrosion and Rayleigh instability in these regions leading to nanowire breakdown. When nanowires break down, more current is forced through other available pathways, causing those regions to then locally increase in temperature. This situation can be observed in Figures 75.d – f. A hotspot present after 10 s, which Figure 75.f indicates is at the highest temperature on the electrode, no longer exists after 60 s. This suggests that some nanowires failed rapidly after current was applied due to this high temperature. As can be observed, it cooled down once current could no longer flow through that pathway, but consequently, the regions around the failed nanowires became hotter. This in turn accelerates nanowire degradation at these points until ultimately, as we observed when higher currents were applied to accelerate failure times, an open circuit exists in a line extending across the electrode. It is important to note that the smallest detected area (pixel resolution) of the thermal imaging camera is 250 μm × 250 μm which corresponds to an area with more than one hundred nanowires. Thus, the temperature of individual nanowires is not directly detectable, and we get an average temperature over the pixel area. In the modelling results reported later, we will see that the temperature variations on the nanoscale are far higher than ones observed on the microscale in thermal maps such as these. In Figures 75.g – i, it is evidenced that the RGO passivation layer smooths out the temperature variation over the Ag NW electrode such that the resulting temperature uniformity appears comparable to that of the ITO electrode. This is likely because of the high thermal conductivity of the RGO (above 1000 $Wm^{-1}.K^{-1}$) compared to air (0.024 $Wm^{-1}.K^{-1}$) and the plastic substrate (0.20 $Wm^{-1}.K^{-1}$) which assists in the lateral distribution of heat over the surface of the electrode.[151],[153,154] The absence of hot spots is one of the reasons why we will later see that the RGO extends the lifetime of Ag NW electrodes under current flow. Also, because the RGO distributes the heat more evenly across the surface, it effectively provides a larger surface area from which the

heat can dissipate and thereby slightly lowers the average surface temperature of the electrode.

Electrode failure under current flow

Figure 76.a shows the average surface temperature (measured with a thermocouple that was attached to the bottom of the substrate) and sheet resistance evolution for an unpassivated 60 ohms/sq Ag NW electrode under 20 mA.cm^{-1} of linear current density. The electrode failed after 120 h (5 days), where failure is defined as when the sheet resistance exceeded 1500 ohms/sq. SEM images of nanowires after electrode failure are shown in Figures 76.b and c, illustrating the two different types of nanowire breakdown that were observed. In Figure 76.b, the presence of nanoparticles on the nanowires indicate nanowire corrosion which eventually lead to electrical discontinuities.[67] Other nanowires (Figure 76.c) are completely melted in addition to damaging the plastic substrate underneath, implying a very high localized temperature. We suggest that these latter nanowires were subjected to very high levels of current and thus heated up and failed quickly, like those associated with the disappearing hotspot in Figures 75.d and e, whereas the corroded nanowires were subject to lower current densities over a longer time period. These issues will be further discussed when the modelling of current levels and temperatures of individual nanowires is presented.
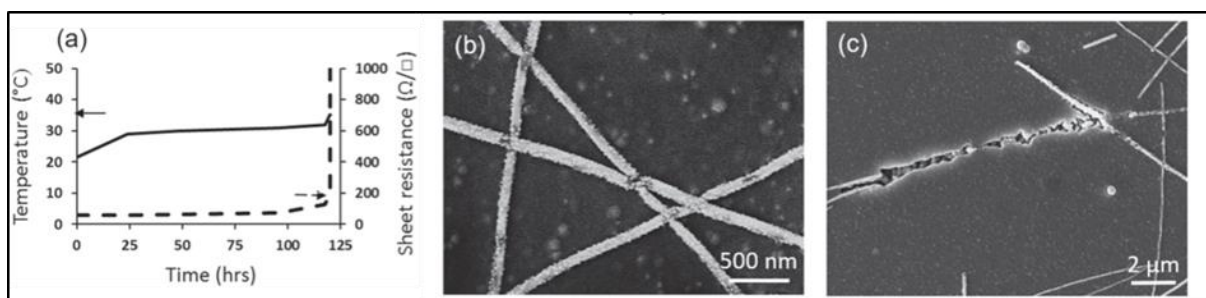
Figure 76: a) Temperature and sheet resistance of an AgNW electrode over time under a linear current density of 20 mA cm^{-1}. b), c) SEM images of nanowires after electrode failure. The nanowires in b) show evidence of accelerated corrosion leading to discontinuities, and in c) a nanowire along with with part of the PET substrate underneath has melted.

Figure 77.a shows the average temperature and sheet resistance of the AgNW-RGO electrodes under a linear current of 20 mA.cm^{-1}. The RGO passivation layer extended the lifetime of the AgNW electrode to 285 h (~12 days). There are three possible mechanisms by which RGO passivates the electrodes: (i) nanowire corrosion is slowed since the RGO impedes air from reaching the nanowires. This is supported by the observed increase in lifetime upon extended annealing at 70 °C with no current flow; (ii) the RGO prevents hotspots (as discussed above) where the fastest degradation occurs; and (iii) the RGO increases the morphological stability of the nanowires and thus increases the temperature at which the nanowires break-up.[159] Indeed, SEM images taken after electrode failure show that the RGO-passivated electrodes do not fail due to NW melting or corrosion (Figure 77.b), which is the case for unpassivated electrodes. Rather, the electrode instead breaks down due to deformation and melting of the PET substrate on a micron length-scale (Figures 77.c and d). The substrate deformation causes breakage in the nanowires and thus electrical discontinuities. A melted substrate indicates that the local temperature of the nanowires exceeds the melting point of PET (~250 °C) during current flow. The silver nanowires, normally unstable at this temperature, remain due to the RGO passivation.[160] Although the thermal imaging data indicated the RGO-passivated electrodes had an average surface temperature of 32 °C under this same current flow (Figure 75.i), the local temperature of some nanowires are much higher. These results demonstrate the inadequacy of annealing a nanowire electrode to assess stability and lifetimes, which is the method used by many others and done above. The Joule heating that would take place in an electrode during solar cell operation, which causes very high localized temperatures, is not incurred. As measured above, the resistance of the RGO-passivated electrode annealed in a furnace at 70 °C only increased by 1.5 times after 12 days, whereas under a current flow causing an average surface temperature of 32 °C, the resistance increased by more than 25 times.
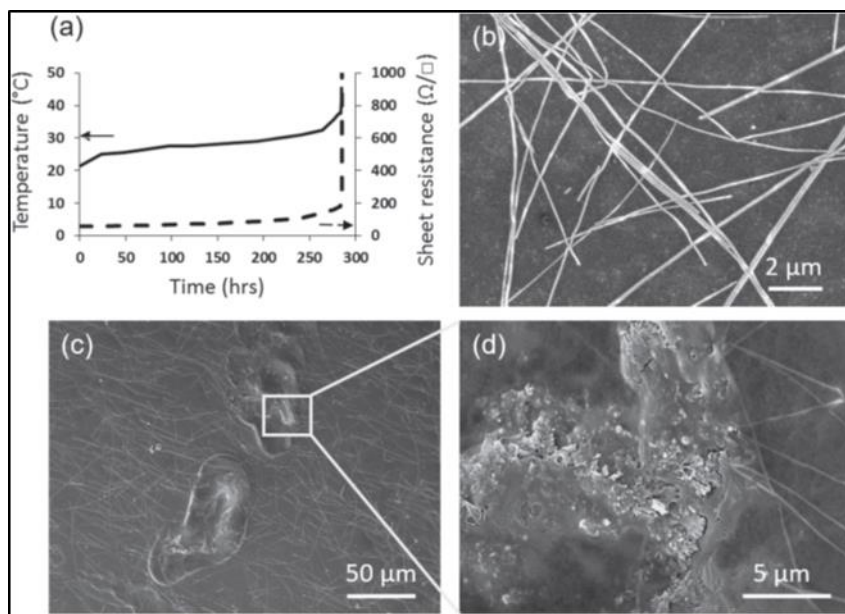
Figure 77: a) Temperature and sheet resistance versus time of a AgNW-RGO electrode under a linear current density of 20 mA cm^{-1}. SEM images after failure of b) a non-melted region and c), d) localized substrate melting.

Joule heating modelling of nanowires in electrodes

Figure 78 shows the results of the COMSOL Joule heating simulations and the steady state temperatures reached by an individual AgNW, an AgNW passivated with RGO, and ITO. It is worth mentioning that at steady state, the whole system is at a similar temperature and thus the coloring indicates only very minor differences in temperature. The colors however are useful to show how heat is dissipated in the system.
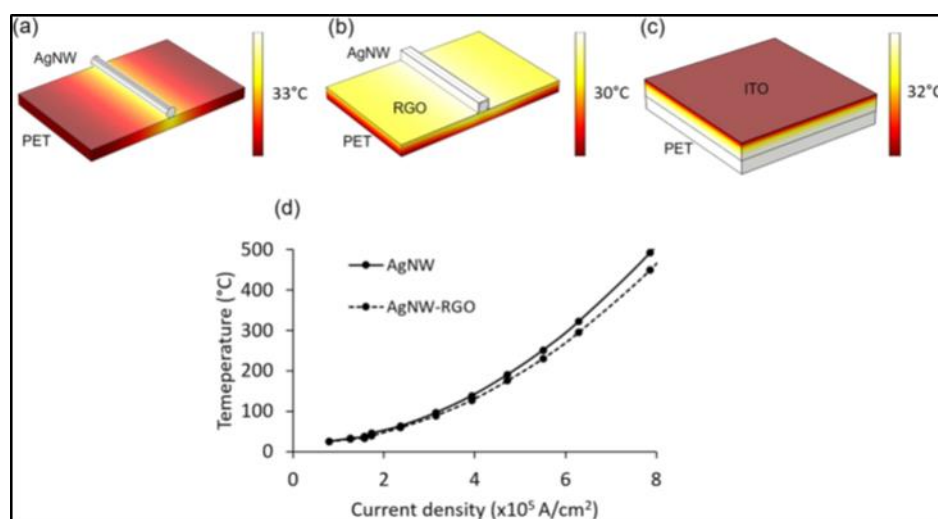
Figure 78: Steady state thermal profile of a (a) AgNW, (b) RGO-passivated AgNW, and (c) 130 nm thick film of ITO on PET when they are carrying the average current density encountered when 20 mA.cm^{-1} is passed across the electrode. (d) Calculated steady state temperature of individual unpassivated and passivated silver nanowires on PET substrates under different current densities.

A single AgNW carrying the average current previously calculated in the section above (1.2×10^5 A.cm^{-2}) reached 33 °C (Figure 78.a) and a RGO-passivated Ag NW reached 30 °C (Figure 78.b). The RGO film helps spread out the heat and reduces the surface temperature by 8%–10%. Our simulated results match closely to experiment: the calculated average surface temperature of the Ag NW electrode under 20 mA.cm^{-1} of current, recorded by the IR camera, was found to be 33 ± 2 °C, and the measured average temperature of the Ag NW-RGO (Figure 75.i) was 32 ± 2 °C. In the case of a 60 ohms/sq, 130 nm thick ITO film on a PET substrate under the calculated ITO average current density of 1.5×10^3 A.cm^{-2} (Figure 78.c), the steady state temperature was calculated to be 32 °C, also close to the 34 ± 2 °C average temperature recorded by the IR camera (Figure 75.c). Although the temperature of a nanowire conducting the average current density is 33 °C, there are some individual nanowire segments in the whole metallic network that can become much hotter. Figure 78.d shows the simulated temperature of silver nanowires on a PET substrate at different current densities. As calculated in the previous section, 0.5% of the nanowire segments in a 60 ohms/sq Ag NW electrode under 20 mA.cm^{-1} current flow are carrying a current density higher than 5.5×10^5 A.cm^{-2}. Figure 78.d shows that the temperature of unpassivated NWs carrying such levels of current exceed 250 °C, a temperature above the melting point of PET. Importantly, at such a temperature unpassivated 90 nm diameter Ag NWs are not thermally stable either.[160] Such nanowires would fail quickly after the current is applied. These nanowire segments are hotter than the hottest spot evidenced in the IR images because, as mentioned above, the camera measures an average temperature of several hundred nanowires. However, the existence of these very hot nanowires still corroborates with our experimental results. The IR data in Figures 75.d and e insinuate that there is a rapid failure of some nanowires, and the SEM image in Figure 77.c indicates the melting of both the nanowire and a localized portion of the PET substrate. Once these high current carrying nanowires break and are no longer

conductive, the current is redistributed amongst the other nanowires. The existence of localized nanoscale hotspots of high temperatures is in stark contrast to ITO electrodes where the current is distributed evenly throughout the film. In an ITO film carrying the same linear current density as the nanowire electrode, all points over the surface are expected to be close to 32 °C. The existence of a non-uniform temperature distribution and localized hotspots reaching 250 °C is a unique issue for nanowire electrodes. Because RGO is not as electrically conductive as the nanowire network, it does not significantly lower the current densities in the nanowires and therefore Joule heating still occurs. Although it initially avoids larger microscale hotspots and slightly lowers the average surface temperature by spreading heat more uniformly over the surface, we can see in Figure 78.d that the temperatures of individual nanowires in the Ag NW-RGO case can still be very high. And because a single layer of RGO does not thoroughly prevent nanowire degradation, as evidenced by the slight resistance increase during annealing (1.5 times after 14 days) and by the observation of some nanowire corrosion in the SEM after extended current flow, the current densities in the nanowires increase over time. As a consequence, this leads to more and more Joule heating until ultimately the PET substrate melts over larger microscale areas (rather than melting only underneath the nanowires in the case of unpassivated electrodes, since the RGO distributes the heat beyond the location of an individual nanowire). This causes the nanowire networks to distort and fail. In addition to concerns about electrode failure, our models show that the temperature of 5.5 ± 0.5% of the unpassivated nanowires and 5.0 ± 0.5% of the RGO-passivated nanowires may exceed 100 °C, which could adversely affect other materials on top of the electrode in a device. Because organic materials are not stable at high temperatures, the maximum operating temperature for organic solar cells and LEDs is commonly below 100 °C.[161–164] This is lower than the melting point of PET and thus these devices require a more

stringent thermal budget. This is another reason why Joule heating in nanowire electrodes is a major concern that needs to be addressed.

Managing Joule heating

Our results show that a passivation layer alone is not sufficient to manage the Joule heating problem in silver nanowire transparent electrodes. In order to reduce Joule heating, the current density in individual nanowires needs to be reduced. One way to achieve this is to increase the density of the nanowires in the electrode so that there are more current pathways. A 20 ohms/sq Ag NW electrode was modelled (Figure 79.a) and the current density distribution in the nanowire segments when 20 mAcm^{-1} of current is applied across the electrode is plotted in Figure 79.b. The average current density in the nanowire segments is $0.6 \pm 0.1 \times 10^5$ A.cm^{-2}, which is half of the average current density expected in a 60 ohms/sq AgNW electrode. The simulation results of Joule heating in the 20 ohms/sq electrodes are shown in Figures 79.c and d. The steady state temperature of the Ag NW and Ag NW-RGO samples under the average current density reached to 27 °C and 25 °C, respectively (Figures 79.c and d), which are 6° and 5° C lower than in the 60 ohms/sq case. In the Ag NW and Ag NW-RGO electrodes, less than $0.006 \pm 0.003\%$ and $0.002 \pm 0.001\%$ of the nanowires, respectively, carry a current that results in a temperature above 250 °C. In addition, only $0.45 \pm 0.15\%$ and $0.15 \pm 0.1\%$ of the nanowires get hotter than 100 °C in the Ag NW and AgNW-RGO electrodes, respectively. Experimentally, 20 mA.cm^{-1} was passed across a 20 ohms/sq unpassivated Ag NW electrode. The surface temperature was 26 °C, 6 °C lower than what was measured for the 60 ohms/sq case (Figure 79.a). The electrode failed after 25 days of sustained current compared to failure after 5 days for the 60 ohms/sq electrode. The effect of elevated currents was also assessed; under a sustained current of 50 mA.cm^{-1}, a 20 ohms/sq Ag NW electrode failed after 7 days. Overall, the effect of Joule heating is reduced in NW electrodes with lower sheet resistance and the lifetime is thus increased. Increasing the

nanowire density in the electrodes has drawbacks however; the electrode transparency would decrease and the material cost would increase. A second way to reduce the current density in individual nanowires is to, of course, have less current flowing across the electrode. In a solar cell this is achieved by making the active area smaller, or in other words, making the electrical contacts (current collectors) closer together, to lower the maximum current levels which occur near a contact. This, however, reduces the efficiency of the solar cells by increasing the surface area covered by the metal bars. Thirdly, because excessive Joule heating leading to NW breakdown is most likely to occur in areas of sparse NWs, the nanowire networks should be made as uniformly dense as possible. However, in a random film there will always be variations in local density. Assembling the NWs into a regularly spaced grid, as has been achieved with some success using NW alignment techniques, or depositing a Ag grid using patterning techniques, would result in a more uniform current distribution and thus avoid hot spots.[66,165–167] This would extend electrode lifetimes though at a cost of a more complex deposition process.
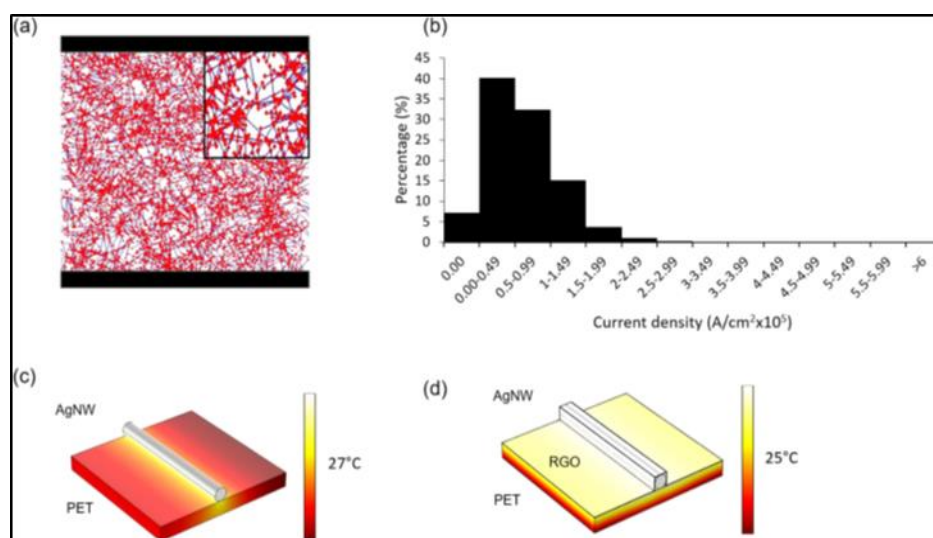
Figure 79: a) Silver nanowire electrode model with a sheet resistance of 20 ohms/sq (red dots show nanowire junctions and endpoints), b)The distribution of current densities in individual nanowire segments (i.e. between two red dots) of the 20 ohms/sq nanowire electrode. Steady-state thermal profile of a, c) Ag NW and d) RGO-passivated Ag NW under the average current density of 0.6×10^5 A.cm^{-2}.

4.1.4. Conclusion

This study demonstrates that the Joule heating taking place in silver nanowire electrodes when they continuously conduct current is a much more serious problem than in conventional transparent homogeneous conductive electrodes like ITO. When a 60 ohms/sq Ag NW electrode conducts current at the levels incurred near the metal contacts of organic solar cells, the resulting Joule heating leads to electrode failure in 5 days. An RGO passivation layer extends the electrode lifetime, but only to 12 days since it cannot prevent the Joule heating that ultimately leads to failure due to localized melting of the plastic substrate. Modelling indicates that the temperature of some individual nanowires under current flow reach much higher temperatures than the average surface temperature recorded. This explains the observation of substrate melting and the faster failure times as compared to electrodes whose lifetimes are assessed by annealing rather than current flow. If silver nanowire electrodes are used in solar cells, OLEDs, or transparent heaters, steps must be taken to reduce the Joule heating problem to extend both the lifetime of the electrode and the rest of the device as well. Lowering the electrode sheet resistance or lowering the current flowed across the electrode would both be effective strategies.

4.2. Passivation of silver nanowires with MuA

Another issue that affects the stability of silver nanowire electrodes is their chemical instability. The lifetime of nanowire electrodes is currently much shorter than ITO. Commercially available AgNWs are stabilized with PVP and they are highly sensitive to daylight and humidity once deposited on a given substrate. After 3 weeks of exposure to ambient air and in the presence of humidity, a study of Elechiguerra et al. showed that a non-uniform layer of Ag_2S crystals could be created at the surface of the silver nanowires.[51] This corrosion has been shown by several studies to increase the sheet resistance of silver nanowire electrodes. For example, Moon observed an increase of sheet resistance of 240 % after 2

months in ambient air conditions.[168] Similarly, Deignan reported that electrodes made of 25 nm diameter silver nanowires degraded to the point of non-conductivity in less than two months.[121]

As shown in Chapter 1, different strategies to improve the chemical stability of electrodes have been implemented. For instance, by encapsulating the nanowires with a polymer or graphene, or by chemically modifying the surface of the nanowire networks with a layer of inorganic material (eg.Al_2O_3, ZnO, TiO_2).[96,103],[97,98,102] Unfortunately, these passivation approaches affect the intrinsic properties of the anisotropic nanostructured networks such as reducing transparency and/or the flexibility of the film, as discussed in Chapter 1 section 1.3.1. Interestingly, passivating the surfaces of the silver nanowires themselves with an organic short molecule, rather than coating an inorganic or organic material over the entire electrode surface, does not affect the transparency of the electrode.[70] A coating of short organic molecules is also inexpensive, easy to implement and does not decrease the electrode's conductivity. Moreover, such methodology should not have a negative effect over the mechanical flexibility of the electrode. Recently, Idier et al. passivated silver nanowires in an electrode with the small molecule triphenylphosphine (PPh_3).[12] Although this work provided decent protection against corrosion, the resistance of the electrode still increased by 500% after exposure to air for 110 days and an even more protective layer is desired.[70] Moreover, it is important to highlight that PPh_3 is a toxic compound.

Because of the attractive qualities of a short molecule passivation, other molecules should be tested to verify their suitability as capping agents. Self-assembled monolayers (SAMs) of the short molecule 11-mercaptoundecanoic (MuA, $HSCH_2(CH_2)_8CH_2COOH$) on gold and silver substrates has been widely explored for many years.[169] This non-toxic molecule can easily be attached to metallic nanostructures through a thiolate bond. [169]

Moreover, Van der Waals and electrostatic forces between the alkyl chains induce a packing order of the MuA monolayer (Figure 80), acting as a barrier against corrosion. Along these lines, Le Beulze and coworkers have shown that silver triangular nanoparticles are more stable when passivated with MuA.[170]
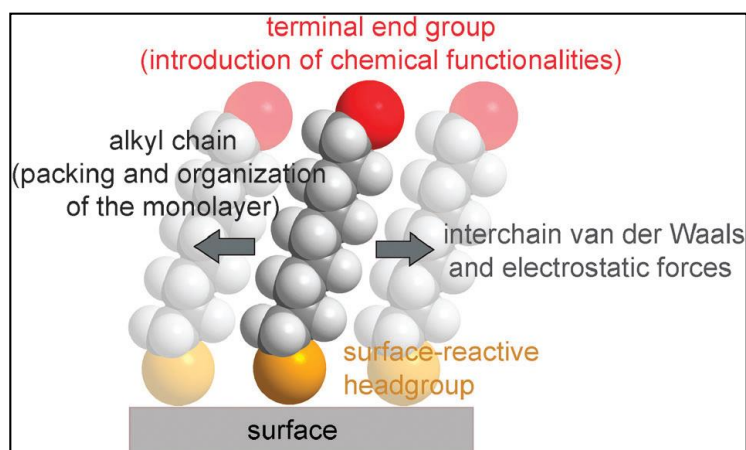
Figure 80: Schematic representation of a self-assembled monolayer of alkanethiol molecules with the surface-reactive head group composed of thiol.[184]

In this section, we investigate the possibility of using MuA to passivate the surface of silver nanowires and enhance their corrosion resistance. We first passivate silver nanowires in solution and prove the presence of MuA on their surfaces. However, these nanowires agglomerate and lead to an inhomogeneous network once deposited on glass. Therefore, we decided to passivate the nanowires after they were deposited as a film. Experiments were performed on commercial silver nanowires or elongated nanowires prepared following the protocol 4.3. Different techniques of characterization were used to probe the PVP-MuA substitution process. Moreover, lifetime testing of the passivated silver nanowire electrodes were performed in the air or in the dark at room temperature. In this manner, a 4-month lifetime study was conducted to evaluate the performance of the passivation on both 70 and 32 nm diameter nanowires under both light and dark conditions. Sheet resistances of passivated silver nanowire electrodes made of thin silver nanowires (32 nm) showed an increase of only 12 % after 4 months of exposure to the air and in the dark. The stability of the

electrodes passivated with MuA drastically changes when stored under light and showed an increase of 277 % for silver nanowires with 70 nm of diameter.
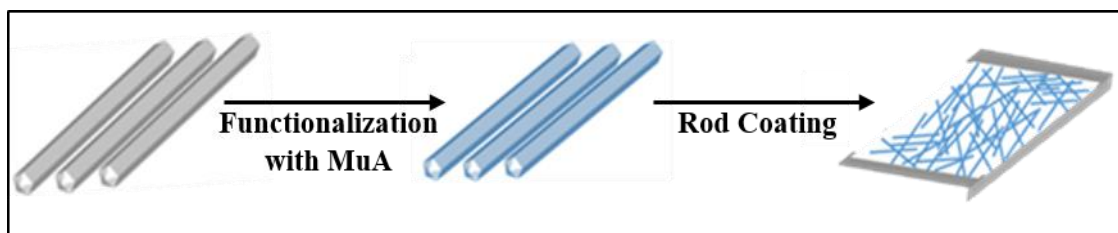
Figure 81: Scheme of the functionalization and elaboration of the AgNW electrodes.

4.2.1. Surface modification of AgNWs in solution

Stock solution of AgNWs (diameter = 70 nm and length = 50 - 100 μm) with a concentration of 20 mg/ml in ethanol was purchased from ACS Materials.

Protocol 4.3: Synthesis of thin AgNWs

In a 100 ml three-necked flask, 166 mg of polyvinylpyrrolidone (PVP-1300 K) and 25 ml of 1,2-propanediol were mixed by magnetic stirring in an oil bath set at 160 °C for 45 minutes. 50 μl of a solution of NaBr dissolved in 1,2-propanediol at a concentration of 50 mM was then added into the flask. After 15 minutes, 10 ml of a solution of $AgNO_3$ dissolved in 1,2-propanediol at a concentration of 100 mM was continuously added drop by drop through a syringe pump at an injection rate of 0.15 ml/min. The reaction proceeded for one hour.

Protocol 4.4: Passivation of the silver nanowires

2 ml of the 70 nm diameter nanowire stock solution described above was mixed with 18 ml of a solution of MuA dissolved in ethanol with a concentration of 0.15 mM. The amount of MuA added was calculated to obtain 10 functions per nm^2 of silver nanowire surface. The mixture was stirred for 1 hour. After 20 minutes of centrifugation at 2000 rpm, the supernatant was removed and 18 ml of the previous solution of MuA was added. The solution was stirred for 30 minutes and 5 ml of ethanol were subsequently added. Then, the solution was shaken rapidly and introduced in an ultrasonic bath in order to redisperse the silver nanowires. 1 ml of the solution was then picked up and dried in order to determine the

new concentration and the volume was then adjusted to get a concentration of 4 mg/ml. The process detailed above was also applied to silver nanowires without MuA functionalization, in order to obtain unpassivated nanowires.

A similar procedure was used for thinner nanowires (diameter = 32 nm) elaborated according the protocol 4.3. 1 ml of the synthesized silver nanowire solution was redispersed in 5 ml of absolute ethanol. This 5 ml were then mixed with 143 µl of a solution of MuA dissolved in ethanol with a concentration of 50 mM.

Protocol 4.5: Fabrication of the electrodes

Unpassivated and passivated silver nanowires were uniformly deposited on glass substrates using a Mayer rod coating method.[171] An annealing treatment in low vacuum is applied to reduce the overlapping nanowire junction resistances. For both types of nanowires, the concentration of the suspension was chosen in order to obtain a sheet resistance lower than 20 Ohms/sq. Silver paste was deposited at the two extremities of the electrodes for conductivity measurements.

AgNW d = 70 nm electrodes: 40 µl of AgNW suspension (4 mg/ml) were coated on a 20 mm x 30 mm glass substrate. This coating was applied 3 more times, with each coating being applied across a different orthogonal direction to obtain a random NW network. The annealing treatment was set at 180 °C for 30 minutes.

AgNW d = 32 nm electrodes: The same procedure as for Ag NW70 was performed with 47 µl of AgNW suspension (5.7 mg/ml) on 24 mm x 32 mm glass substrates. The annealing treatment was set at 160 °C for 30 minutes.

Sample preparation for SERS measurements

SERS experiments on silver nanowires immersed in ethanol were carried out using home-made glass liquid cells following a three-step procedure. A 20 µL volume of concentrated ethanolic solution of PVP-coated AgNWs (5 mM) was first dried into the cell to

116

allow for the formation of localized AgNW stacks. A 20 µL volume of ethanol was then slowly added in order to avoid the complete dispersion of stacks. A few microliters of an ethanolic solution of MuA were finally injected to reach the desired MuA concentration (500 µM or 100 µM) into the cell and start the PVP-MuA substitution.

Single nano-object optical spectroscopy analysis and simulation framework

Colocalized total internal reflection Raman scattering (TIR Raman) instrument consists of a topographic tapping-mode AFM (atomic force microscopy) and diffraction-limited DFRSM (dark-field Rayleigh scattering microscopy) and allows the realization of spectra of single PVP-coated nanowires deposited on glass substrate. DFRSM measurements give information on the finding of the best excitation wavelength (561 nm) used for the measurements of the spectra of the single nano-objects and to get the best Enhanced Factor, such work being confirmed by FDTD simulations (Finite-difference time-domain). In order to carry out TIR Raman measurements, a laser (Cobalt, 561nm) was launched in a polarization-maintaining single mode fiber. The emerging light was focused on a 50 µm diameter pinhole using two coupled 10x objectives between which a band pass filter was introduced to clean the fiber Raman signal and a half-wave plate to control the polarization state at the sample (p or s polarization).This part of the work will not be detailed in the present Thesis and further information can be found in a recently submitted publication.

X-ray photoelectron spectroscopy (XPS) measurements were carried out using a Thermo Fisher Scientific K-Alpha spectrometer with a monochromated Al Kα source (E=1486.6 eV). The X-ray spot size was 200 µm and charge compensation was used on insulating samples. The spectrometer was calibrated with monocrystalline gold and silver foils (binding energies of 84.0 eV for Au 4f7/2 and 368.25 eV for Ag 3d5/2). Surveys were acquired at a 200 eV pass energy and the high resolution spectra were acquired with a pass

energy of 40 eV. ThermoScientific Avantage software was used for fitting and quantification (Scofield table).

As previously described, MuA passivation was performed on 70 nm and 32 nm diameter AgNWs. Figures 82 and 83 show electron microscopy images of the two families of silver nanowires, both being initially capped with PVP.
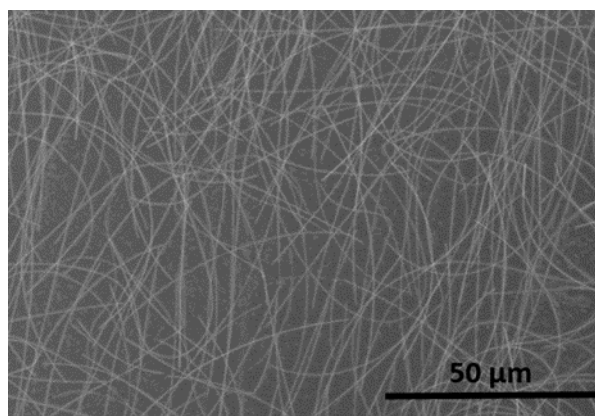
Figure 82: SEM image of the 70 nm diameter AgNWs supplied by ACS materials.
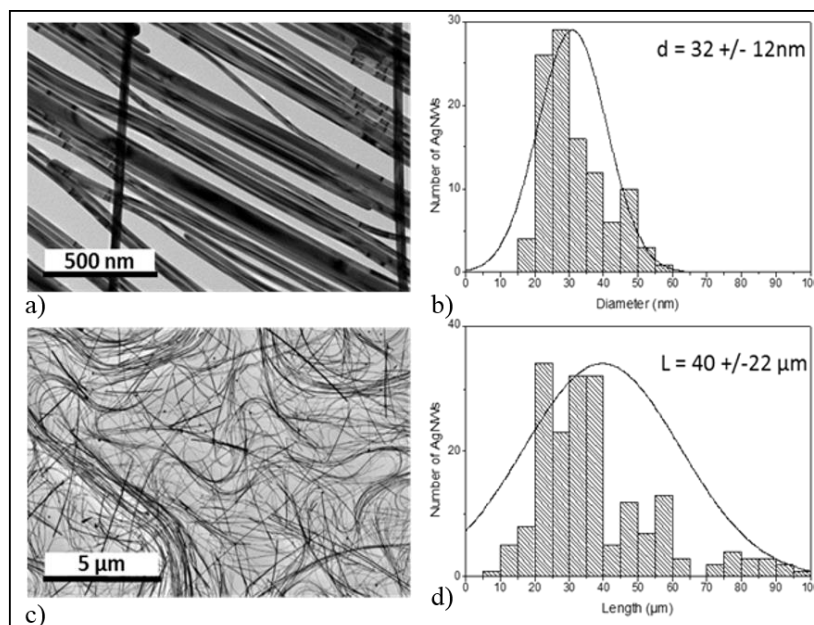
Figure 83: a) and c) TEM images of the AgNWs synthesized according to the protocol 4.3. b) and d) Diameter and length size distributions, respectively.

For surface modification, the AgNW suspension was incubated with a solution of the thiolate molecule overnight (Protocol 4.4). Figure 84 shows the TEM images of the PVP- and MuA-coated AgNWs. Before the surface modification, a thin amorphous layer of the polymer

118

can be seen on the surface of the silver nanowire, having an approximative thickness 5 nm (Figure 84). On the other hand, MuA molecules cannot be observed by TEM after surface functionalization. Even with an atomic resolution microscopy (ARM) analysis performed at the Plateforme Castaing in Toulouse (France), MuA molecules were extremely difficult to characterize (Figure 84).
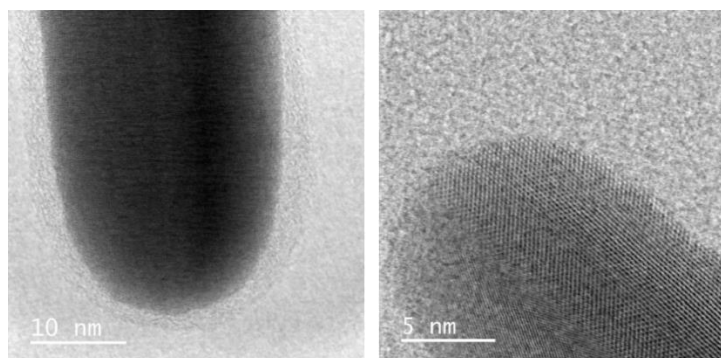
Figure 84: TEM image of the silver nanowires before (left) and after (right) passivation with MuA.

In order to determine if MuA functionalization has been successfully achieved, UV-Vis absorption spectroscopy was performed on untreated silver nanowires (i.e. those passivated with PVP) and silver nanowires passivated with MuA. This technique should allow us to observe a redshift of the plasmonic band of the silver nanowires after functionalization, given the nucleophilic character of the thiolated molecule.[172],[173] The UV-Visible absorption spectra of the colloidal suspension of PVP- and MuA-coated Ag NWs are shown in Figure 85. The initial PVP-stabilized silver solution has a main absorption band around 374 nm (and a shoulder at about 353 nm) that corresponds to absorption along the short axes of the nanowires. On the other hand, MuA-coated AgNWs possess an absorption band slightly red-shifted that is centered around 378 nm. Interestingly, the MuA-protected silver nanowires remain stable in solution, even after several months at ambient temperature in the presence of air. These materials are even stable in a strong oxidative medium such as H_2O_2, that can easily destroy PVP-coated silver nanowires. Such observations suggest that the small MuA organic

molecules attached onto the entire nanowire surface, i.e. on both the ends and on the lateral facets of the elongated nanostructures.
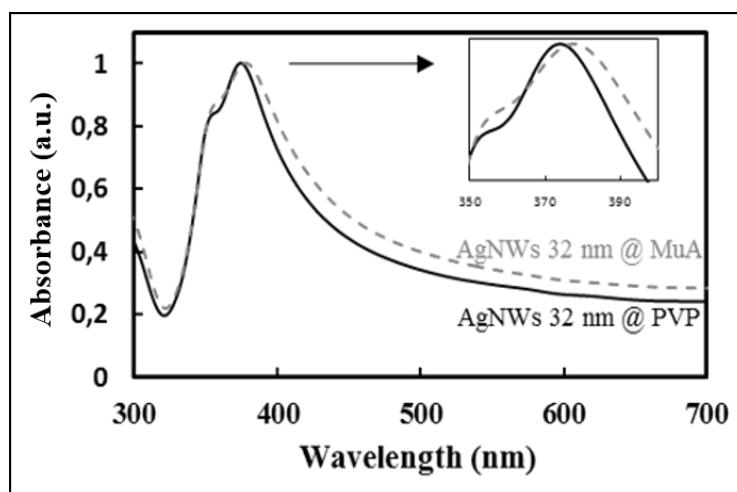
Figure 85: UV-Vis absorption spectra of silver nanowires before and after passivation.

Previous spectroscopic investigations on the binding of the PVP onto silver surfaces by FTIR (Fourier Transform infrared spectroscopy) have demonstrated that the PVP chains attach by the chemical adsorption of the oxygen and nitrogen atoms. The Ag-S bond is stronger than the Ag-O and the Ag-N ones and explains why PVP could be replaced by MuA.[174,175]

4.2.2. Mechanisms of replacement of PVP by MuA

XPS analyses were performed on samples that were dried at room temperature on glass substrates. AgNW@PVP and AgNW@MuA samples as well as Ag_2S as a reference were analyzed. Firstly, in the PVP sample a broad and intense band due to C-C bonding at 285 eV and a band with lower intensity at a slightly higher binding energy ~287.5 eV could be observed (Figure 86.a). This latter is assigned to a carbon atom bound to one oxygen with double bond (C=O). On the other hand, a band assigned to COOH bonding at 289.4 eV appears on the AgNW@MuA sample (Figure 86.c), that may come from the COOH group present in the MuA structure. Interestingly, XPS spectrum of AgNW@PVP contains only a signal corresponding to a C=O (carbonyl group), without trace of a COOH (carboxylic acid

120

functionality). Such XPS results are in accordance with the UV-Vis spectroscopy and confirm that MuA molecules reached the surface of the PVP-coated silver nanowires. This finding implies that PVP molecules originally linked to AgNWs through a coordination bond have been replaced by smaller MuA.
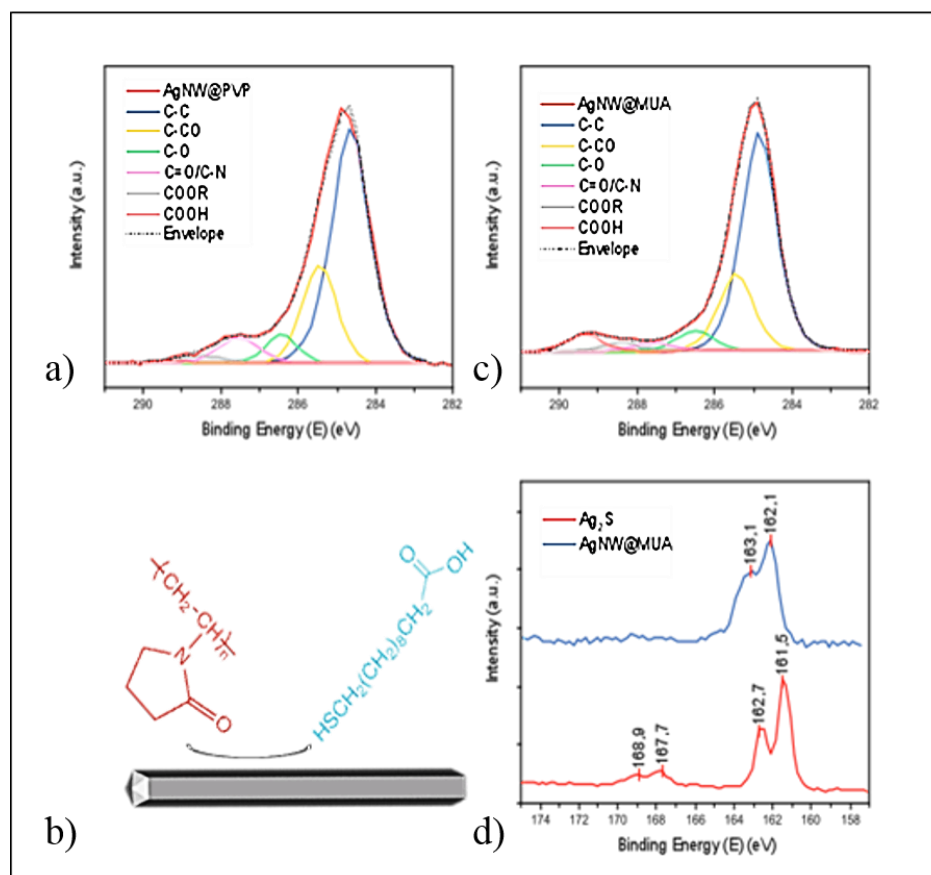
Figure 86: XPS C 1s region scans of a) AgNW@PVP and c) AgNW@MuA samples. b) Scheme of the PVP-MUA substitution on the silver NW surface, and d) 2p region scans of a reference Ag_2S and AgNW@MUA.

Figure 86.d displays a representative S2p region scan of the AgNW@MuA sample (blue curve). For comparison, reference Ag_2S region scan is shown (red curve). The spectrum of the AgNW@MuA reveals a peak at 163.1 and 162.1 eV due to Ag-S bonding. These observations evidence non-surprisingly that the MuA is bounded to the metal via the thiol groups rather than the carboxyl ones. The thiol groups chemisorb onto the metal to form a silver-thiolate bond:

$$R\text{-}S\text{-}H + Ag^0_n \longrightarrow R\text{-}S\text{-}Ag^+Ag^{0\bullet}_n + \tfrac{1}{2} H_2$$

Furthermore, it is interesting to note that no trace of sulfur oxide is observed on the AgNW@MuA sample, whereas a peak due to SO_2 is found on the Ag_2S bulk reference (in the 167-168 eV area). This observation further confirms that the MuA-functionalized silver nanowires are stable against chemical oxidation.

Figure 87 displays SERS spectra associated with both PVP-coated and MuA-coated AgNWs corresponding to the initial and final products of the PVP-MuA substitution as well as the Raman spectrum of the surrounding solution (containing ethanol, free PVP and excess MuA molecules) after PVP desorption and a reference spectrum of ethanol measured using normal Raman spectroscopy. PVP and MuA molecules exhibit very different Raman fingerprints (Figure 87). Two marker bands have been selected, namely the C=O stretching vibration centered at 1766 cm^{-1} for PVP and the C-S stretching vibration centered at 630 cm^{-1} for MuA (highlighted in green and blue respectively in Figure 87). The wavenumber of the C=O mode of PVP is consistent with several reports in the literature where it has been identified to range between 1750 and 1769 cm^{-1} when PVP is bound to the surface of Ag nanoparticles.[176–178] In contrast, free PVP molecules exhibit a C=O stretching vibration centered at 1776 cm^{-1} due to the increased force constant of the C=O bond. The wavenumber of the C-S stretching vibration of MuA nicely matches the value expected for the Gauche conformation of the molecule adsorbed on a silver surface.[179,180] Marker bands of the Trans conformation, such as specific C-S and C-C stretching vibrations at 692 cm^{-1} and 1102 cm^{-1} respectively, emerge also but, as they overlap with other vibrations assigned to PVP and free MuA molecules, it turns out hard to draw a definitive conclusion from their study.[179,180]
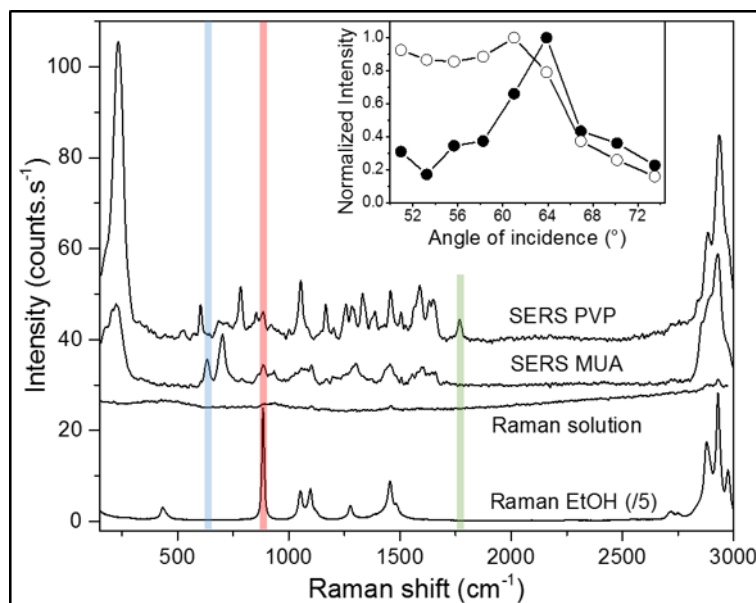
Figure 87: SERS spectra of PVP and MuA adsorbed on stacks of AgNWs, Raman spectrum (under evanescent excitation) of the ethanolic solution after PVP-MuA substitution, and normal Raman spectrum of ethanol (with intensity divided by a factor 5 for the sake of clarity).

Finally, in order to take into account possible intensity variations between SERS spectra, the marker band of ethanol at 885 cm^{-1} was chosen as an internal reference. Even though the bulk Raman signal of ethanol is very weak in regions void of AgNWs under evanescent field excitation (Figure 87), it can be easily detected nearby stacks of AgNWs due to some electromagnetic enhancement of its vibration modes (bands highlighted in red in Figure 87). Figures 88.B and 89.B present the change in the intensity ratio I_{PVP}/I_{EtOH} and I_{MUA}/I_{EtOH} as a function of time, where I_{PVP}, I_{MUA} and I_{EtOH} are integrated intensities of the 1766, 630 and 855 cm^{-1} Raman bands respectively. Two spectra are also plotted to illustrate the observed changes (Figures 88.A and 89.A). The PVP-MuA substitution mechanism seems to proceed in two main steps. For t<τ_{PVP}≈40 min, PVP molecules are replaced by their MuA counterparts as reflected by the intensity decay of the I_{PVP}/I_{EtOH} ratio which nullifies for t>τ_{PVP} (Figure 88.B), congruent with the disappearance of the band centered at 1766 cm^{-1} (grey solid line in Figure 88.A) and the emergence of the 1776 cm^{-1} C=O band of free PVP molecules (grey dashed line in Figure 88.A).

123
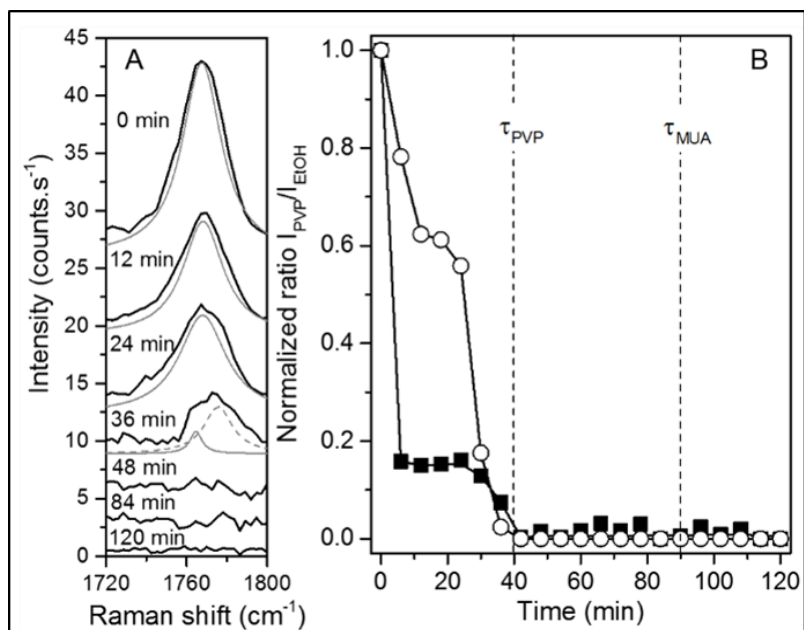
Figure 88: A) SERS spectra obtained upon exciting a bundle of Ag NWs at 561 nm in contact with a 100 µM MuA solution for 0, 12, 24, 36, 48, 84 and 120 min (black solid lines). The band centered at 1766 cm^{-1} is assigned to the C=O mode of bound PVP molecules (grey solid lines). The peak at 1776 cm^{-1} (grey dashed line) can be assigned to the C=O mode of free PVP molecules. B) Normalized intensity ratio of the C=O band (PVP) at 1766 cm^{-1} and a marker band assigned to ethanol at 885 cm^{-1} as a function of time for two different concentrations of the MuA solution, namely 500 µM (filled squares) and 100 µM (open circles). Each curve corresponds to the average value of 2 kinetics performed in the same experimental conditions.
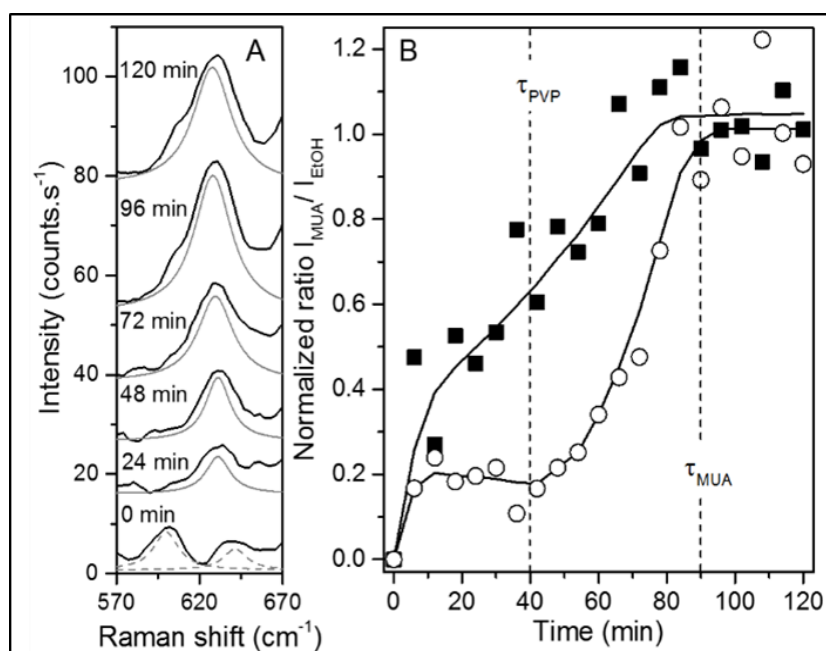
Figure 89: A) SERS spectra obtained upon exciting a bundle of Ag NWs at 561 nm in contact with a 100 µM MuA solution for 0, 24, 48, 72, 96 and 120 min (black solid lines). The band centered at 630 cm^{-1} is assigned to the C-S mode of bound MuA molecules (grey solid lines). Peaks at different wavenumbers are indicated with grey dashed lines. B) Normalized intensity ratio of the C-S band (MuA) at 630 cm^{-1} and a marker band assigned to ethanol at 885 cm^{-1} as a function of time for two different concentrations of the MuA solution, namely 500 µM (filled squares) and 100 µM (open circles). Each curve corresponds to the average value of 2 kinetics performed in the same experimental conditions.

This derives from the ability of MuA molecules to adsorb on silver by forming COO-Ag or S-Ag bonds.[179] This competition between the two anchor terminal sites of MuA molecules leads to a partial covering of AgNWs through strong Ag-S covalent bonds for t< τ_{PVP}. For t>τ_{PVP}, MuA molecules tend to adopt the more stable orientation by breaking COO-Ag bonds to create S-Ag bonds until τ_{MuA} is reached. This process is slower than the MuA functionalization of bare silver which is almost complete within 60 min,[179] which suggests the existence of a retardation effect induced by the necessary removal of PVP molecules. Note that it was not possible to follow the intensity change of the COO-Ag Raman band expected[179] at 1394 cm^{-1} owing to unfortunate band overlaps. Finally, for t>τ_{MuA}, all the AgNWs are covered with MuA molecules adsorbed via covalent Ag-S bonds.

This 2-step mechanism of the PVP-MuA substitution presents a peculiar dependence as a function of the MuA concentration. For 500 µM and 100 µM MuA solutions, τ_{PVP} and τ_{MuA} are not affected, but each step appears globally slower at the lowest 100 µM concentration. Concerning the PVP desorption after injection of a 500 µM MuA solution (Figure 88.B), the intensity ratio I_{PVP}/I_{EtOH} falls down quickly within 6 min and reaches a plateau ($I_{PVP}/I_{EtOH}\approx0.15$) before vanishing at τ_{PVP}. In contrast, for a 100 µM MuA solution, the initial decrease lasts 12 min and the plateau occurs at higher intensity ratio ($I_{PVP}/I_{EtOH}\approx0.18$). Regarding the C-S bond formation (Figure 89.A), the I_{MUA}/I_{EtOH} ratio increases gradually for a 500 µM MuA solution while, after a short initial surge, it stabilizes at $I_{MUA}/I_{EtOH}=0.19$ during 40 min before pursuing its rise for a 100 µM MuA solution.

In order to explain this atypical behavior, it is worth recalling that both portions of single AgNWs and hot spots at contact points between AgNWs contribute to the detected SERS signal. The molecular accessibility of hot spot regions is clearly reduced with respect to isolated sections of AgNWs. Therefore, these latter areas react first with MuA molecules. For a large excess MuA concentration (500 µM), most of hot spot regions can be simultaneously

functionalized. However, at lower MuA concentration (100 µM), the PVP-MuA substitution slows down due to the steric hindrance and leads to intermediate plateaus corresponding to incubation times before triggering the PVP-MuA substitution (for $t < \tau_{PVP}$) or the MuA reorientation (for $\tau_{MuA} < t < \tau_{PVP}$) mechanisms in hot spot regions.

4.2.3. Chemical stability of MuA-passivated Ag nanowire networks

The modified MuA-silver nanowires were deposited onto glass substrates according the protocol 4.5. Figure 90.a and b show SEM images of an electrode made of AgNWs@PVP and AgNWs@MuA respectively. Unfortunately, the passivated silver nanowires did not spread uniformly onto the glass substrate. Contrarily to the Ag@PVP nanowires, the Ag@MuA nanowires have a strong tendency to aggregate upon the deposition process. Such effect is associated to the weak repulsion generated by the MuA-capped Ag nanowires.
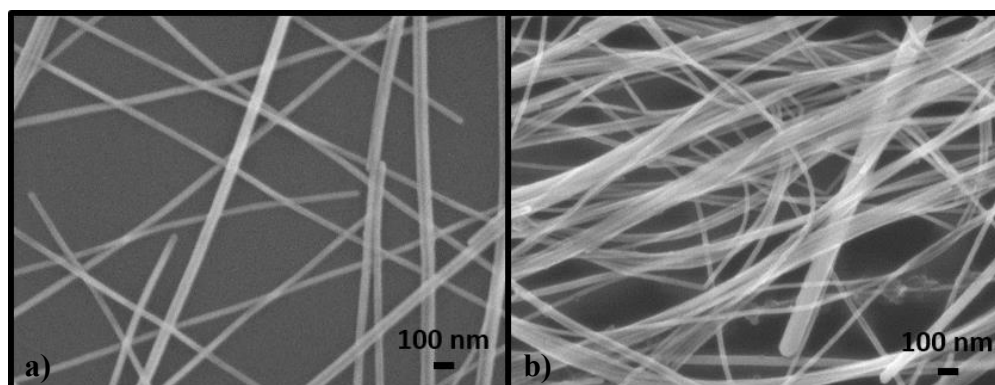
Figure 90: SEM images of electrodes consisting of a) silver nanowires passivated with PVP and b) silver nanowires passivated with MuA.

4.2.4. Surface modification of silver nanowires deposited on a substrate

To overcome this problem, an alternative method of MuA passivation was investigated. The surface modification was performed on the Ag@PVP nanowires after they were deposited on a given substrate, rather than in solution before deposition (Figure 91).
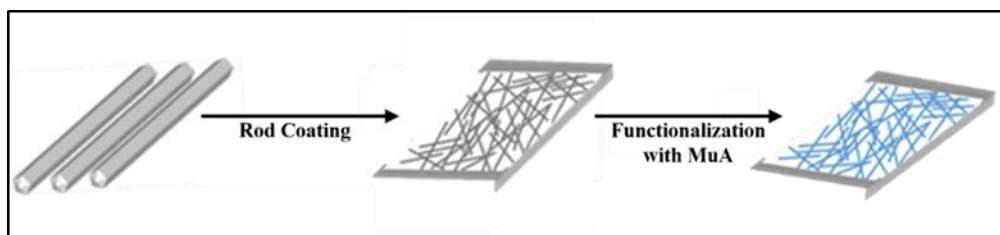
Figure 91: Scheme of the passivation of the AgNW Network.

Protocol 4.6: **Fabrication of the electrodes**

40 µl of AgNW d = 70nm suspension (purchased from ACS Materials) diluted to a concentration of 4 mg/ml were coated on a 20 mm x 30 mm glass substrate. This coating was applied 3 more times, with each coating being applied across a different orthogonal direction to obtain a random NW network. The annealing treatment was set at 180 °C for 30 minutes.

Protocol 4.7: **Passivation of the electrodes**

The 70 nm diameter NW electrodes were immersed in a solution of MuA/ethanol at a 1.8 mM concentration of MuA for one hour to functionalize the silver nanowires already deposited on the substrate. The electrode was then removed and immersed a second time in the MuA/ethanol solution for 30 minutes.

Lifetime study

The lifetime study was performed by storing electrodes in a non-hermetic box at ambient temperature and ambient atmosphere (relative humidity = 80%). One box was left open to expose the electrodes to light and the other one was covered to keep them in the dark. The properties of the electrodes were investigated over a period of 4 months. In this manner, the sheet resistances were measured twice a week during the first two months and once a week during the last two months. Sheet resistances of the electrodes were measured by two-point probe measurements using a multimeter. Quoted resistance is an average of eight measurements performed on electrodes. Finally, transparency was measured at 550 nm with a spectrophotometer and using plain glass as a reference.

Figure 92 shows SEM images of a network before and after passivating the AgNWs with MuA. The density and uniformity of the network before and after passivation are similar. Therefore, passivating AgNWs with MuA post-deposition avoids the problem of Ag@MuA agglomerating in solution.
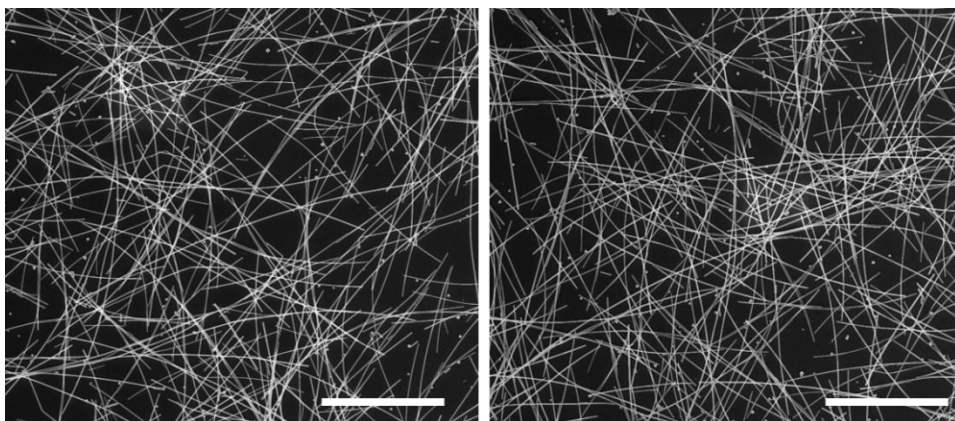
Figure 92: SEM images of the networks of Ag@PVP (left) and Ag@MuA (right) elaborated following the scheme described in Figure 91. Scale bar 10 µm.

Chemical analysis was performed on the random network of AgNW after the MuA passivation in order to ensure that the surface modification was homogeneous. A chemical maping was performed using an EDX (Energy-dispersive X-ray) spectrometer which was coupled to an SEM at the Plateforme CASTAING in Toulouse, France. Probing the sulfur was very difficult since the element is present at low concentration compared to silver. Nevertheless, and in opposition to the Ag@PVP network (not shown here), S can be detected in low amounts (Figure 93), demonstrating once again the presence of MuA.
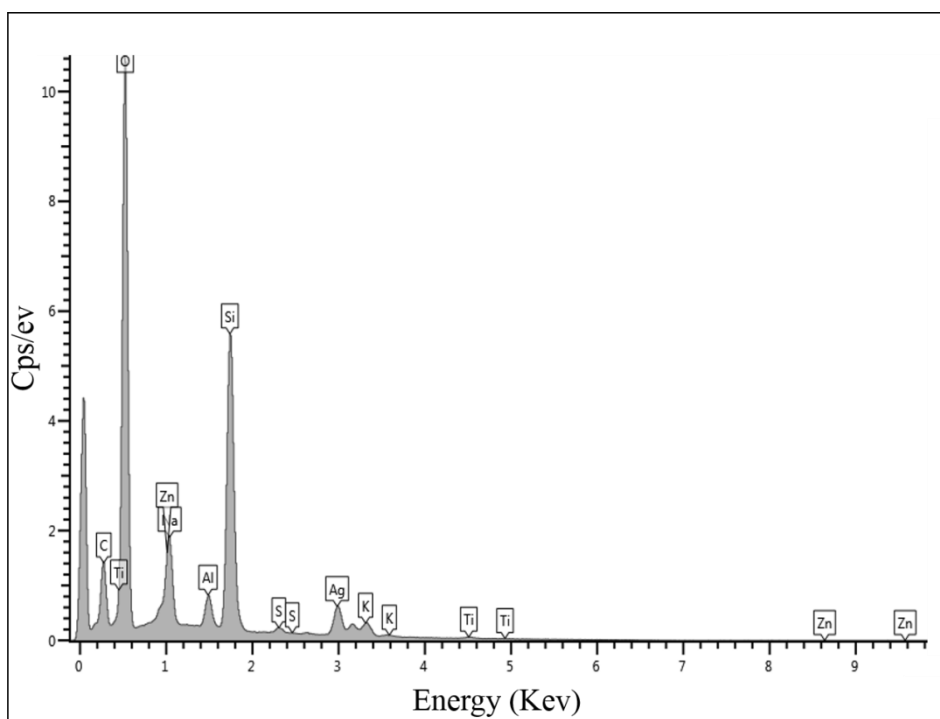
Figure 93: Spectrum corresponding to the chemical analysis of the MuA-passivated electrode.

4.2.5. Lifetime of the silver nanowire electrodes

The evolution over time of the electrical resistance and optical transparency of the passivated and non-passivated electrodes has been thoroughly investigated. Along these lines, the electrode were fabricated according the protocols 4.6 and 4.7, while the concentration of the suspension was chosen in order to obtain a sheet resistance lower than 20 Ohms/sq. Measurements were performed on both electrodes protected from light and electrodes exposed to ambient light.

4.2.5.1.   Impact of the MuA on the intrinsic properties of the electrodes

The initial sheet resistances and transparencies of the unpassivated and passivated nanowire electrodes are presented in Table 4.1. The values of both electrodes are similar indicating that the MuA molecule did not negatively affect the electrical and the optical properties of the electrodes. Moreover, the evolution of the electrical resistance of the electrodes protected from the light over time is reported in Figure 94.

129

Table 4.1: Initial sheet resistances and transparencies of the passivated and unpassivated AgNW electrodes

	Ag NW Network passivated PVP	Ag NW Network passivated MuA
Commercial Ag NWs d = 70 nm	Rs = 9.0 +/- 1.0 Ohm/Sq T = 85 +/- 1 %	Rs = 8.8 +/- 0.4 Ohm/Sq T = 86 +/- 1 %

Figure 94: Evolution of the sheet resistance of unpassivated (black solid line) and passivated (grey solid line) AgNW electrodes.

The sheet resistance of the reference sample (AgNW@PVP) increased significantly, by 277% (i.e. 2.8X), over a period of 4 months. In this case, the increase has been assigned to the progressive oxidation and sulfurization of the silver nanowires, causing a degradation of the silver nanowire network. On the other hand, when MuA-capped silver nanowires are measured, the sheet resistance of the electrodes only increases by 34% with respect to the original value. Interestingly, these results highlight the drastic improvement in electrode stability under air achieved with this small organic molecule.

The different evolution of the resistance versus time in the same two networks stored and exposed to daylight have been evaluated (Figure 95). In this case, the reference electrode presents a strong degradation after 4 months of storage, with an increment in sheet resistance of 20718% over this period of time. This finding suggests that light may act as a catalyst through a photo-oxidation process: electrons could be removed from Ag^0 by photon-absorption, facilitating the interaction of photo-oxidated Ag^+ with O_2 and H_2S available in the air. Such reaction could lead to the formation of AgO, Ag_2O and Ag_2S.[181] On the other hand, the electrical resistivity of AgNW meshes covered by a layer of MuA experienced a dramatically lower effect, leading to an increase in sheet resistance of 225%.

Figure 95: Evolution of the sheet resistance of unpassivated (black solid line) and passivated (grey solid line).

In order to obtain a more complete understanding of the evolution experienced by the different electrodes under study, their optical properties over time have been analyzed (Table 4.2). It is important to remark that transparency was less frequently measured than the sheet resistance given the fact that the window tint meter can remove some nanowires from the surface during the measurement process, thus affecting the reliability of the measurement. In this case another set of electrodes were used for measurements and the decrease in

transparency is expressed in percentage. Interestingly, our results show that capping the electrodes with MuA does not affect the overall optical properties of the electrodes (independently of their storage under light or in the dark). These observations confirm that MuA is a promising passivation agent for AgNW electrodes.

	Storage under light		Storage in the dark	
	AgNW electrodes unpassivated	AgNWs electrodes passivated with MuA	AgNW electrodes unpassivated	AgNWs electrodes passivated with MuA
After 4 days	+ 0,4 %	+ 0,75 %	+0,78%	-0,05%
After 3 months	- 3,0 %	- 2,3 %	-1,05 %	- 2,1 %
After 4 months	- 4,5 %	- 4,1 %	- 1,8 %	- 3,0 %

Table 4.2: Evolution of the transparency of passivated and non-passivated electrodes over time.

4.2.5.2. Lifetime stabilities of electrodes based on thin nanowires

Similar experiments have been performed on electrodes based on thinner nanowires, known to be more fragile than the ones based on "thick nanowires". Electrodes were fabricated and passivated following protocols 4.8 and 4.9.

Protocol 4.8: Fabrication of the electrodes

4 coating stages have been implemented. Each one of them consists in the deposition of 47 µl of AgNWs (d = 32 nm and a concentration of 5.7 mg/ml) onto 24 mm x 32 mm glass substrates in 4 orthogonal directions to obtain a random NW network. The annealing treatment was set at 160 °C for 30 minutes.

Protocol 4.9: Passivation of the electrodes

The 32 nm diameter NW electrodes were immersed in a solution of MuA/ethanol at a higher concentration of MuA (18 mM) for one hour to functionalize the silver nanowires already deposited on the substrate. The electrode was then removed and immersed a second time in a solution of MuA/ethanol (18 mM) for 30 minutes. The benches were placed on a

rocking platform (Bio-Rad's rocking platforms) for a continuous agitation of the reagents on the electrodes.

The evolution of the properties of the different electrodes obtained is represented in Figure 96. In this case similar trends to previous observations made for thicker Ag NW (d = 70 nm) electrodes can be observed on both the optical and the electrical properties. Along these lines, a 48% increase of sheet resistance was observed for non-passivated electrodes versus 12% for MuA-passivated electrodes when stored in the dark. On the other hand, in the case of electrodes exposed to daylight the average resistance increase was 10960 % for the non-passivated electrodes versus 588% for those passivated with MuA. One could postulate that the difference in relative increase of the resistance for the two studied networks ("thick" and "thin" NWs) may originate from the difference in density of nanowires deposited: the resistance of dense networks is more important than that of sparser ones since more alternative pathways exist for the current to flow if a pathway becomes too corroded to conduct current.[6] In our study, thin nanowires are shorter than thick ones, thus a higher density of the former is required to reach a similar initial resistance than that obtained for the 70 nm nanowires.

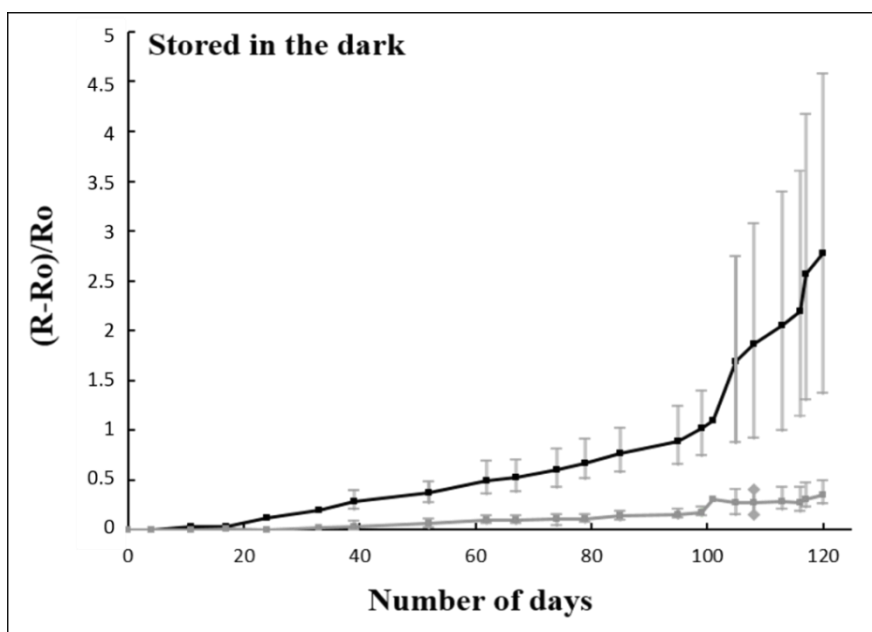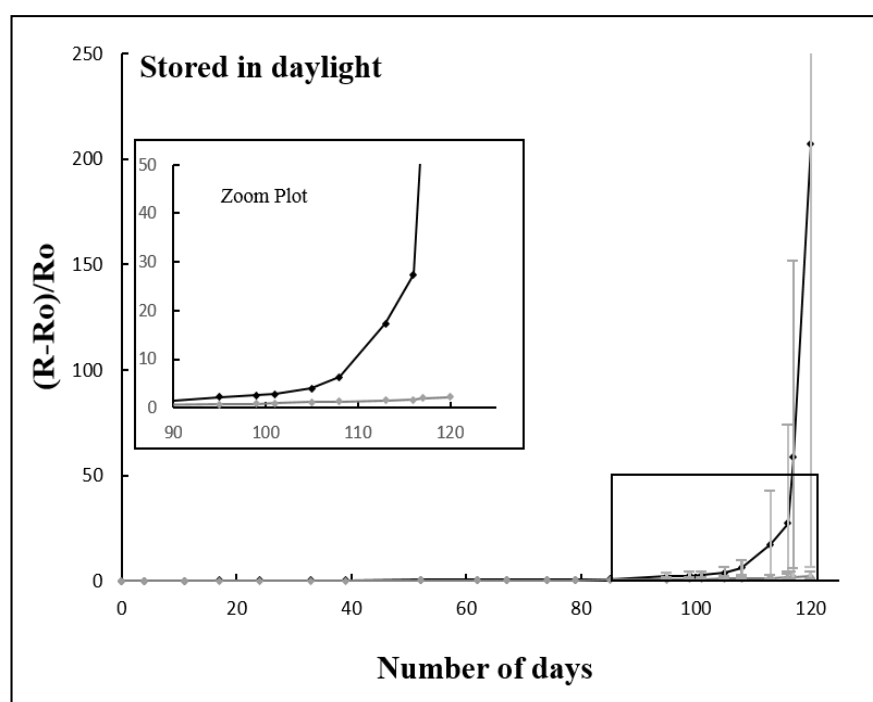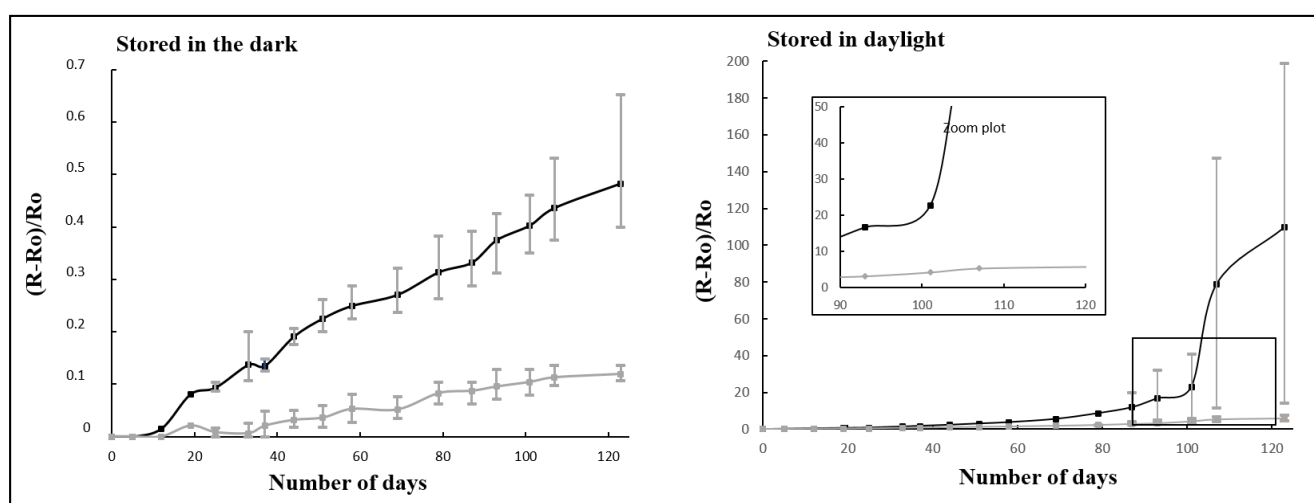
Figure 96: Evolution of the sheet resistance of unpassivated (black solid line) and passivated (grey solid line) electrodes in the dark (left) and under daylight (right).

Similar experiments performed on electrodes based on thinner nanowires were reproduced with PPh$_3$ instead of MuA following protocols 4.8 and 4.10.

Protocol 4.10: Passivation of the electrodes with PPh$_3$

The 32 nm diameter NW electrodes were passivated with a solution of PPh$_3$ in ethanol (18 mM) following protocol 4.9.

The chemical stability of the electrodes passivated with PPh$_3$ is similar to the stability of the electrodes passivated with MuA (Figure 97). More precisely, a 588% increase of resistance was observed for MuA passivated electrodes versus 722% for PPh$_3$ passivated electrodes (both samples being stored in daylight).
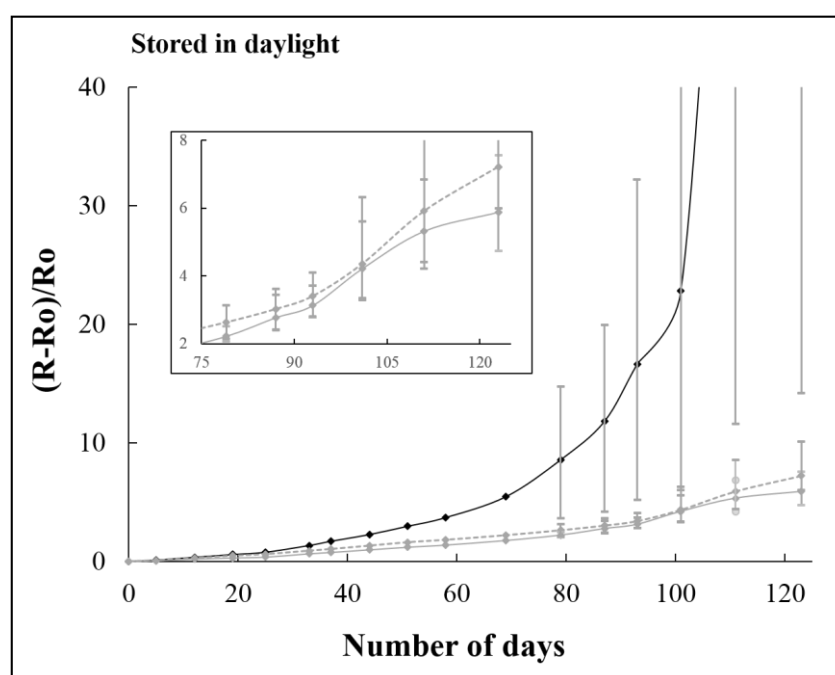
Figure 97: Evolution of the resistance of unpassivated (black solid line), passivated MuA (grey solid line), passivated PPh$_3$ (grey dashed line) and in the daylight.

The previous study of PPh$_3$ passivation showed an increase of sheet resistance of 500% (10 Ω/sq to 60 Ω/Sq) after 3.5 months in air in the dark.[70] The differences in the resistance increase observed between MuA and PPh$_3$-passivated electrodes must reflect chemical differences at the silver surface. One possibility is that the MuA forms a dense and ordered monolayer on silver that limits corrosion:[169] upon exposure to the solution of

alkanethiol (type of MuA molecule) the surface reacts with thiols and the resulting monolayer on silver contain no (or little) silver oxide. Along these lines, the oxide must be removed during the formation of the monolayer of MuA by reduction or displacement by the thiols. In contrast, the formation of the PPh$_3$ passivation layer could allow the formation of oxide prior to the complete functionalization. In this manner, such oxidized surface may reacts with PPh$_3$ and the resulting passivated layer contains some similar oxide that may favor the corrosion of silver over time.

4.2.5.3.   Conclusion

This study evidences that MuA is a promising passivation agent for silver nanowire networks in terms of chemical stability. We have proved that MuA can easily replace PVP on the silver nanowire surface. XPS and SERS-TIR analysis show important evidence on both the stability of thiolate bonding over time and the mechanisms of the replacement of the PVP by MuA. We conclude that a minimum of 90 minutes of exchange reaction are needed to completely replace the PVP at the surface of the silver nanowires. Along these lines, the replacement of the PVP by MuA proceeds within two steps: (i) a fast anchoring of the MUA on the metal surface via the formation of COO-Ag and S-Ag bonds within a few minutes and (ii) a slow reorganization of MUA molecules over a period of tens of minutes to form a self-assembled monolayer.

Interestingly, the passivation of AgNWs with MuA allows to improve their protection against oxidation. For electrodes made of thin Ag@PVP exposed to daylight, the average resistance increase was 10960 % versus 588% for those passivated with MuA. The sheet resistance of thicker nanowires increased even less (225%) due to their higher chemical stability. The functionalization protocol can be implemented both in solution or directly onto already-deposited nanowires. Nevertheless, the bad colloidal stability of the AgNWs leads to a better results when the passivation is performed directly on the electrodes.

The intrinsic properties of the network, namely the conductivity and transparency, were not affected by this approach. As already seen in Chapter 1, the transparency decreased when silver nanowires were passivated with metal oxide (TiO_2 or ZnO, -6%) or graphene (-3%) which is not the case when PPh_3 or MuA are used.[70,95,107] Unfortunately, having a short molecule instead of PVP does not lead to an increase in conductivity because of the colloidal instability of the silver nanowires. For instance, TiO_2 allows an increase of an order of 50 Ohm/Sq.[98]

Strategies to improve the passivation further will have to be implemented in order to obtain even more stable systems under light exposure. In this manner, we believe that it may be interesting to explore the passivation capability of alkanethiols with longer carbon chains. Similarly, the chemical modification of the carboxyl group of the MuA layer anchored on metal surface could be tested as well: i.e. benzene cycles could be attached to MuA via the formation of an amide bond. Since benzene has a strong density of electrons and silver is more electrophile under light, a continuous transfer of electrons from the benzene moieties to the silver surface could be created (aromatic mesomeric effect (+M)). This effect may result in an increase of the chemical stability of the electrodes given that the silver nanowires would be fed with a continuous transfer of electrons.

4.3. Conclusion of the Chapter

Lifetime and stabilities issues were tackled in this chapter. The Joule heating generated by working electrodes was first investigated. The results showed that graphene passivation enhances the thermal stability of silver nanowire electrodes by more homogeneously distributing heat across the network. The lifetime of the electrode were extended to only 12 days because the joule heating effect is still present. In this manner, graphene does not prevent Joule heating in the nanowires and local points of high temperature ultimately shift the failure mechanism from nanowire degradation to melting of the

underlying plastic substrate. Moreover, graphene has also the tendency to decrease the transparency of the electrodes.

Regarding the electrode stability over time, we have demonstrated that MuA is a promising passivation agent for silver nanowires. The molecule itself does not affect negatively the conductivity or transparency of the electrode and is extremely cheap, both characteristics contributing to the commercial viability of this passivation method. A method to functionalize the surfaces of silver nanowires with MuA has also been developed and a novel Surface Enhanced Raman Spectroscopy method has been used to prove that the molecule forms a complete self-assembled monolayer onto the metallic surface.

Conclusion and future work

Transparent electrodes based on silver nanowires are continuously being investigated for their application in optoelectronic devices as a replacement for ITO. The study presented herein focused on the performance enhancement of such electrodes. Our strategies based on simulations[57] and previous research[61,88] lead to the elaboration of both ultra-long silver nanowires and branched silver nanowires to improve electrode conductivity. Moreover, since the thermal and chemical stability of the silver nanowires is a major issue for their application in real devices, an additional part of our research is focused on the elaboration of more robust silver nanowires.

In **chapter 2**, nanowires with a mean length of 130 μm and a diameter of 124 nm (aspect ratio of 1050) were synthesized in high yield in relatively short reaction times (80 minutes). It was shown that an easy variation of the initial concentration of the molecular precursors could be used to tune the aspect ratio of the silver nanowires. In this manner, a range of nanowire batches with aspect ratios varying from 1000 to 1130 is accessible. These original nanostructures were subsequently used for the elaboration of transparent electrodes using three different deposition processes onto the glass substrates: spin coating, spray coating and Mayer rod coating. On an adapted substrate, Mayer rod coating revealed itself as the most suitable method to get homogeneous networks when ultra-long silver nanowires are used. Such methodology leads to high transparency and high conductivity at room temperature. Thermal treatment has been shown to have a very small influence on the decrease of the sheet resistance. In this work, we could elaborate electrodes with a sheet resistance lower than 5 Ω/Sq and with a transparency of 94 %. Such Haacke factor was rarely reported for nanowire electrodes. Future work includes the replacement of HCl by a mixture of HBr and HCl which could induce the elaboration of thinner silver nanowires while keeping

the same lengths.[182] The ultra-long silver nanowires having thinner diameter (but still higher than 50 nm) should induce more transparency for an equivalent conductivity and scatter less light. Preliminary syntheses were performed by replacing HCl with HBr, which indeed lead to the formation of thinner nanowires. Surprisingly, a second population of silver nanorings with diameters of approximatively 15 µm could be observed as well (Figure 98). Unfortunately, their yield is low in comparison to the population of silver nanowires.
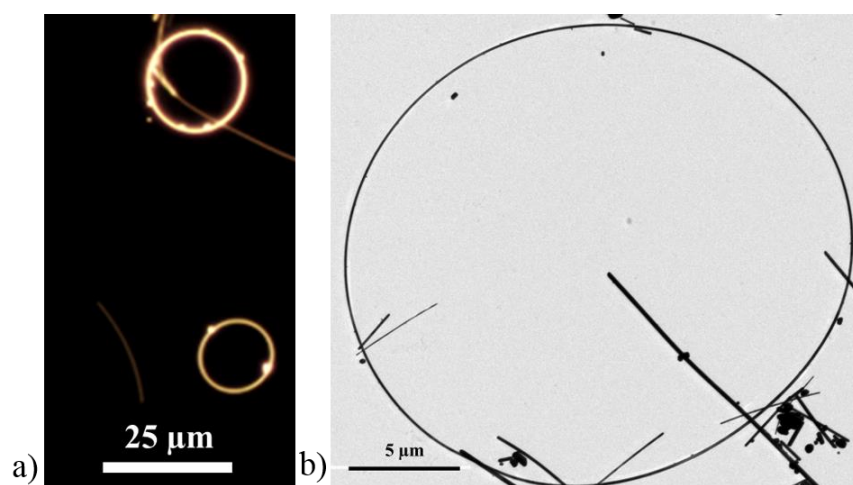
Figure 98: Dark field image of silver nanowires and nanorings and TEM image of a silver nanoring

A further step in this direction would consist of their assembly into a film via dip-coating a substrate in the nanoring solution, allowing a "Olympic-like" organization of these nanorings (Figure 99). Numerous percolation pathways could then be obtained for a low density of nanostructures. Moreover, a modification of the diameter of the Ag rings may lead to the modification of the transparency of the entire electrode.
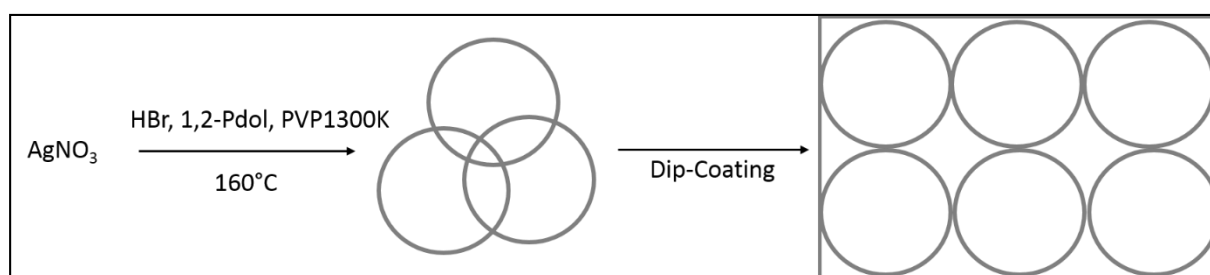
Figure 99: Scheme of fabrication of silver nanowires based on metallic nanorings.

In **chapter 3**, the goal consisted in the synthesis of branched silver nanowires. Based on the synthesis of silver nanowires from multiply twinned platinum seeds developed by Younan Xia few years ago,[15] a first strategy consisted in the growth of silver from platinum tripods. No branches could be obtained following this protocol and the dissolution of the platinum tripods was observed. Such dissolution may come from the elevated temperature at which the polyol process took place. Therefore, the growth of silver from platinum tripods (length of the branches ≈ 50 nm) was performed in water at lower temperature, thus leading to the emergence of only one branch emerged from the tripod. Moreover, this protocol can also lead to the dissolution of one branch or to the formation of a Pt tripod totally encompassed within a nanowire. These promising results have lead our work towards the study of the growth mechanism of silver from platinum seeds in the polyol process. Along these lines, our findings suggest that one silver nanowire does not grow from one platinum seed but from several ones. Such nascent nanostructures have been defined by ARM as an organic preform full of crystallites containing both silver and platinum, the latter metal being dissolved throughout the reaction. In this manner, we believe that the platinum seeds act as catalysts in the synthesis of Ag nanowires. Consequently, other strategies have been developed in order to obtain branched nanowires, including the addition of foreign ions or by using two different surfactants during the polyol process. Unfortunately, both approaches have proven to be ineffective towards the synthesis of high quality samples. A last strategy has been induced concerning the use of ultra-sounds during the polyol process, allowing the synthesis of branched nanowires and "boomerang-like" shaped silver nanowires. Even though such results seem promising, the limited length of the nanostructures obtained (≈ 6 μm) reduces their interest to enhance the performance of conductivity of the electrodes in comparison to ultra-long silver nanowires.

We believe that the synthesis of branched nanowires from platinum tripods could be developed by using platinum tripods having longer branches (200 nm). Since it is possible to create one silver branch from one platinum tripod branch, it should be possible to obtain three branches by tuning the kinetics of the reaction. Having longer branches should facilitate the deposition of silver onto every single branch before their total dissolution (Figure 100).
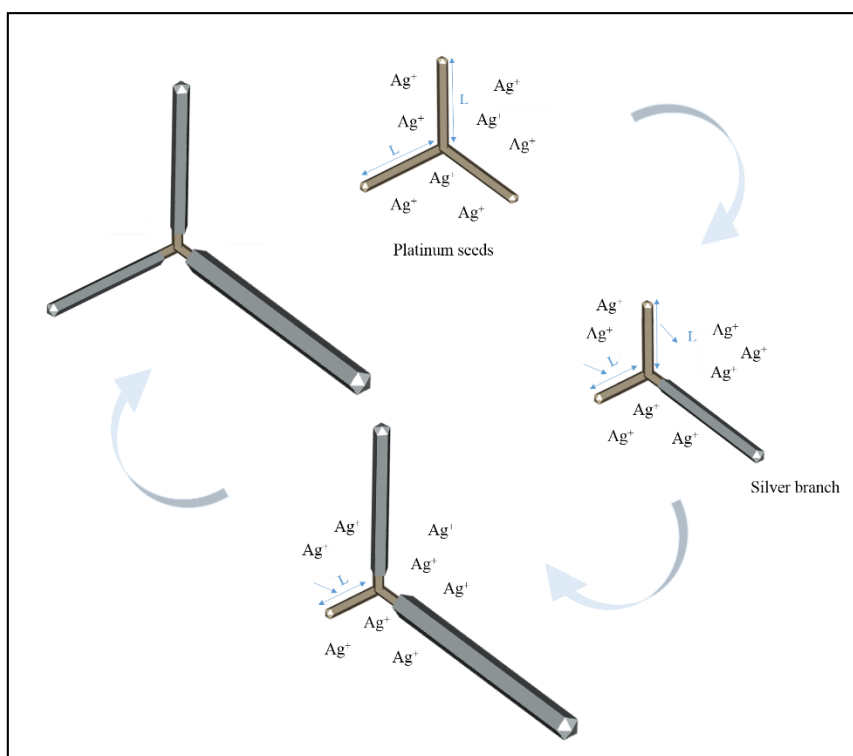
Figure 100: Schematic representation of the growth of silver on Pt tripods seed with long branches length.

The synthesis was also performed on another type of branched structure: Pd/Cu tetrapods. In this case, even though silver did not grow from the tip of the tetrapods but from their core, resulting in interesting pyramidal core-shell nanoparticles. Similar results are observed when silver grows from platinum tripods at a lower concentration of capping agent. Both core shell Pt@Ag triangles and Pd/Cu@Ag pyramids have interesting features for plasmonic studies. By using this synthesis route, future works could thus be performed to further expand this novel family of nanostructures (Figure 101).
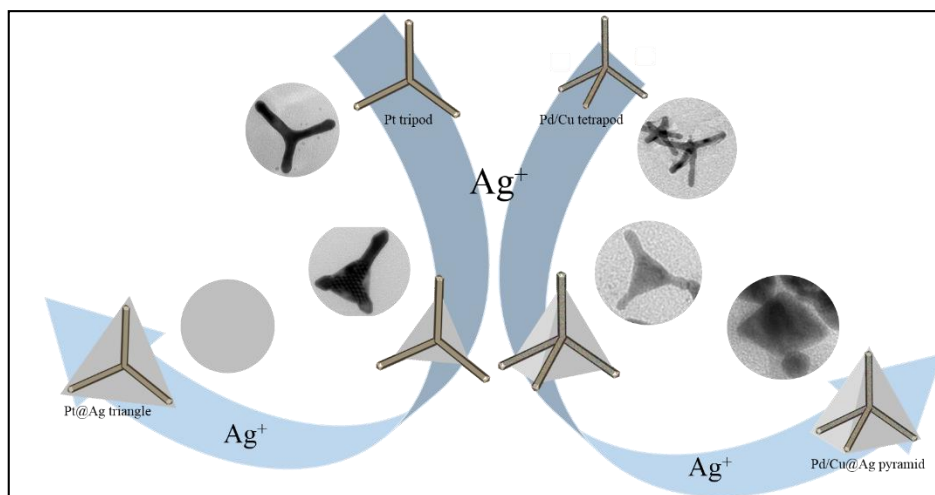
Figure 101: Schematic representation of the plasmonic nanostructures of unconventional morphologies.

In the **last chapter** of the thesis, chemical and thermal stability issues of Ag nanowires were tackled. In collaboration with H.Hosseinzadeh Khaligh, the Joule heating problem in silver nanowire transparent electrodes was investigated. Thermal properties of silver nanowires and hybrid silver nanowire/graphene electrodes were treated in comparison with electrodes made of ITO. The results showed that graphene passivation enhanced the thermal stability of the silver nanowire electrodes by limiting the number of hot spots in the network and thus inducing a more homogeneously-distributed heat when current passes through it. However, the graphene passivation does not prevent Joule heating in the nanowires and local points of high temperature ultimately shift the failure mechanism from nanowire degradation to melting of the underlying plastic substrate. Strategies to manage Joule heating include increasing the nanowire density in the film, reducing the current flowing across the electrodes, and ensuring the nanowires are uniformly dense across the film. The second part of this chapter focused on the chemical instability of silver nanowires. Although, as shown in the first part of the chapter, graphene can slow the chemical degradation of nanowires, like most other passivation it decreases the transparency of the electrodes. With a different approach, the protection of transparent electrodes against oxidation without altering their properties of transparency and conductivity was performed using a short molecule as

passivating agent. In opposition to classical methods which coat silver nanowire films with a continuous passivation layer such as graphene or metal oxide,[95,96,98,103,138] the passivation of the silver nanowire surfaces only with a short molecule such as trioctylphosphine[70] seemed to us as a valuable alternative with lower impact on the optical and mechanical properties of the electrodes. In this work, we have demonstrated that MuA is a promising passivation agent for silver nanowires, leading to longer lifetimes. Moreover, Surface Enhanced Raman Spectroscopy allowed us to observe that such a molecule forms a complete self-assembled monolayer on the surface of the nanowires. A lifetime study was been performed over 4 months on two different sets of transparent electrodes composed by thick and thin silver nanowires. In both cases the passivation leads to overall improved stability. The decrease of the electrical properties over time still exists but it is slowed, which makes MuA a promising agent for the protection against the oxidation of silver nanowires. Additional work consists of grafting a benzene cycle having an amine function, which could allow a continuous electron feeding of the silver nanowires by the mesomeric effect.

As mentioned above, the aim of our work is to enhance the electrical and optical properties of nanowire electrodes as well as their stability over time under working conditions. Improvement of the performance of the electrodes was reached by rod coating ultra-long silver nanowires on glass substrates. Even though these nanostructures have been already presented in the literature, the synthesis presented in this manuscript is new, cheap and extremely fast allowing dimension-controlled nanostructures. And most importantly, nanowires with the highest aspect ratio between length and diameter ever reported was achieved. Furthermore, low resistance could be achieved without annealing which has numerous advantages. The synthesis of "novel" nanostructures such as "branched silver nanowires" remains a challenge. This thesis helps to select the chemical processes needed to develop synthetic routes of a novel family of complex nano-objects with interesting

plasmonic properties. We found that the coating of graphene on silver nanowire networks can induce better thermal stability. Moreover, the coating of such structures with MuA leads to improved electrical stabilities in comparison to silver nanowires with the PVP that remains from their polyol synthesis. Investigations on the mechanisms of replacement of PVP by MuA proved a complete replacement.

References

[1]   D. Bellet, M. Lagrange, T. Sannicolo, S. Aghazadehchors, V. Nguyen, D. Langley, D. Muñoz-Rojas, C. Jiménez, Y. Bréchet, N. Nguyen, *Materials (Basel).* **2017**, *10*, 570–586.

[2]   Y. Zhu, H. Ji, H.-M. Cheng, R. S. Ruoff, *Natl. Sci. Rev.* **2017**, 1–12.

[3]   L. He, S. C. Tjong, *Mater. Sci. Eng. R Reports* **2016**, *109*, 1–101.

[4]   J. Meiss, C. L. Uhrich, K. Fehse, S. Pfuetzner, M. K. Riede, K. Leo, in *Photonics Eur. Photonics Sol. Energy Suystems II, Ed. Andreas Gombert, Proc. SPIE, Vol. 7002, 700210,* (Ed.: A. Gombert), **2008**, pp. 700210–700219.

[5]   S. Bae, S. J. Kim, D. Shin, J.-H. Ahn, B. H. Hong, *Phys. Scr.* **2012**, *T146*, 014024–014032.

[6]   D. S. Ghosh, *Ultrathin Metal Transparent Electrodes for the Optoelectronics Industry*, Springer International Publishing, Heidelberg, **2013**.

[7]   C.-C. Lee, P.-C. Huang, K.-S. Wang, *Materials (Basel).* **2016**, *9*, 850–860.

[8]   F. Dauzou, P. C. P. Bouten, A. Dabirian, Y. Leterrier, C. Ballif, M. Morales-Masis, *Org. Electron. physics, Mater. Appl.* **2016**, *35*, 136–141.

[9]   H. Kim, J. S. Horwitz, G. P. Kushto, Z. H. Kafafi, D. B. Chrisey, *Appl. Phys. Lett.* **2001**, *79*, 284–286.

[10]   R. K Narashimha, *Indian J. Pure Appl. Phys.* **2004**, *42*, 201–204.

[11]   Q. Huang, W. Shen, X. Fang, G. Chen, Y. Yang, J. Huang, R. Tan, W. Song, *ACS Appl. Mater. Interfaces* **2015**, *7*, 4299–4305.

[12]   S. E. Skrabalak, B. J. Wiley, M. Kim, E. V. Formo, Y. Xia, *Nano Lett.* **2008**, *8*, 2077–2081.

[13]   N. M. Abbasi, H. Yu, L. Wang, Zain-Ul-Abdin, W. A. Amer, M. Akram, H. Khalid, Y. Chen, M. Saleem, R. Sun, et al., *Mater. Chem. Phys.* **2015**, *166*, 1–15.

[14]   J.-Y. Lin, Y.-L. Hsueh, J.-J. Huang, J.-R. Wu, *Thin Solid Films* **2015**, *584*, 243–247.

[15]   Y. Sun, Y. Yin, B. T. Mayers, T. Herricks, Y. Xia, *Chem. Mater.* **2002**, *14*, 4736–4745.

[16]   M. Tsuji, K. Matsumoto, P. Jiang, R. Matsuo, X. L. Tang, K. S. N. Kamarudin, *Colloids Surfaces A Physicochem. Eng. Asp.* **2008**, *316*, 266–277.

[17]   M. N. Gueye, A. Carella, N. Massonnet, E. Yvenou, S. Brenet, J. Faure-Vincent, S. Pouget, F. Rieutord, H. Okuno, A. Benayad, et al., *Chem. Mater.* **2016**, *28*, 3462–3468.

[18]   T. Sannicolo, M. Lagrange, A. Cabos, C. Celle, J. P. Simonato, D. Bellet, *Small* **2016**, *12*, 6052–6075.

[19] C. H. Tsai, S. Y. Hsu, T. W. Huang, Y. T. Tsai, Y. F. Chen, Y. H. Jhang, L. Hsieh, C. C. Wu, Y. S. Chen, C. W. Chen, et al., *Org. Electron. physics, Mater. Appl.* **2011**, *12*, 2003–2011.

[20] B. L. Groenendaal, F. Jonas, D. Freitag, H. Pielartzik, J. R. Reynolds, **2000**, 481–494.

[21] N. Kim, S. Kee, S. H. Lee, B. H. Lee, Y. H. Kahng, Y. R. Jo, B. J. Kim, K. Lee, *Adv. Mater.* **2014**, *26*, 2268–2272.

[22] K. I. Bolotin, K. J. Sikes, Z. Jiang, M. Klima, G. Fudenberg, J. Hone, P. Kim, H. L. Stormer, *Solid State Commun.* **2008**, *146*, 351–355.

[23] S. H. Keshmiri, M. Rezaee-Roknabadi, S. Ashok, *Thin Solid Films* **2002**, *413*, 167–170.

[24] D. Wang, Y. Mei, G. Huang, *J. Semicond.* **2018**, *39*, 011002–011024.

[25] W. Yang, C. Wang, *J. Mater. Chem. C* **2016**, *4*, 7193–7207.

[26] S. Bae, H. K. Kim, Y. Lee, X. Xu, J.-S. Park, Y. Zheng, J. Balakrishnan, D. Im, T. Lei, Y. Il Song, et al., *Nat. Nanotechnol.* **2009**, *5*, 1–5.

[27] W. Choi, I. Lahiri, R. Seelaboyina, Y. S. Kang, *Crit. Rev. Solid State Mater. Sci.* **2010**, *35*, 52–71.

[28] J. D. Roy-Mayhew, I. A. Aksay, *Chem. Rev.* **2014**, *114*, 6323–6348.

[29] L. Sun, B. Fugetsu, *J. Am. Chem. Soc.* **2013**, *80*, 1339–1339.

[30] F. Torrisi, T. Hasan, W. Wu, Z. Sun, A. Lombardo, T. S. Kulmala, G. W. Hsieh, S. Jung, F. Bonaccorso, P. J. Paul, et al., *ACS Nano* **2012**, *6*, 2992–3006.

[31] R. Kumar, R. M. Kumar, D. Lahiri, I. Lahiri, *Surf. Coatings Technol.* **2016**, *309*, 931–937.

[32] M. S. Fuhrer, *Science (80-.).* **2000**, *288*, 494–497.

[33] R. M. Pasquarelli, D. S. Ginley, R. O'Hayre, *Chem. Soc. Rev.* **2011**, *40*, 5406–5441.

[34] Z. Li, Y. Jia, J. Wei, K. Wang, Q. Shu, X. Gui, H. Zhu, A. Cao, D. Wu, *J. Mater. Chem.* **2010**, *20*, 7236–7240.

[35] D. S. Ghosh, L. Martinez, S. Giurgola, P. Vergani, V. Pruneri, *Opt. Lett.* **2009**, *34*, 325–327.

[36] B. O'Connor, C. Haughn, K. H. An, K. P. Pipe, M. Shtein, *Appl. Phys. Lett.* **2008**, *93*, 1–4.

[37] P. B. Catrysse, S. Fan, *Nano Lett.* **2010**, *10*, 2944–2949.

[38] H.-J. Choi, S. Choo, P.-H. Jung, J.-H. Shin, Y.-D. Kim, H. Lee, *Nanotechnology* **2015**, *26*, 055305–055313.

[39]   F. Selzer, C. Floresca, D. Kneppe, L. Bormann, C. Sachse, N. Weiß, A. Eychmüller, A. Amassian, L. Müller-Meskamp, K. Leo, *Appl. Phys. Lett.* **2016**, *108*, 163302–163306.

[40]   J. Du, S. Pei, L. Ma, H. M. Cheng, *Adv. Mater.* **2014**, *26*, 1958–1991.

[41]   R. Wang, H. Ruan, *J. Alloys Compd.* **2016**, *656*, 936–943.

[42]   B. Li, S. Ye, I. E. Stewart, S. Alvarez, B. J. Wiley, *Nano Lett.* **2015**, *15*, 6722–6726.

[43]   H. Wu, L. Hu, M. W. Rowell, D. Kong, J. J. Cha, J. R. McDonough, J. Zhu, Y. Yang, M. D. McGehee, Y. Cui, *Nano Lett.* **2010**, *10*, 4242–4248.

[44]   T. Gao, B. Wang, B. Ding, J. Lee, P. W. Leu, *Nano Lett.* **2014**, *14*, 2105–2110.

[45]   N. Kumar, R. Kumar, S. Kumar, S. K. Chakarvarti, *Radiat. Phys. Chem.* **2016**, *119*, 44–50.

[46]   H. Hosseinzadeh Khaligh, K. Liew, Y. Han, N. M. Abukhdeir, I. A. Goldthorpe, *Sol. Energy Mater. Sol. Cells* **2015**, *132*, 337–341.

[47]   D. Langley, G. Giusti, C. Mayousse, C. Celle, D. Bellet, J.-P. Simonato, *Nanotechnology* **2013**, *24*, 452001–452021.

[48]   M. Amjadi, A. Pichitpajongkit, S. Lee, S. Ryu, I. Park, *ACS Nano* **2014**, *8*, 5154–5163.

[49]   T. Kim, Y. W. Kim, H. S. Lee, H. Kim, W. S. Yang, K. S. Suh, *Adv. Funct. Mater.* **2013**, *23*, 1250–1255.

[50]   C. N. Leavitt, "Silver Nanowires in Breakthrough Medical Application," can be found under http://www.cambrios.com/news/clearohm®-silver-nanowires-breakthrough-medical-application, **n.d.**

[51]   J. L. Elechiguerra, L. Larios-Lopez, C. Liu, D. Garcia-Gutierrez, A. Camacho-Bragado, M. J. Yacaman, *Chem. Mater.* **2005**, *17*, 6042–6052.

[52]   J. Jiu, J. Wang, T. Sugahara, S. Nagao, M. Nogi, H. Koga, K. Suganuma, M. Hara, E. Nakazawa, H. Uchida, *RSC Adv.* **2015**, *5*, 27657–27664.

[53]   D. P. Langley, M. Lagrange, G. Giusti, C. Jiménez, Y. Bréchet, N. D. Nguyen, D. Bellet, *Nanoscale* **2014**, *6*, 13535–13543.

[54]   S. De, J. N. Coleman, *MRS Bull.* **2011**, *36*, 774–781.

[55]   M. Lagrange, **2015**.

[56]   K. Zilberberg, T. Riedl, *J. Mater. Chem. A* **2016**, *4*, 14481–14508.

[57]   M. Marus, A. Hubarevich, R. J. W. Lim, H. Huang, A. Smirnov, H. Wang, W. Fan, X. W. Sun, *Opt. Mater. Express* **2017**, *7*, 1105–1112.

[58]   E. C. Garnett, W. Cai, J. J. Cha, F. Mahmood, S. T. Connor, M. Greyson Christoforo, Y. Cui, M. D. McGehee, M. L. Brongersma, *Nat. Mater.* **2012**, *11*, 241–249.

[59] B. Park, I. G. Bae, Y. H. Huh, *Sci. Rep.* **2016**, *6*, 1–9.

[60] G.-H. Lim, K. Ahn, S. Bok, J. Nam, B. Lim, *Nanoscale* **2017**, *9*, 8938–8944.

[61] S. M. Bergin, Y.-H. Chen, A. R. Rathmell, P. Charbonneau, Z.-Y. Li, B. J. Wiley, *Nanoscale* **2012**, *4*, 1996–2004.

[62] S. Ye, A. R. Rathmell, Z. Chen, I. E. Stewart, B. J. Wiley, *Adv. Mater.* **2014**, *26*, 6670–6687.

[63] C3Nano, "C3Nano," **n.d.**

[64] S. De, T. M. Higgins, P. E. Lyons, E. M. Doherty, P. N. Nirmalraj, W. J. Blau, J. J. Boland, J. N. Coleman, *ACS Nano* **2009**, *3*, 1767–1774.

[65] T. Araki, J. Jiu, M. Nogi, H. Koga, S. Nagao, T. Sugahara, K. Suganuma, *Nano Res.* **2014**, *7*, 236–245.

[66] J. Van De Groep, P. Spinelli, A. Polman, *Nano Lett.* **2012**, *12*, 3138–3144.

[67] H. H. Khaligh, I. A. Goldthorpe, *Nanoscale Res. Lett.* **2013**, *8*, 235–241.

[68] C. Mayousse, C. Celle, A. Fraczkiewicz, J.-P. Simonato, *Nanoscale* **2015**, *7*, 2107–2115.

[69] B. Vaagensmith, Q. Qiao, *IEEE J. Photovoltaics* **2016**, *6*, 1549–1553.

[70] J. Idier, W. Neri, C. Labrugère, I. Ly, P. Poulin, R. Backov, *Nanotechnology* **2016**, *27*, 105705–105712.

[71] F. Fievet, F. Fievetvincent, J. P. Lagier, B. Dumont, M. Figlarz, *J. Mater. Chem.* **1993**, *3*, 627–632.

[72] Y. Xia, Y. Xiong, B. Lim, S. E. Skrabalak, *Angew. Chemie - Int. Ed.* **2009**, *48*, 60–103.

[73] M. Tsuji, N. Miyamae, S. Lim, K. Kimura, X. Zhang, S. Hikino, M. Nishio, *Chrystal Growth Des.* **2006**, *6*, 1801–1807.

[74] W. M. Schuette, W. E. Buhro, *ACS Nano* **2013**, *7*, 3844–3853.

[75] R. R. Da Silva, M. Yang, S. Il Choi, M. Chi, M. Luo, C. Zhang, Z. Y. Li, P. H. C. Camargo, S. J. L. Ribeiro, Y. Xia, *ACS Nano* **2016**, *10*, 7892–7900.

[76] P. Zhang, I. Wyman, J. Hu, S. Lin, Z. Zhong, Y. Tu, Z. Huang, Y. Wei, *Mater. Sci. Eng. B Solid-State Mater. Adv. Technol.* **2017**, *223*, 1–23.

[77] C. Wang, B. Cheng, H. Zhang, P. Wan, L. Luo, Y. Kuang, X. Sun, *Nano Res.* **2016**, *9*, 1532–1542.

[78] B. Wiley, Y. Sun, B. Mayers, Y. Xia, *Chem. - A Eur. J.* **2005**, *11*, 454–463.

[79] V. B. Nam, D. Lee, *Nanomater. (Basel, Switzerland)* **2016**, *6*, 47–64.

[80] B. Wiley, T. Herricks, Y. Sun, Y. Xia, *Nano Lett.* **2004**, *4*, 1733–1739.

[81]   Whitcomb, D. R. (**2014**). U.S. Patent No. 8,741,026. Washington, DC: U.S. Patent and Trademark Office.

[82] K. E. Korte, S. E. Skrabalak, Y. Xia, *J. Mater. Chem.* **2008**, *18*, 437–441.

[83] B. Wiley, Y. Sun, Y. Xia, *Langmuir* **2005**, *21*, 8077–8080.

[84] M. Plissonneau, L. D'Alençon, T. Lemercier, M. Tréguer-Delapierre, *Silver Nanowires Synthesis*, **2017**, 60/073789.

[85] J. Jiu, T. Araki, J. Wang, M. Nogi, T. Sugahara, S. Nagao, H. Koga, K. Suganuma, E. Nakazawa, M. Hara, et al., *J. Mater. Chem. A* **2014**, *2*, 6326–6330.

[86] Y. Mao, H. Yang, C. Hu, J. Guo, X. Meng, Y. Yang, *J. Mater. Sci. Mater. Electron.* **2017**, *28*, 5308–5314.

[87] L. José Andrés, M. Fe Menéndez, D. Gómez, A. Luisa Martínez, N. Bristow, J. Paul Kettle, A. Menéndez, B. Ruiz, *Nanotechnology* **2015**, *26*, 1–9.

[88] S. Wang, Y. Tian, S. Ding, C. Wang, *Mater. Res. Express* **2016**, *3*, 1–9.

[89] B. Bari, J. Lee, T. Jang, P. Won, S. H. Ko, K. Alamgir, M. Arshad, L. J. Guo, *J. Mater. Chem. A* **2016**, *4*, 11365–11371.

[90] Y. Zhang, J. Guo, D. Xu, Y. Sun, F. Yan, *ACS Appl. Mater. Interfaces* **2017**, *9*, 25465–25473.

[91] J. H. Lee, P. Lee, D. Lee, S. S. Lee, S. H. Ko, *Cryst. Growth Des.* **2012**, *12*, 5598–5605.

[92] F.-Z. Cong, H. Wei, X.-R. Tian, H.-X. Xu, *Front. Phys.* **2012**, *7*, 521–526.

[93] I. Seshadri, G. L. Esquenazi, T. Cardinal, T. Borca-Tasciuc, G. Ramanath, *Nanotechnology* **2016**, *27*, 175601–175608.

[94] F. S. F. Morgenstern, D. Kabra, S. Massip, T. J. K. Brenner, P. E. Lyons, J. N. Coleman, R. H. Friend, *Appl. Phys. Lett.* **2011**, *99*, 1–4.

[95] P. Ramasamy, D.-M. Seo, S.-H. Kim, J. Kim, *J. Mater. Chem.* **2012**, *22*, 11651–11657.

[96] D. G. Lee, D. Lee, J. S. Yoo, S. Lee, H. S. Jung, *Nano Converg.* **2016**, *3*, 20–27.

[97] A. T. Pham, X. Q. Nguyen, D. H. Tran, V. Ngoc Phan, T. T. Duong, D. C. Nguyen, *Nanotechnology* **2016**, *27*, 1–7.

[98] T. Bin Song, Y. S. Rim, F. Liu, B. Bob, S. Ye, Y. T. Hsieh, Y. Yang, *ACS Appl. Mater. Interfaces* **2015**, *7*, 24601–24607.

[99] M.-H. Yeh, P.-H. Chen, Y.-C. Yang, G.-H. Chen, H.-S. Chen, *ACS Appl. Mater. Interfaces* **2017**, *9*, 10788–10797.

[100] A. Yoshida, N. Toshima, *J. Electron. Mater.* **2016**, *45*, 2914–2919.

[101] D. Y. Choi, H. W. Kang, H. J. Sung, S. S. Kim, *Nanoscale* **2013**, *5*, 977–983.

[102] S. Chen, L. Song, Z. Tao, X. Shao, Y. Huang, Q. Cui, X. Guo, *Org. Electron. physics, Mater. Appl.* **2014**, *15*, 3654–3659.

[103] R. Chen, S. R. Das, C. Jeong, M. R. Khan, D. B. Janes, M. A. Alam, *Adv. Funct. Mater.* **2013**, *23*, 5150–5158.

[104] Y. Ahn, Y. Jeong, Y. Lee, *ACS Appl. Mater. Interfaces* **2012**, *4*, 6410–6414.

[105] Y. Ahn, Y. Jeong, Y. Lee, *ACS Appl. Mater. Interfaces* **2012**, *4*, 6410–6414.

[106] G. S. Liu, J. S. Qiu, D. H. Xu, X. Zhou, D. Zhong, H. P. D. Shieh, B. R. Yang, *ACS Appl. Mater. Interfaces* **2017**, *9*, 15130–15138.

[107] H. H. Khaligh, L. Xu, A. Khosropour, A. Madeira, M. Romano, C. Pradére, M. Tréguer-Delapierre, L. Servant, M. A. Pope, I. A. Goldthorpe, *Nanotechnology* **2017**, *28*, 425703–425715.

[108] S. Wang, Y. Tian, S. Ding, Y. Huang, *Mater. Lett.* **2016**, *172*, 175–178.

[109] K. Takahashi, S. Yokoyama, T. Matsumoto, J. L. Cuya Huaman, H. Kaneko, J.-Y. Piquemal, H. Miyamura, J. Balachandran, *New J. Chem.* **2016**, *40*, 8632–8642.

[110] D. Derivatives, A. Espinosa, M. A. Gallo, J. Campos, A. Enbena, **1986**, *24*, 754–757.

[111] Y. Liu, J. Zhang, H. Gao, Y. Wang, Q. Liu, S. Huang, C. F. Guo, Z. Ren, *Nano Lett.* **2017**, *17*, 1090–1096.

[112] Y. Li, S. Guo, H. Yang, Y. Chao, S. Jiang, C. Wang, *RSC Adv.* **2018**, *8*, 8057–8063.

[113] "MAYER ROD, METER BAR, ADHESIVE COATING," can be found under http://www.holoeast.com/machines/coating/adhesive-coating-Meyer-Bar.html, **n.d.**

[114] F. Aziz, A. F. Ismail, *Mater. Sci. Semicond. Process.* **2015**, *39*, 416–425.

[115] J. F. Taylor, *Met. Finish.* **2001**, *99*, 16–21.

[116] T. Sannicolo, N. Charvin, L. Flandin, S. Kraus, D. T. Papanastasiou, C. Celle, J. Simonato, D. Muñoz-Rojas, C. Jiménez, D. Bellet, *ACS Nano* **2018**, *12*, 4648–4659.

[117] A. Höpe, in *Spectrophotometry Accurate Meas. Opt. Prop. Mater.* (Eds.: T. Lucatorto, A.C. Parr, K. Baldwin), Elsevier Science Inc., **2014**, pp. 179–219.

[118] J. Li, S. L. Zhang, *Phys. Rev. E - Stat. Nonlinear, Soft Matter Phys.* **2009**, *80*, 1–4.

[119] F. Basarir, F. S. Irani, A. Kosemen, B. T. Camic, F. Oytun, B. Tunaboylu, H. J. Shin, K. Y. Nam, H. Choi, *Mater. Today Chem.* **2017**, *3*, 60–72.

[120] A. T. Bellew, H. G. Manning, C. Gomes da Rocha, M. S. Ferreira, J. J. Boland, *ACS Nano* **2015**, *9*, 11422–11429.

[121] G. Deignan, I. A. Goldthorpe, *RSC Adv.* **2017**, *7*, 35590–35597.

[122] S. Maksimuk, X. Teng, H. Yang, *Phys. Chem. Chem. Phys.* **2006**, *8*, 4660–4663.

[123] L. Zhang, S.-I. Choi, J. Tao, H.-C. Peng, S. Xie, Y. Zhu, Z. Xie, Y. Xia, *Adv. Funct. Mater.* **2014**, *24*, 7520–7529.

[124] T. K. Sau, C. J. Murphy, *J. Am. Chem. Soc.* **2004**, *126*, 8648–8649.

[125] S. Cheong, J. D. Watt, R. D. Tilley, *Nanoscale* **2010**, *2*, 2045–2053.

[126] H. Liu, Y. Xu, Y. Qin, W. Sanderson, D. Crowley, C. H. Turner, Y. Bao, *J. Phys. Chem. C* **2013**, *117*, 17143–17150.

[127] Y. T. Chu, K. Chanda, P. H. Lin, M. H. Huang, *Langmuir* **2012**, *28*, 11258–11264.

[128] B. Pang, Y. Zhao, H. Luehmann, X. Yang, L. Detering, M. You, C. Zhang, L. Zhang, Z. Y. Li, Q. Ren, et al., *ACS Nano* **2016**, *10*, 3121–3131.

[129] S. Maksimuk, X. Teng, H. Yang, *J. Phys. Chem. C* **2007**, *111*, 14312–14319.

[130] K. Park, R. A. Vaia, *Adv. Mater.* **2008**, *20*, 3882–3886.

[131] J. P. Franey, M. Hill, **1985**, *25*, 133–143.

[132] S. Karim, M. E. Toimil-Molares, A. G. Balogh, W. Ensinger, T. W. Cornelius, E. U. Khan, R. Neumann, *Nanotechnology* **2006**, *17*, 5954–5959.

[133] B. Deng, P. C. Hsu, G. Chen, B. N. Chandrashekar, L. Liao, Z. Ayitimuda, J. Wu, Y. Guo, L. Lin, Y. Zhou, et al., *Nano Lett.* **2015**, *15*, 4206–4213.

[134] X. Zhang, X. Yan, J. Chen, J. Zhao, *Carbon N. Y.* **2014**, *69*, 437–443.

[135] G. I. V. and G. A. Nair R R, Wu H A, Jayaram P N, *Science (80-.).* **2012**, *335*, 442–444.

[136] B. T. Liu, H. L. Kuo, *Carbon N. Y.* **2013**, *63*, 390–396.

[137] K. Naito, N. Yoshinaga, E. Tsutsumi, Y. Akasaka, *Synth. Met.* **2013**, *175*, 42–46.

[138] S. B. Yang, H. K. Choi, D. S. Lee, C. G. Choi, S. Y. Choi, I. D. Kim, *Small* **2015**, *11*, 1293–1300.

[139] D. Lee, H. Lee, Y. Ahn, Y. Lee, *Carbon N. Y.* **2015**, *81*, 439–446.

[140] S. Nanowire, L. Hu, H. S. Kim, J. Lee, P. Peumans, Y. Cui, *ACS Nano* **2010**, *4*, 2955–2963.

[141] H. H. Khaligh, **2013**, 25–30.

[142] H. Hosseinzadeh Khaligh, I. A. Goldthorpe, *Nanoscale Res. Lett.* **2014**, *9*, 1–5.

[143] D. C. Marcano, D. V. Kosynkin, J. M. Berlin, A. Sinitskii, Z. Sun, A. Slesarev, L. B.

Alemany, W. Lu, J. M. Tour, *ACS Nano* **2010**, *4*, 183–191.

[144] H. Pron, C. Bissieux, *Quant. Infrared Thermogr. J.* **2004**, *1*, 229–240.

[145] M. A. Green, *Prog. Photovoltaics Res. Appl.* **2015**, *23*, 1202–1202.

[146] M. Jørgensen, J. E. Carlé, R. R. Søndergaard, M. Lauritzen, N. A. Dagnæs-Hansen, S. L. Byskov, T. R. Andersen, T. T. Larsen-Olsen, A. P. L. Böttiger, B. Andreasen, et al., *Sol. Energy Mater. Sol. Cells* **2013**, *119*, 84–93.

[147] M. Niggemann, B. Zimmermann, J. Haschke, M. Glatthaar, A. Gombert, *Thin Solid Films* **2008**, *516*, 7181–7187.

[148] P. T. Tsai, K. C. Yu, C. J. Chang, S. F. Horng, H. F. Meng, *Org. Electron. physics, Mater. Appl.* **2015**, *22*, 166–172.

[149] J. Yang, D. Vak, N. Clark, J. Subbiah, W. W. H. Wong, D. J. Jones, S. E. Watkins, G. Wilson, *Sol. Energy Mater. Sol. Cells* **2013**, *109*, 47–55.

[150] M. Romano, C. Pradere, J. Toutain, C. Hany, J. C. Batsale, *Quant. Infrared Thermogr. J.* **2014**, *11*, 134–160.

[151] P. Kumar, F. Shahzad, S. Yu, S. M. Hong, Y. H. Kim, C. M. Koo, *Carbon N. Y.* **2015**, *94*, 494–500.

[152] A. Bid, A. Bora, A. K. Raychaudhuri, *Phys. Rev. B - Condens. Matter Mater. Phys.* **2006**, *74*, 1–8.

[153] R. . Montgomery, *J. Meteorol.* **1947**, *4*, 193–196.

[154] C. Lopes, M. Felisberti, *Polym.Test* **2004**, *23*, 637–643.

[155] X. Li, Y. Zhu, W. Cai, M. Borysiak, B. Han, D. Chen, R. D. Piner, L. Colombo, R. S. Ruoff, *Nano Lett.* **2009**, *9*, 4359–4363.

[156] G. Eda, G. Fanchini, M. Chhowalla, *Nat. Nanotechnol.* **2008**, *3*, 270–274.

[157] J. S. Woo, J. T. Han, S. Jung, J. I. Jang, H. Y. Kim, H. J. Jeong, S. Y. Jeong, K. J. Baeg, G. W. Lee, *Sci. Rep.* **2014**, *4*, 1–6.

[158] S. Hong, H. Lee, J. Lee, J. Kwon, S. Han, Y. D. Suh, H. Cho, J. Shin, J. Yeo, S. H. Ko, *Adv. Mater.* **2015**, *27*, 4744–4751.

[159] Y. C. G. Kwan, Q. L. Le, C. H. A. Huan, *Sol. Energy Mater. Sol. Cells* **2016**, *144*, 102–108.

[160] J. Y. Lee, S. T. Connor, Y. Cui, P. Peumans, *Nano Lett.* **2008**, *8*, 689–692.

[161] I. T. Sachs-Quintana, T. Heumüller, W. R. Mateker, D. E. Orozco, R. Cheacharoen, S. Sweetnam, C. J. Brabec, M. D. McGehee, *Adv. Funct. Mater.* **2014**, *24*, 3978–3985.

[162] E. A. Katz, D. Faiman, S. M. Tuladhar, J. M. Kroon, M. M. Wienk, T. Fromherz, F. Padinger, C. J. Brabec, N. S. Sariciftci, *J. Appl. Phys.* **2001**, *90*, 5343–5350.

[163] K. J. Bergemann, R. Krasny, S. R. Forrest, *Org. Electron. physics, Mater. Appl.* **2012**, *13*, 1565–1568.

[164] T. T. Thao, T. Q. Trung, V.-V. Truong, N. N. Dinh, *J. Nanomater.* **2015**, *2015*, 1–7.

[165] S. Duan, Q. Niu, J. Wei, J. He, Y. Yin, Y. Zhang, *Phys. Chem. Chem. Phys.* **2015**, *17*, 8106–8112.

[166] D. Whang, S. Jin, Y. Wu, C. M. Lieber, *Nano Lett.* **2003**, *3*, 1255–1259.

[167] B. Sciacca, J. Van De Groep, A. Polman, E. C. Garnett, *Adv. Mater.* **2016**, *28*, 905–909.

[168] I. K. Moon, J. Il Kim, H. Lee, K. Hur, W. C. Kim, H. Lee, *Sci. Rep.* **2013**, *3*, 1–7.

[169] J. J. Gooding, S. Ciampi, *Chem. Soc. Rev.* **2011**, *40*, 2704–18.

[170] A. Le Beulze, E. Duguet, S. Mornet, J. Majimel, M. Tréguer-Delapierre, S. Ravaine, I. Florea, O. Ersen, *Langmuir* **2014**, *30*, 1424–1434.

[171] C.-H. Liu, X. Yu, *Nanoscale Res. Lett.* **2011**, *6*, 75–83.

[172] S. K. Ghosh, S. Nath, S. Kundu, K. Esumi, T. Pal, *J. Phys. Chem. B* **2004**, *108*, 13963–13971.

[173] P. Mulvaney, *Langmuir* **1996**, *12*, 788–800.

[174] M. Kumar, P. Devi, A. Kumar, *J. Mater. Sci. Mater. Electron.* **2017**, *28*, 5014–5020.

[175] T. Zhao, R. Sun, S. Yu, Z. Zhang, L. Zhou, H. Huang, R. Du, *Colloids Surfaces A Physicochem. Eng. Asp.* **2010**, *366*, 197–202.

[176] C. H. Moran, M. Rycenga, Q. Zhang, Y. Xia, *J. Phys. Chem. C* **2011**, *115*, 21852–21857.

[177] M. A. Mahmoud, C. E. Tabor, M. A. El-Sayed, *J. Phys. Chem. C* **2009**, *113*, 5493–5501.

[178] Y. Gao, P. Jiang, D. F. Liu, H. J. Yuan, X. Q. Yan, Z. P. Zhou, J. X. Wang, L. Song, L. F. Liu, W. Y. Zhou, et al., *J. Phys. Chem. B* **2004**, *108*, 12877–12881.

[179] C. Ma, J. M. Harris, *Langmuir* **2012**, *28*, 2628–36.

[180] M. Bryant, J. Pemberton, *J. Am. Chem. Soc.* **1991**, *113*, 8284–8293.

[181] N. Grillet, D. Manchon, E. Cottancin, F. Bertorelle, C. Bonnet, M. Broyer, J. Lerm??, M. Pellarin, *J. Phys. Chem. C* **2013**, *117*, 2274–2282.

[182] J. Ma, M. Zhan, *RSC Adv.* **2014**, *4*, 21060–21071.

[183] H. Sim, S. Bok, B. Kim, M. Kim, G. H. Lim, S. M. Cho, B. Lim, *Angew. Chemie - Int. Ed.* **2016**, *55*, 11814–11818.

[184] J. L. C. Fajín, F. Teixeira, J. R. B. Gomes, M. N. D. S. Cordeiro, *Theor. Chem. Acc.* **2015**, *134*, 67–80.

Résumé de thèse

Introduction générale

Les électrodes transparentes sont des composantes utilisées dans de nombreux dispositifs optoélectroniques comme les cellules solaires, les écrans tactiles et les films chauffants transparents...[1] Ces électrodes sont fabriquées, depuis les années cinquante, essentiellement à partir d'oxydes métalliques. L'oxyde le plus utilisé est l'oxyde d'indium-étain (ITO) en raison de son excellente conductivité électronique (de l'ordre de 10^{-4} Ω/cm) et de sa transparence élevée dans le domaine du visible (supérieure à 80%).[2] En dépit de ses propriétés, les électrodes à base d'ITO souffrent de fortes limitations : elles sont produites par un procédé relativement coûteux et elles sont très fragiles, ce qui proscrit leur utilisation au sein de dispositifs optoélectroniques flexibles. De nouveaux matériaux transparents et conducteurs (TCM) ont été développés ces dernières années afin de remplacer l'ITO : l'oxyde d'aluminium zinc (AZO)[3], l'oxyde de fluor dopé à l'étain (FTO)[4], des matériaux nanostructurés. Bien que les oxydes (AZO et FTO) présentent des propriétés optoélectroniques comparables à celles de l'ITO, ils possèdent une résistivité élevée, une certaine rugosité, et sont élaborées par des méthodes de synthèse onéreuses. Les réseaux nanostructurés, par exemple à base de nano-fils métalliques (Figure 1), présentent l'avantage de permettre le transport électronique sur de grandes distances tout en garantissant des espaces pour la transmission de la lumière, ce qui les rend compatibles avec la réalisation d'électrodes transparentes performantes.
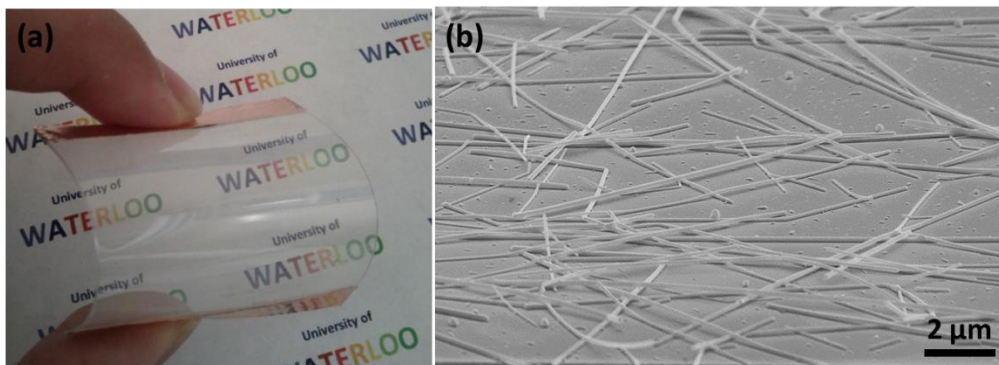

Figure 1 : (a) Image d'une électrode transparente réalisée à base de nanofils métalliques déposés sur un substrat plastique, (b) image MEB du réseau bidimensionnel.

Les réseaux de nano-fils d'argent peuvent être élaborés sur des supports flexibles et sur des grandes surfaces via des procédés simples à mettre en œuvre tels que le spray-coating, le

rod-coating, etc...[5–7] Leur moindre coût et la disponibilité des matières premières en font ainsi des systèmes très recherchés pour la nouvelle génération d'électrodes.

Le but de ces travaux de thèse est de (i) concevoir et de synthétiser des nano-fils d'argent sur mesure afin d'obtenir des dispositifs aux propriétés opto-électroniques supérieures à celles des dispositifs commerciaux à base d'ITO, (ii) modifier la surface des réseaux de nano-fils métalliques pour résoudre leurs problèmes de stabilité chimique et thermique. Le contrôle de la synthèse colloïdale devrait permettre de générer des nano-fils métalliques à facteur de forme très élevé et/ou présentant une architecture inhabituelle, i.e. avec des ramifications. De tels systèmes sont très recherchés pour la fabrication d'électrodes très performantes. La modification de surface des nanostructures à l'aide de molécules organiques devrait permettre aux électrodes de conserver leur propriétés opto-électroniques et de limiter la corrosion des fils d'argent généralement observée au cours du temps.

Cette thèse s'inscrit dans le cadre du programme international IDS-FunMat (International Doctoral School in Function Materials) et implique l'université de Waterloo au Canada et l'université de Bordeaux en France. Elle a été menée dans le groupe de recherche « Chimie des nanomatériaux », à l'ICMCB (Institut de la chimie de la matière condensée de Bordeaux) et dans l'équipe du professeur Irene Goldthorpe de l'Institut De Nanotechnologie de Waterloo (WIN), à l'Université de Waterloo. Des analyses de spectroscopie et de thermique ont été réalisées en collaboration avec le Groupe Spectroscopie Moléculaire (GSM) de l'Institut des Sciences Moléculaires et avec le groupe de mesures thermiques de l'Institut de Mécanique et Ingénierie de Bordeaux

1. Etat de l'art

Les électrodes à base de fils d'argent font actuellement l'objet d'un grand nombre de recherches car elles ont des propriétés optoélectroniques comparables voire supérieures à celles de l'ITO, ainsi que celles de nombreuses nanostructures organiques ou inorganiques: les nanotubes de carbone[8], le graphène[9], les nano-fils de cuivre[10] (Figure 2). L'argent est le métal qui a la plus haute conductivité électrique. Par ailleurs, de nombreux procédés simples à mettre en œuvre permettent de synthétiser des nano-fils d'argent à l'échelle du gramme. Plusieurs entreprises proposent à la vente des solutions de nano-fils d'argent : Blue Nano, Seashell, Cambrios, etc. A partir d'une solution de nano-fils dispersés dans un solvant donnée, il est possible de réaliser des réseaux percolants via divers procédés d'impression, peu coûteux, et transférables à l'échelle industrielle.[11]
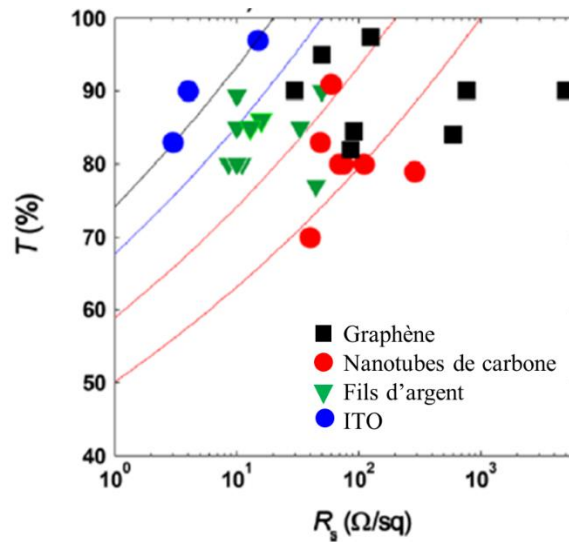
Figure 2 : Comparaison des propriétés optoélectroniques de matériaux à base de graphène, nanotubes de carbone, fils d'argent et ITO.[11]

Pour diminuer la rugosité des réseaux bidimensionnels, améliorer la qualité des jonctions et donc la conductivité globale de l'électrode, différentes stratégies ont été proposées dans la littérature telles que l'application d'une pression mécanique et/ou d'un recuit en température.[12] Le schéma ci-dessous illustre les modifications du réseau de nano-fils d'argent avant et après un recuit thermique.
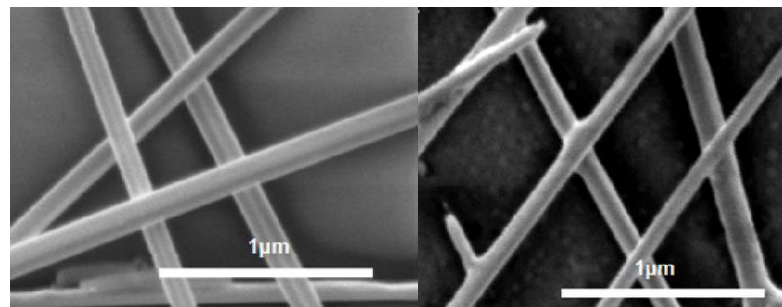

Figure 3 : Images de microscopie à balayage d'un réseau de fils d'argent (a) avant et (b) après traitement thermique.[12]

Même si les réseaux percolants présentent des propriétés optoélectroniques excellentes, plusieurs verrous sont à considérer afin de pouvoir prétendre à une intégration réussie transférable à l'échelle industrielle. Afin d'avoir un réseau très conducteur, il est nécessaire d'avoir un réseau de nanostructures assez dense pour permettre au courant de circuler d'un point à l'autre de l'électrode. Si le réseau n'est pas assez dense, aucun chemin de conduction macroscopique n'est possible (schéma A de la Figure 4). A l'inverse, si le réseau est trop dense : le réseau est percolant et les porteurs de charge peuvent être transportés sur

157

toute la surface de l'électrode. Mais, le dispositif présentera, alors, une faible transparence (Schéma C de la Figure 4). La haute résistance électrique aux jonctions est également problématique. Plus le nombre de nanostructures est élevé, plus le nombre de jonctions augmente.
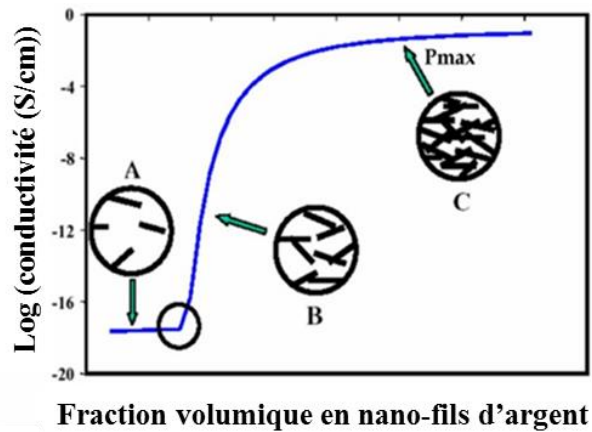

Figure 4 : Conductivité d'un réseau de fils d'argent en fonction de sa fraction volumique en nano-fils.

Un autre inconvénient des électrodes à base de nano-fils d'argent est la faible stabilité des nano-objets sur le substrat notamment en fonctionnement. Des problèmes d'oxydation, de sulfuration et/ou d'électromigration peuvent se produire.[13] Ces processus peuvent être freinés en déposant une fine couche d'oxyde métallique (Al_2O_3, TiO_2) ou de polymère conducteur sur le réseau.[14,15] Mais, ces approches peuvent affecter les propriétés optiques des électrodes (transparence) et réduire leur flexibilité.

Afin de pallier aux faiblesses des électrodes transparentes à base de fils d'argent, nous avons exploré trois stratégies dans ce travail de thèse. Nous avons exploré de nouvelles approches de synthèse et de modification de surface des nanofils d'argent pour développer des électrodes transparentes plus performantes et plus stables. Nous avons tout d'abord examiné la possibilité d'élaborer des nanostructures d'argent différentes de celles commercialisées : (i) des fils d'argent ultra-longs (ii) des fils d'argent branchés. Enfin, afin de limiter la corrosion des nano-fils d'argent, conduisant à une augmentation de la résistance au cours du temps, (iii) nous avons passivé la surface des nanofils d'argent par de petites molécules organiques susceptibles de protéger les nanostructures contre l'oxydation sans perturber les propriétés intrinsèques des électrodes.
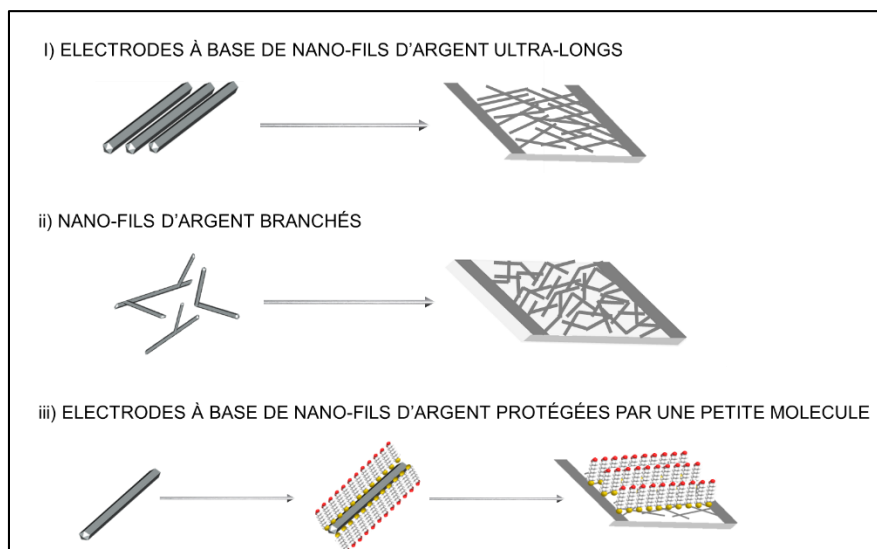
Figure 5 : Représentation schématique des objectifs de la thèse.

2. Elaboration d'électrodes transparentes à base de nano-fils d'argent ultra-longs

Des paramètres clés du procédé polyol de synthèse des fils d'argent, ont été modifiés pour élaborer des fils d'argent ultra-longs. En jouant sur un certain nombre de paramètres expérimentaux (nature du polyol, concentration des précurseurs, ratio des précurseurs), des fils bien calibrés en taille (i.e. avec une longueur moyenne de 130 μm et un diamètre moyen de 124 nm) ont été obtenus à l'échelle du gramme. Leur rapport d'aspect est le plus élevé élaboré en voie polyol (Figure 6).
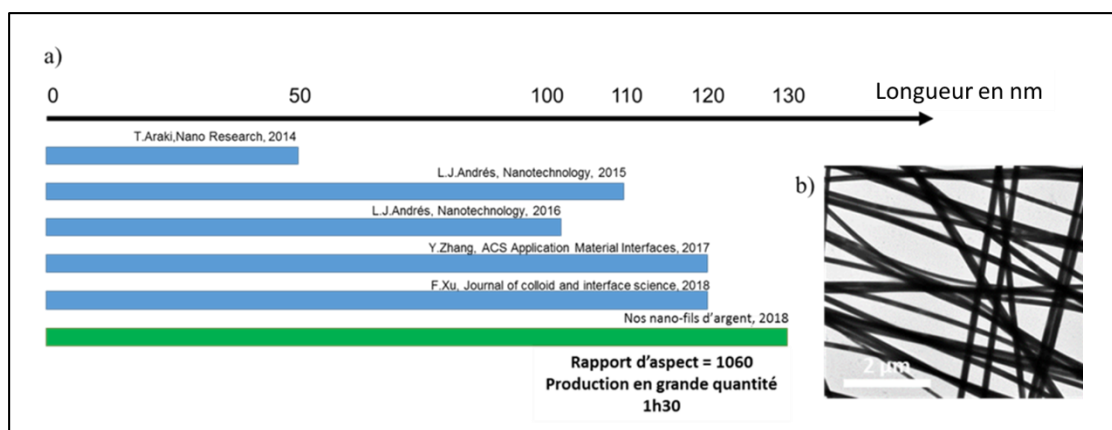

Figure 6 : (a) Comparaison de la longueur des nano-fils d'argent ultra-longs obtenus dans la littérature [16–19] et ceux élaborés au cours de ce travail de thèse, (b) Image de microscopie électronique à transmission des nano-fils d'argent formés au cours de ce projet.

Ces nano-fils ultra-longs ont été déposés sur un substrat flexible ou non par plusieurs méthodes de dépôt (dip-coating, spray-coating, Rod Meyer). Les performances des réseaux ainsi formé ont été évaluées optiquement en utilisant un spectrophotomètre UV, et électriquement en utilisant un multimètre à deux pointes ou à quatre pointes.

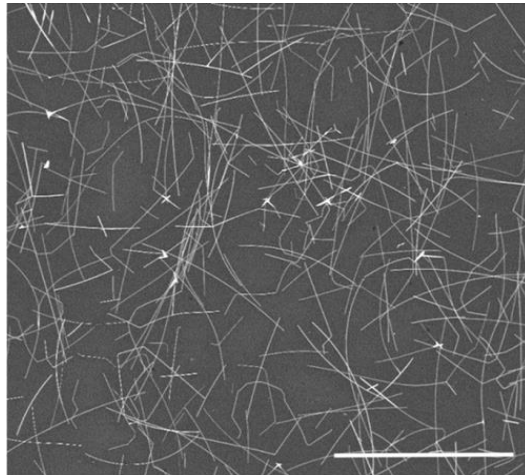Comme mentionné précédemment, les électrodes à base de nano-fils, sont

Figure 7 : Image de microscopie à balayage d'un réseau de fils d'argent ultra-longs élaboré par rod-coating. Barre d'échelle = 100 nm.

généralement très peu conductrices à l'issue de l'étape du dépôt. Un recuit thermique ou l'application d'une pression permet la soudure des jonctions. Contrairement à ces observations, nous avons observé des valeurs très intéressantes de conductivité à l'issue du dépôt. Un traitement thermique induit une très faible diminution de la résistance des réseaux élaborés par différents procédés d'impression ("roll to roll', 'spray coating',etc…) . Ces résultats sont extrêmement intéressants car ils démontrent que le contact entre les nano-fils est excellent, même à température ambiante.

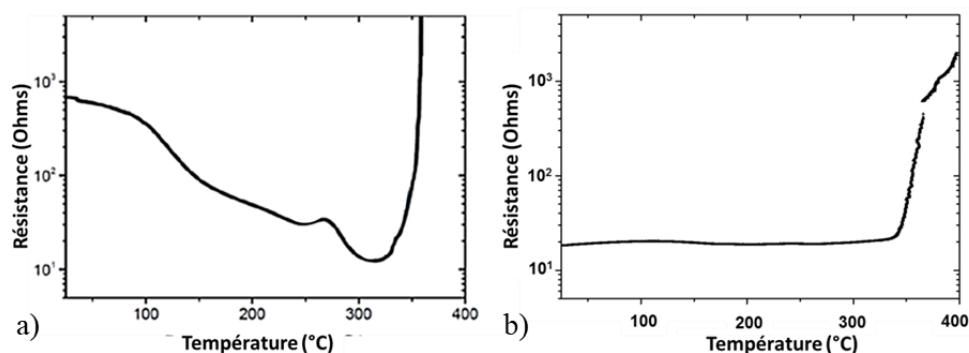
Figure 8: Evolution de la résistance en fonction de la température d'une electrodes transparentes elaboree a) avec des fils commerciaux[12] et b) avec les fils d'argent ultra-longs synthetisés dans le cadre de ce travail de thèse.

160

Par ailleurs, nous avons observé que les nano-fils ultra-longs étaient de très bons candidats pour élaborer des électrodes très performantes. Les électrodes réalisées sur substrat rigide présentent des performances à la hauteur des attentes établies. En effet, les électrodes présentent une excellente transparence (T = 94% à une longueur d'onde de 550 nm) pour une faible résistance (Rs = 5 Ω/Sq).

3. La synthèse de nanofils d'argent de morphologie non conventionnelle

Plusieurs stratégies de synthèse ont été envisagées pour élaborer des nanofils présentant des ramifications : (i) synthèse à partir de germes de morphologie 'tripodes' de platine (ii) application d'ultra-sons au cours de la croissance de fils conventionnels.
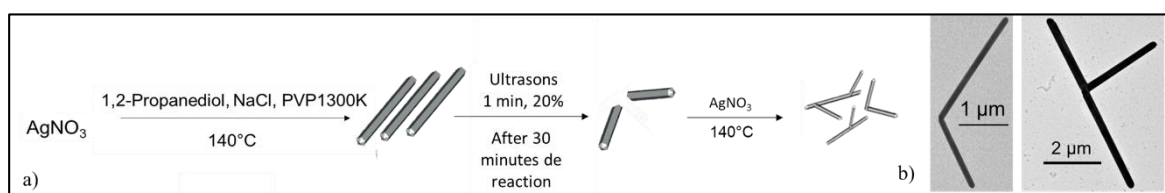

Figure 9: a) Schéma de principe de la synthèse de fils d'argent branches par application d'ultra-sons au cours de la croissance des fils d argent et b) Image de microscopie a transmission des structures obtenues.

Seule la deuxième approche s'est avérée concluante et a permis de générer des nano-fils d'argent de forme « Y » ou de type « boomerangs » (Figure 9) Cependant, la longueur des branches est trop courte et ne favorise pas à l'heure actuellement la percolation des réseaux bidimensionnels.

4. Amélioration des stabilités chimique et thermique des électrodes à base de nanofils d'argent

Concernant la stabilité des électrodes, nous avons tout d'abord examiné les problèmes de stabilité des électrodes en fonctionnement. Du fait de l'effet Joule, l'application d'une tension conduit généralement à une augmentation de température du réseau bidimensionnel et éventuellement à une dégradation des nano-fils. Grâce à des études d'analyse thermique *in situ*, nous avons montré que la stabilité thermique des électrodes à base de nanofils d'argent pouvait être accrue en les recouvrant d'un feuillet de graphène.[20] Le graphène permet de limiter le nombre de points chauds du réseau et homogénéiser la température des électrodes en fonctionnement (Figure 10).
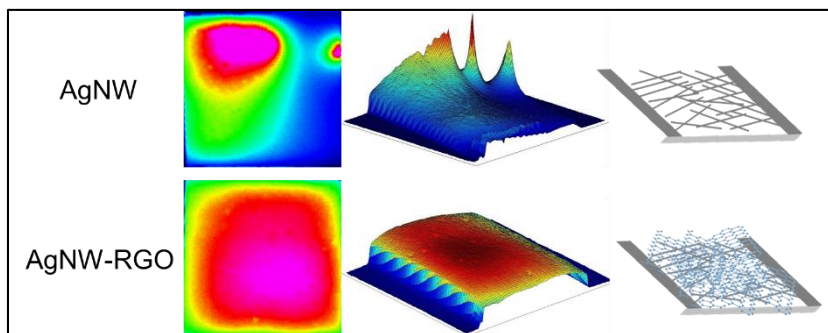
Figure 10: Images thermiques et représentation schématique des électrodes transparentes.[20]

En ce qui concerne la stabilité chimique des électrodes, la corrosion des nano-fils d'argent au cours du temps est un problème majeur limitant leur exploitation commerciale. La molécule, 11-mercaptoundecanoic acid (MuA), a été identifiée comme une molécule très intéressante pour limiter le processus de corrosion de fils d'argent à l'air. Nous avons montré, au cours de ce travail de thèse, via des analyses de microscopie haute résolution, des analyses spectrophotométriques, XPS et SERS que la modification de surface des nanofils pouvait être effectuée en solution ou sur des fils déposés sur un substrat. La dynamique de passivation a été suivie en détail via des analyses SERS originales menées à l'échelle de la particule unique. L'ancrage du PVP se produit en deux étapes : substitution du PVP par le MUA ; ancrage des molécules de MUA via leur fonction thiol. Par ailleurs, une analyse temporelle des performances des électrodes a montré que les électrodes modifiées en surface par du MuA étaient bien plus robustes vis à vis des processus de corrosion que celles non passivés (Figure 11). Ce résultat est très prometteur car la molécule de MUA est un agent de passivation peu onéreux. En outre, elle permet aux réseaux bidimensionnels de conserver ses performances de transparence et de conductivité.
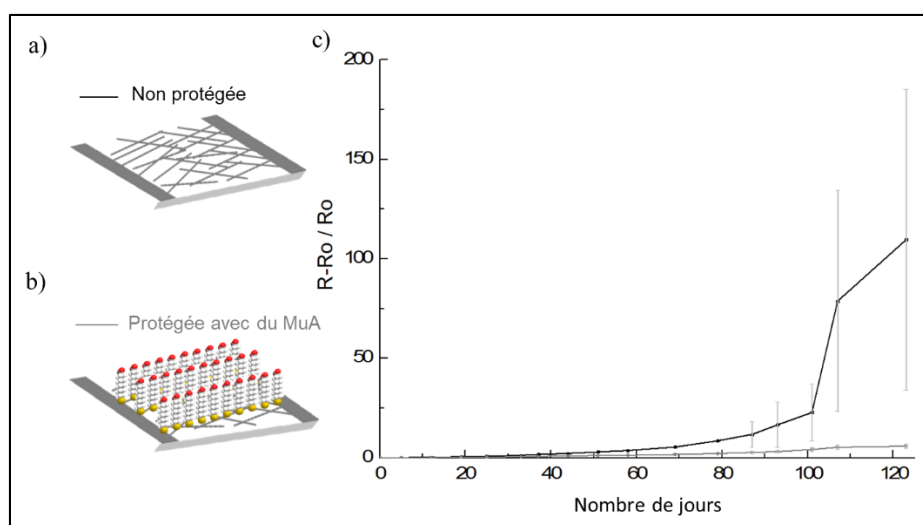
Figure 11: Représentation schématique des électrodes transparentes a) à base de fils d'argent, b) à base de fils d'argent passivés avec du MuA et c) modification de la résistance de l'électrode en fonction du temps d'exposition à la lumière des électrodes passivés (gris foncé) ou non (gris clair).

Conclusion

Ces travaux de thèse ont permis de démontrer le potentiel des réseaux de nano-fils pour la réalisation d'électrodes transparentes performantes. L'utilisation de nanofils d'argent ultra-longs sous forme de réseaux 2D percolants nous a permis de tirer profit du haut niveau de conduction des fils métalliques tout en conservant une très bonne transparence grâce au vide dans le maillage du réseau. L'approche développée pour élaborer des fils ultra-longs est simple à mettre à œuvre et permet de générer des lots de nano-objets bien calibrées en taille, à l'échelle du gramme. En outre, leur état de surface permet d'assurer un bon contact au niveau des nanofils sur un substrat, flexible ou non, à température ambiante. Ces résultats offrent des perspectives très intéressantes pour élaborer des électrodes transparentes démontrant des propriétés optoélectroniques supérieures à celles de l'ITO, et qui plus est flexibles. Comme aucun post-traitement énergivore n'est nécessaire pour obtenir de très hauts niveaux de transparence et de conduction électrique. Ces résultats sont donc très encourageants pour l'industrie. En ce qui concerne la stabilité des réseaux à base de nanofils à l'air, nous avons démontré que passiver les réseaux avec du MUA permettait de limiter considérablement les processus de corrosion à la lumière ou dans le noir. Cela offre de nombreuses perspectives très intéressantes pour l'avenir des électrodes à base de nanofils métalliques.

Références

[1]   T. Sannicolo, M. Lagrange, A. Cabos, C. Celle, J. Simonato, D. Bellet, *Small* **2016**, *12*, 6052–6075.

[2]   J. Meiss, C. L. Uhrich, K. Fehse, S. Pfuetzner, M. K. Riede, K. Leo, *Photonics Sol. Energy Syst. II* **2008**, *7002*, 1–9.

[3]   Q. Huang, W. Shen, X. Fang, G. Chen, Y. Yang, J. Huang, R. Tan, W. Song, *ACS Appl. Mater. Interfaces* **2015**, *7*, 4299–4305.

[4]   M. A. Lazar, W. A. Daoud, *RSC Adv.* **2012**, *2*, 447–452.

[5]   R. M. Pasquarelli, S. Ginley, R. O. Hayre, *Chem. Soc. Rev.* **2011**, *40*, 5406–5441.

[6]   Y. Meng, X. Xu, H. Li, Y. Wang, E. Ding, Z. Zhang, H. Geng, *Carbon N. Y.* **2014**, *70*, 103–110.

[7]   D. Bellet, M. Lagrange, T. Sannicolo, S. Aghazadehchors, V. H. Nguyen, D. P. Langley, D. Muñoz-rojas, C. Jim, Y. Bréchet, N. D. Nguyen, *Materials (Basel).* **2017**, *10*, 1–16.

[8]   I. Jeon, Y. Matsuo, S. Maruyama, *Top. Curr. Chem.* **2018**, *376*, 1–28.

[9]   J. D. Roy-mayhew, I. A. Aksay, *Chem. Rev.* **2014**, *114*, 6323–6348.

[10]   V. B. Nam, D. Lee, *nanomaterials* **2016**, *6*, 1–17.

[11]   D. Langley, G. Giusti, C. Mayousse, C. Celle, D. Bellet, J. Simonato, *Nanotechnology* **2013**, *24*, 45001–45021.

[12]   G. Giusti, D. P. Langley, M. Lagrange, R. Collins, C. Jimenez, Y. Bréchet, D. Bellet, *Nanotechnology* **2014**, *11*, 785–795.

[13]   J. L. Elechiguerra, L. Larios-lopez, C. Liu, D. Garcia-gutierrez, A. Camacho-bragado, M. J. Yacaman, *Chem. Mater* **2005**, *17*, 6042–6052.

[14]   T. Song, Y. S. Rim, F. Liu, B. Bob, S. Ye, Y. Hsieh, Y. Yang, *ACS Appl. Mater. Interfaces* **2015**, *7*, 24601–24607.

[15]   R. Chen, S. R. Das, C. Jeong, M. R. Khan, D. B. Janes, M. A. Alam, *Adv. Funct. Mater.* **2013**, *23*, 5150–5158.

[16]   T. Araki, J. Jiu, M. Nogi, H. Koga, S. Nagao, T. Sugahara, *Nano Res.* **2014**, *7*, 236–245.

[17]   L. J. Andrés, M. F. Menéndez, D. Gómez, A. L. Martínez, N. Bristow, J. P. Kettle, A. Menéndez, B. Ruiz, *Nanotechnology* **2015**, *26*, 265201–265210.

[18]   Y. Zhang, J. Guo, D. Xu, Y. Sun, F. Yan, *ACS Appl. Mater. Interfaces* **2017**, *9*, 25465–25473.

[19]   F. Xu, W. Xu, B. Mao, W. Shen, Y. Yu, R. Tan, W. Song, *J. Colloid Interface Sci.* **2018**, *512*, 208–218.

[20]   H. H. Khaligh, L. Xu, A. Khosropour, A. Madeira, M. Romano, C. Pradère, M. Tréguer-Delapierre, L. Servant, M. A. Pope, I. A. Goldthorpe, *Nanotechnology* **2017**, *28*, 425703–425715.